Available online at www.sciencedirect.com
SCIENCE DIRECT®
Tectonophysics 366 (2003) 1–53
TECTONOPHYSICS
www.elsevier.com/locate/tecto

Tectonics of the Qinling (Central China): tectonostratigraphy, geochronology, and deformation history

Lothar Ratschbacher[a,*], Bradley R. Hacker[b], Andrew Calvert[c], Laura E. Webb[d], Jens C. Grimmer[a], Michael O. McWilliams[e], Trevor Ireland[f], Shuwen Dong[g], Jianmin Hu[g]

[a] *Institut für Geologie, Technische Universität Bergakademie Freiberg, Bernhard von Cottastrasse 2, Freiberg Sachsen D-09599, Germany*
[b] *Department of Geological Sciences, University of California, Santa Barbara, CA 93160, USA*
[c] *U.S. Geological Survey, 345 Middlefield Road, MS-910 Menlo Park, CA 94025, USA*
[d] *Department of Earth Sciences, Syracuse University, Syracuse, NY 13244-1070, USA*
[e] *Department of Geology and Environmental Sciences, Stanford University, Stanford, CA 94305-2215, USA*
[f] *Research School of Earth Sciences, The Australian National University, Canberra, Australia*
[g] *Chinese Academy of Geological Sciences, Beijing, PR China*

Received 5 April 2002; accepted 5 February 2003

Abstract

The Qinling orogen preserves a record of late mid-Proterozoic to Cenozoic tectonism in central China. High-pressure metamorphism and ophiolite emplacement (Songshugou ophiolite) assembled the Yangtze craton, including the lower Qinling unit, into Rodinia during the ~1.0 Ga Grenvillian orogeny. The lower Qinling unit then rifted from the Yangtze craton at ~0.7 Ga. Subsequent intra-oceanic arc formation at ~470–490 Ma was followed by accretion of the lower Qinling unit first to the intra-oceanic arc and then to the Sino-Korea craton. Subduction then imprinted a ~400 Ma Andean-type magmatic arc onto all units north of the northern Liuling unit. Oblique subduction created Silurian–Devonian WNW-trending, sinistral transpressive wrench zones (e.g., Lo-Nan, Shang-Dan), and Late Permian–Early Triassic subduction reactivated them in dextral transpression (Lo-Nan, Shang-Xiang, Shang-Dan) and subducted the northern edge of the Yangtze craton. Exhumation of the cratonal edge formed the Wudang metamorphic core complex during dominantly pure shear crustal extension at ~230–235 Ma. Post-collisional south-directed shortening continued through the Early Jurassic. Cretaceous reactivation of the Qinling orogen started with NW–SE sinistral transtension, coeval with large-scale Early Cretaceous crustal extension and sinistral transtension in the northern Dabie Shan; it presumably resulted from the combined effects of the Siberia–Mongolia — Sino-Korean and Lhasa – West Burma — Qiangtang–Indochina collisions and Pacific subduction. Regional dextral wrenching was active within a NE–SW extensional regime between ~60 and 100 Ma. An Early Cretaceous Andean-type continental magmatic arc, with widespread Early Cretaceous magmatism and back-arc extension, was overprinted by shortening related to the collision of Yangtze–Indochina Block with the West Philippines Block. Strike–slip and normal faults associated with Eocene half-graben basins record Paleogene NNE–SSW contraction and WNW–ESE extension. The Neogene(?) is characterized by normal faults and NNE-trending sub-horizontal extension. Pleistocene(?)–Quaternary NW–SE extension and

* Corresponding author. Tel.: +49-3731-393758; fax: +49-3731-393597.
E-mail address: lothar@geo.tu-freiberg.de (L. Ratschbacher).

doi:10.1016/S0040-1951(03)00053-2

NE–SW contraction comprises sinistral strike–slip faults and is part of the NW–SE extension imposed across eastern Asia by the India–Asia collision.

Keywords: Structural geology; Ar/Ar thermochronology; Proterozoic to Cenozoic tectonics; Ultrahigh-pressure orogeny; Qinling; Dabie Shan

1. Introduction

The Qinling orogen of central China stretches from the Qin mountain range south of Xian 1500 km westward through the Qilian Shan (Deng, 1996) and at least 600 km eastward through the Dabie Shan (Okay et al., 1993); it continues northeastward through the Sulu area (Enami and Zhang, 1990) of the Shandong peninsula into the Imjingang fold belt of Korea (Chough et al., 2000; Fig. 1). To elucidate the exhumation of high (HP) to ultrahigh-pressure (UHP) metamorphic rocks, we recently studied the Triassic–Jurassic tectonic unroofing of the Hong'an–Dabie Shan segment of the orogen (Hacker et al., 2000), and its Cretaceous

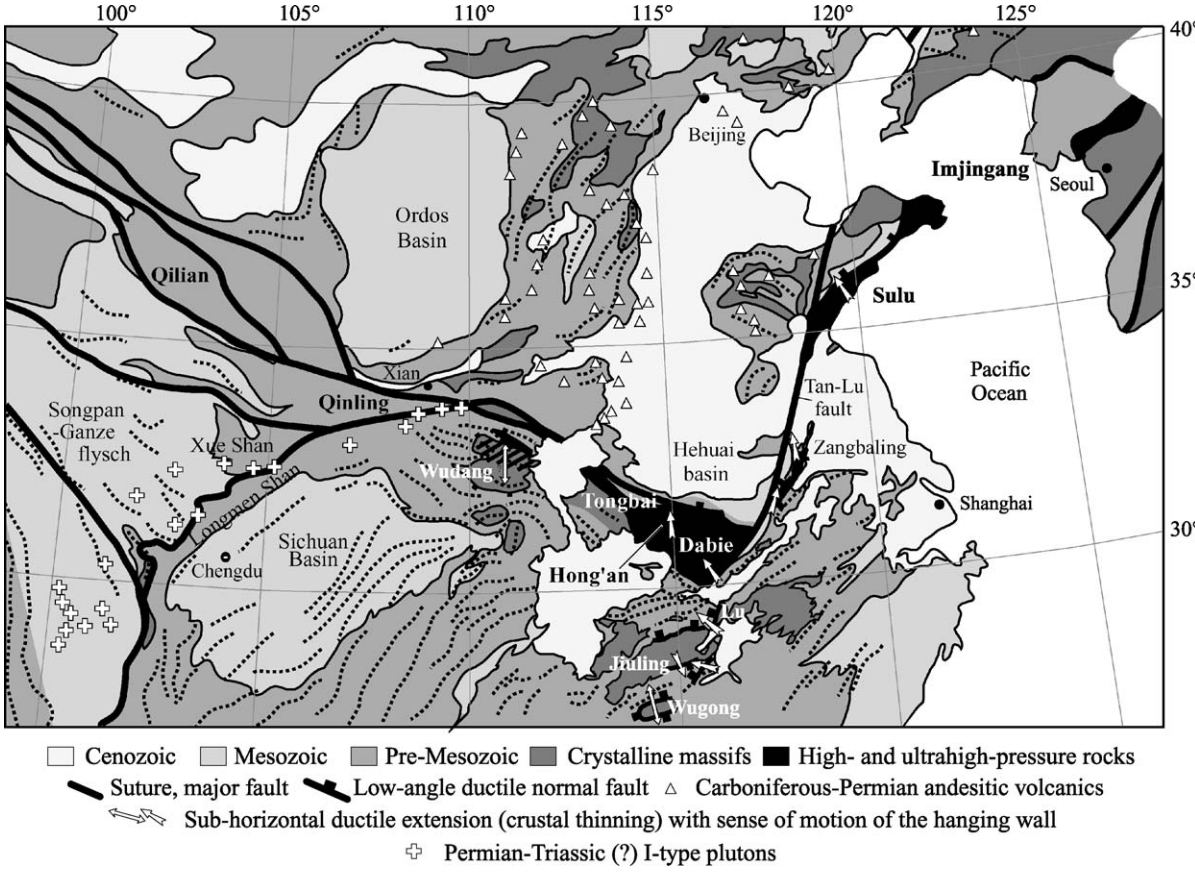

Fig. 1. The early Mesozoic Qilian–Qinling–Tongbai–Hong'an–Dabie–Sulu–Imjingang collisional orogen in eastern Asia. Structural interpretations of sub-horizontal extension in crystalline basement domes from Faure et al. (1996), Wallis et al. (1999), Lin et al. (2000), Hacker et al. (2000), and our data. Andesitic volcanic rocks from Zhang (1997) and Permian–Triassic plutons from R.G.S. Sichuan (1991) and R.G.S. Shaanxi (1989) suggest a pre-Late Permian arc related to subduction. The high-pressure metamorphism in the Wudang Shan basement complex is demonstrated unequivocally only in its northern part, whereas only spotty data coverage exists in the south; we indicate this by the bar shades.

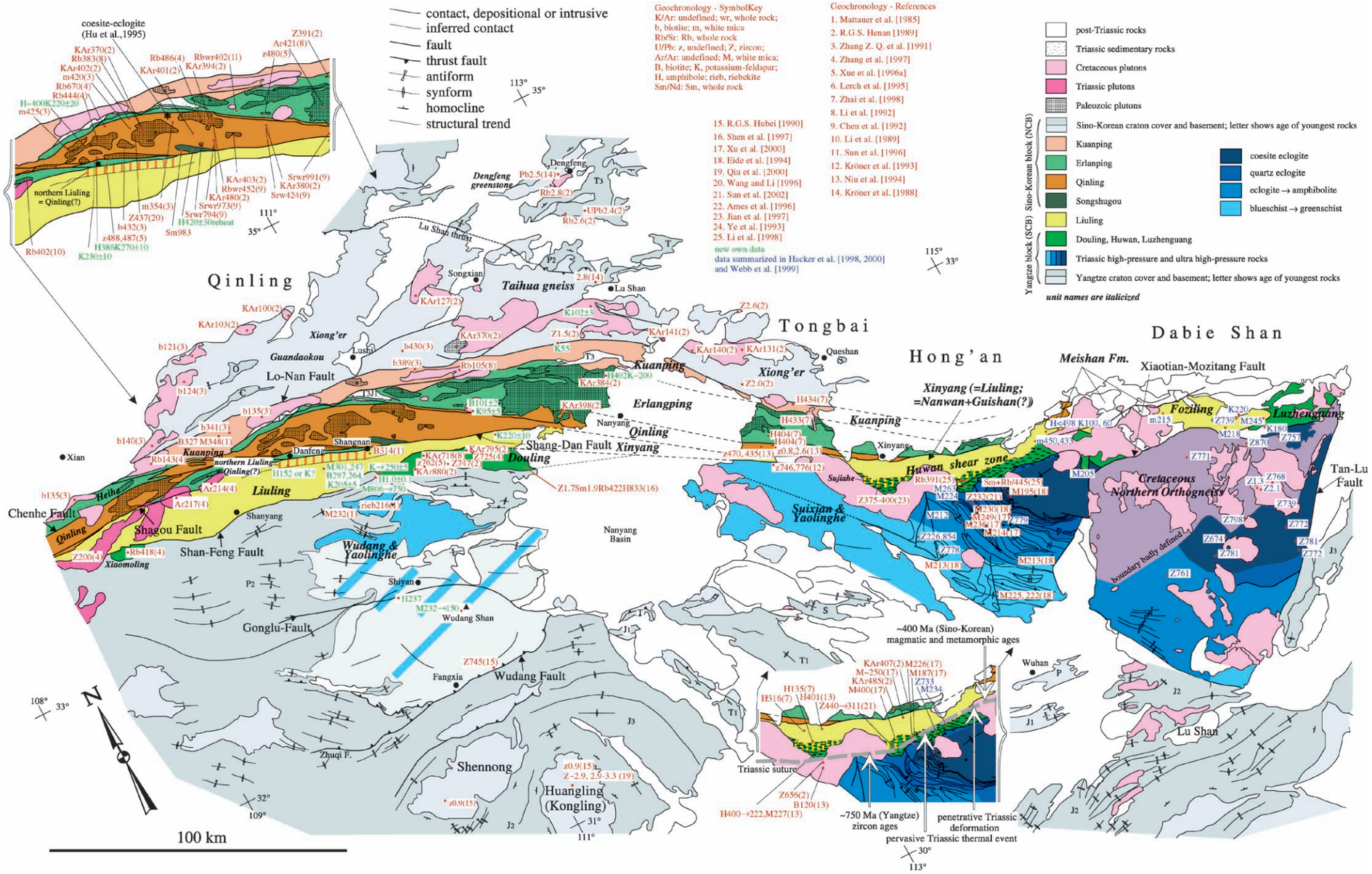

Fig. 2. Correlation of Paleozoic rock units through Qinling–Tongbai–Hong'an–Dabie, zones of high- and ultrahigh-pressure Triassic metamorphism, distribution of Early Cretaceous plutons, trend of major Triassic fold trains in the Yangtze-craton foreland cover fold-thrust belt (adapted from 1:500,000 province maps of China), and reliable geochronologic ages (those older than 800 Ma are in Ga). K-feldspar gives cooling through ~ 200 °C or an age range (marked by →) in case of an Ar-loss profile; the latter applies also for some hornblende and muscovite data. For a complete coverage of U/Pb, Rb/Sr, and $^{40}Ar/^{39}Ar$ ages from the Dabie and Hong'an Shan see Hacker et al. (1998, 2000), Ratschbacher et al. (2000), and references therein. The high-pressure metamorphism in the Wudang Shan basement complex is demonstrated unequivocally only in its northern part, whereas only spotty data coverage exists in the south; we indicate this by the bar shades (Eide et al., 1994).

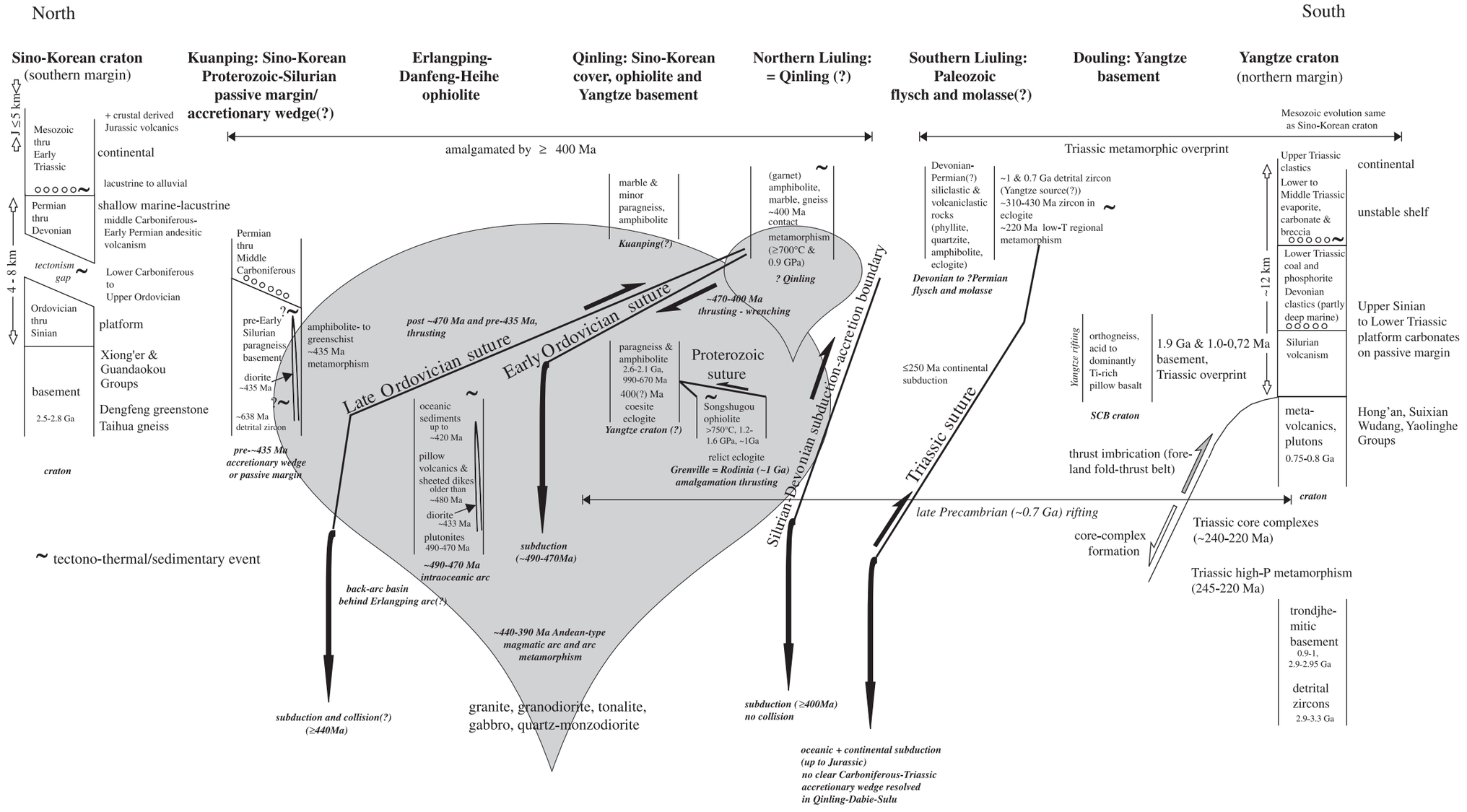

Fig. 3. Geologic units, tectono-thermal/sedimentary events, facies interpretation, radiometric ages, and tectonic interpretation of the Paleozoic–early Mesozoic Qinling orogenic belt. Intra-oceanic arc formation (Erlangping–Danfeng–Heihe) between ~ 490 and 470 Ma was followed by accretion of the lower Qinling micro-continent to the intra-oceanic arc, and to the Sino-Korean craton. Subduction underneath the northern Liuling unit imprinted the ~ 400 Ma Andean-type magmatic arc on the Sino-Korean craton plus Qinling assemblage. A subduction signature is again evident during the Carboniferous to Late Permian on the Sino-Korean craton, when the Paleo-Tethys was subducted northward producing the andesitic magmatism on the Sino-Korean craton and within the Liuling unit, where eclogites locally have late Carboniferous metamorphism. In the Late Permian–Early Triassic, the leading edge of the Yangtze craton was subducted to >150 km and subsequently exhumed by crustal extension.

and Cenozoic overprint (Ratschbacher et al., 2000). Exhumation was primarily accomplished by lithosphere-scale normal shear within and along the top of the upward and eastward moving HP–UHP continental wedge. Several issues pertinent to this UHP orogeny, however, must be addressed outside the HP and UHP rocks of Hong'an–Dabie. (1) How is the position of the Triassic suture between the Yangtze and Sino-Korean cratons expressed in the Qinling area (Fig. 2)? (2) How does the Sino-Korean craton in Tongbai–Hong'an–Dabie correlate with the more complete sequence in Qinling, what tectonothermal signature do they have, and is Triassic deformation widespread north of the suture, that is, in the hanging wall of the Triassic orogen? (3) How is the large-scale Triassic crustal extension of Dabie–Hong'an expressed in the Qinling? (4) The orogenic architecture of the world's largest UHP exposure, the Hong'an–Dabie Shan, is dominated by Cretaceous and Cenozoic structures that contributed to exhumation from mid-crustal depths. How widespread are Cretaceous and Cenozoic tectonics in the Qinling area?

This paper establishes a first-order correlation of rock units from the Qinling in the west to the Dabie Shan in the east and portrays the unit boundaries in terms of structural geometry, kinematics, and age of deformation. We focus on the Triassic orogeny, but to accomplish a comprehensive view of the Qinling, we add new and review existing data on the major units and deformation zones of the Qinling encompassing the late mid-Proterozoic to Recent. We close with speculative scenarios for the middle and late Proterozoic, Ordovician–Silurian, Triassic, Cretaceous, and Cenozoic tectono-thermal/sedimentary events.

2. Geologic units of the Qinling–Dabie orogen

Clear definition and subdivision of the rock units that comprise the Qinling–Dabie orogen (Figs. 2 and 3) remain elusive principally because units were initially divided using relatively young strike–slip faults as boundaries. The correlation of rock units across these strike–slip faults and the delineation of units using earlier, more fundamental, but cryptic, structures is evolving, but still incomplete. This section describes the major units of the Qinling orogen from north to south.

2.1. Sino-Korean craton

In the Qinling area, the oldest rocks in the Sino-Korean basement are the 2.5- to 2.8-Ga Taihua gneiss and Dengfeng greenstone (Kröner et al., 1988). These, and the Xiong'er and Guandaokou Groups, are overlain by a 4- to 8-km-thick Sinian (late Proterozoic to Early Cambrian) to Triassic section (Ma, 1989; R.G.S. Henan, 1989; Fig. 3). The Sinian through Ordovician rocks are platform-facies sandstone, stromatolitic dolomite, limestone, mudstone and rare evaporites, basaltic flows and pyroclastics. Late Ordovician through Early Carboniferous rocks are locally absent in the Qinling, probably indicating tectonism. Devonian to Permian (and locally Triassic in Henan Province) rocks are shallow marine or lacustrine (R.G.S. Henan, 1989). The middle Carboniferous to Lower Permian coal-bearing series contain andesitic volcanic rocks (Zhang, 1997). Sediment deposition changed markedly on the Sino-Korean craton in the Early Triassic when lacustrine to alluvial conglomerate, arkosic sandstone, and siltstone were laid down; this continental environment persisted throughout the Mesozoic. During the Jurassic, continental clastic sedimentation on both the Sino-Korean and Yangtze cratons was accompanied by deposition of up to 5 km of calc-alkaline, crustal-derived, intermediate-composition volcanic rocks: tuff, volcanogenic sandstone, and some lava (R.G.S. Anhui, 1987; R.G.S. Henan, 1989; R.G.S. Hubei, 1990).

2.2. Kuanping: Proterozoic–Silurian passive margin or accretionary wedge

Crystalline rocks of the Sino-Korean craton abut directly against metamorphic rocks of the core of the Qinling orogen, without an intervening sedimentary sequence that can confidently be interpreted as depositional cover to the craton. The Kuanping unit (Fig. 3), chiefly amphibolite- to greenschist-facies marbles and two-mica quartz schists, could represent part of the metamorphosed south-facing passive margin of the Sino-Korean craton (Wang et al., 2000) or an accretionary wedge (see below). It contains detrital zircon with a Pb–Pb age of 638 Ma (Lerch, 1993), is unconformably overlain by middle Carboniferous to Permian sedimentary rocks (Xue et al., 1996b), yielded a $^{40}Ar/^{39}Ar$ metamorphic hornblende age of 434 ± 2

Ma, and is intruded by a diorite of the same age (Zhai et al., 1998); it thus predates the Early Silurian. Vergence of the fold-thrust belt of pre-Carboniferous age within the Kuanping unit is northward (Xue et al., 1996b) and/or southward (Mattauer et al., 1985).

2.3. Erlangping–Danfeng–Heihe: Ordovician–Silurian (~490–470 Ma) intraoceanic arc ophiolite

Ophiolitic rocks within the Qinling orogen include the Heihe, Danfeng, and Erlangping units (Figs. 2 and 3). They include greenschist- to amphibolite-facies massive and pillowed volcanic rocks, sheeted dikes, plutonic rocks, chert, wackes, limestones, and turbiditic siliciclastic rocks (Xue et al., 1996a); at least some of the siliciclastic rocks interfinger with the volcanic rocks. The sediments contain Cambrian–Ordovician radiolaria (Zhang and Tang, 1983), Ordovician gastropods and corals (Li et al., 1990; You et al., 1993), Yangtze-affinity Early Cambrian(?) radiolaria, Silurian corals (Wang, 1989), and Ordovician–Devonian(?) radiolaria (Cui et al., 1995), indicating Ordovician–Silurian (though possibly longer) sedimentation; the youngest fossils of clearly defined age are Ludlovian–Wenlockian (419–428 Ma) radiolaria (Wang, 1989). Trace element contents indicate that the basaltic, andesitic, and dacitic volcanic rocks erupted in an intra-oceanic arc (Zhang et al., 1989, 1994; Sun et al., 1996; Xue et al., 1996b). Trondjhemites, tonalites, gabbros, and rare pyroxenites comprise a modest portion of the unit, and, at least in the Danfeng area, intrude the volcanic sequence (Xue et al., 1996a); they give single-grain Pb/Pb ages of 470, 480, 487, 487, and 488 Ma (Reischmann et al., 1990; Xue et al., 1996a), and a K–Ar age of unknown type of 485 Ma (R.G.S. Henan, 1989; all K/Ar ages from the study area should be viewed with caution because of the documented presence of excess ^{40}Ar in some samples, e.g., Zhai et al., 1998). A Rb/Sr isochron of 486 ± 15 Ma from a pluton (Zhang et al., 1997) and two Pb/Pb single zircon ages of 470 Ma (Kröner et al., 1993) in the Qinling unit might also be part of this intrusive series. These relationships imply that the volcanic rocks are older than ~480 Ma, consonant with a Sm/Nd isochron of 447 ± 41 Ma on a suite of volcanic and hypabyssal rocks (Zhang et al., 1989), and with a 433 Ma $^{40}Ar/^{39}Ar$ hornblende age on a cross-cutting diorite (Zhai et al., 1998). Sedimentary rocks of Erlangping type are reportedly disconformable on the Kuanping (R.G.S. Henan, 1989) or the Qinling units (Huang and Wu, 1992), but until the pseudostratigraphies and contact relationships among the units are better understood, we view these observations with caution. An early (seafloor?) oligoclase + actinolite metamorphism of the ophiolitic rocks was overprinted by regional greenschist to amphibolite facies discussed below.

2.4. Qinling: Yangtze basement and Sino-Korean cover?

The Qinling unit includes a variety of rocks and its internal structure is not well understood (Fig. 3). The structurally lowest rocks are biotite–plagioclase gneisses, amphibolites, calc-silicate rocks, garnet–sillimanite gneiss, and marble (Xue et al., 1996b). Indications that they are Proterozoic come from whole-rock Rb/Sr ages on gneisses of 991 ± 1, 794 ± 32 (Chen et al., 1991), and 670 ± 40 Ma (Zhang et al., 1997), Pb/Pb single-zircon ages of 2.1 (Zhang et al., 1991), 0.8 and 2.6 Ga (Kröner et al., 1993), and granitoid U/Pb zircon ages of 0.7 and 2.7 Ga (lower and upper intercepts, respectively; Zhang et al., 2001). The upper Qinling unit consists of marble with minor amphibolite and garnet–sillimanite gneiss (You et al., 1993). Often grouped within the Qinling unit is the Songshugou ophiolite, which includes an amphibolite body. The amphibolite contains relicts of an eclogite-facies metamorphism (Liu and Zhou, 1995) estimated by Zhang (1996) to have occurred at >750–770 °C and 1.2–1.6 GPa. Li et al. (1991) obtained a garnet–hornblende–whole-rock Sm/Nd age on the amphibolite of 1.0 ± 0.1 Ga, and we obtained a $^{40}Ar/^{39}Ar$ hornblende spectrum indicating a thermal event at 420 ± 30 Ma (Fig. 4a, Tables 1 and 2). Eclogite lenses, probably within the northern margin of the Qinling unit, contain coesite (Fig. 2; Hu et al., 1995). Hu et al. (1996) obtained a garnet–hornblende–omphacite–rutile–whole-rock Sm/Nd age on this eclogite of 400 ± 16 Ma.

Whether the Qinling unit belongs to the Sino-Korean or Yangtze cratons remains an open issue. Zhang et al. (1989) correlated the lower Qinling unit with the Sino-Korean basement, whereas Huang and Wu (1992) correlated the lower Qinling unit with the Douling and Wudang units (Yangtze craton) based on lithology. Xue et al. (1996b) used the prevalence of

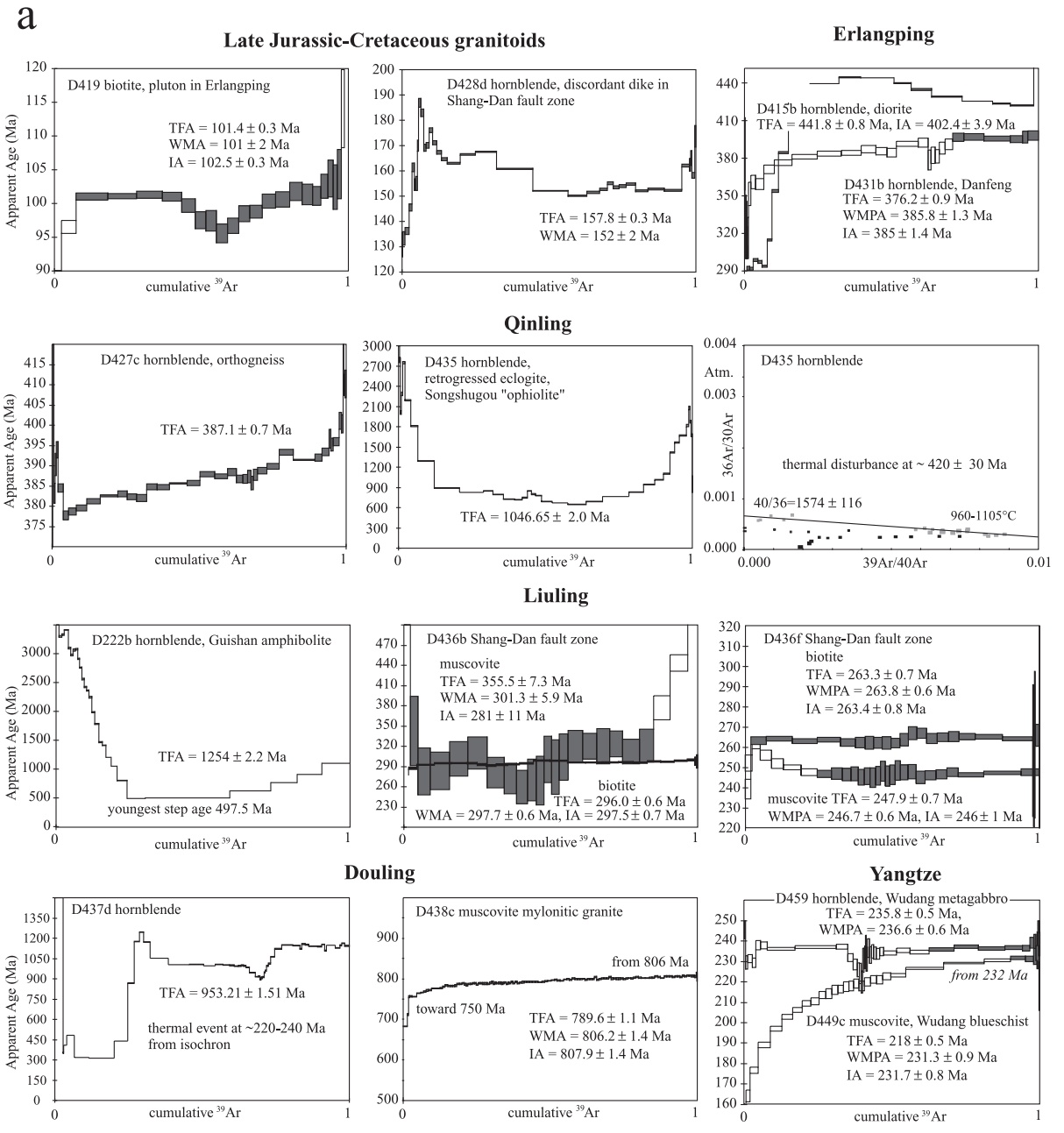

Fig. 4. New $^{40}Ar/^{39}Ar$ data. (a) Hornblende, muscovite, biotite. See Table 1 for sample location and Table 2 for age data and interpretations. Weighted mean ages (WMA) and weighted mean plateau ages (WMPA) were calculated using shaded steps. TFA, total fusion age. Uncertainties are 1σ. (b) Diffusion-domain analysis of metamorphic K-feldspars, shown are Arrhenius plot, log r/r_0 plot, release spectrum, and range of cooling histories.

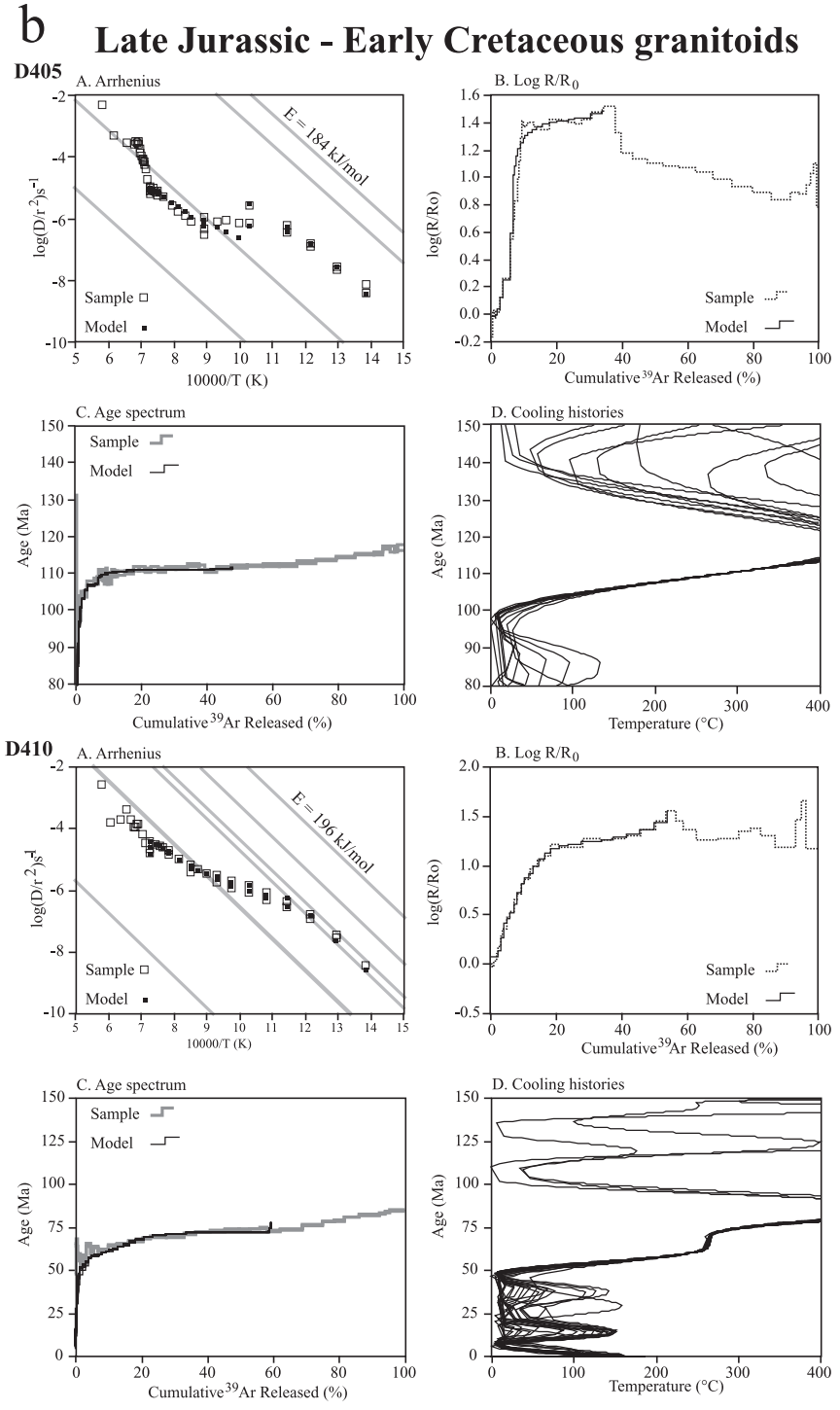

Fig. 4 (*continued*).

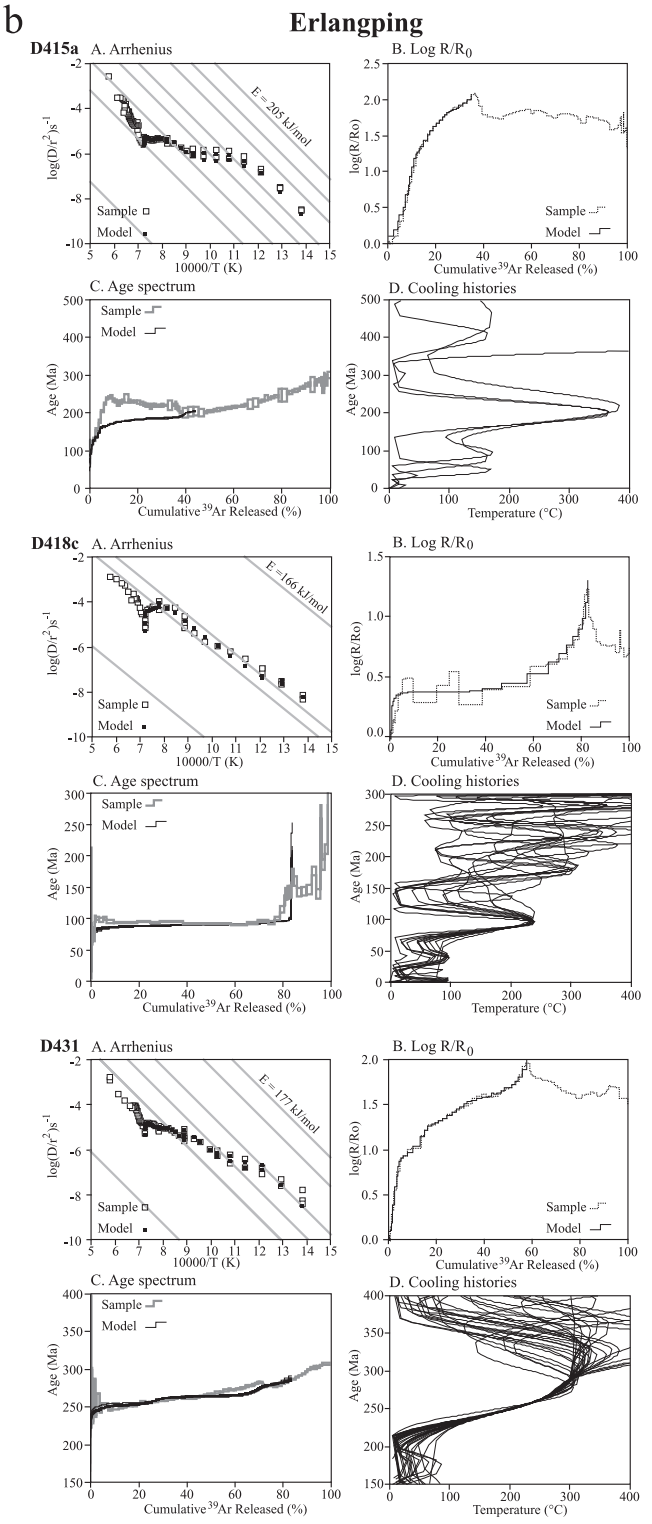

Fig. 4 (*continued*).

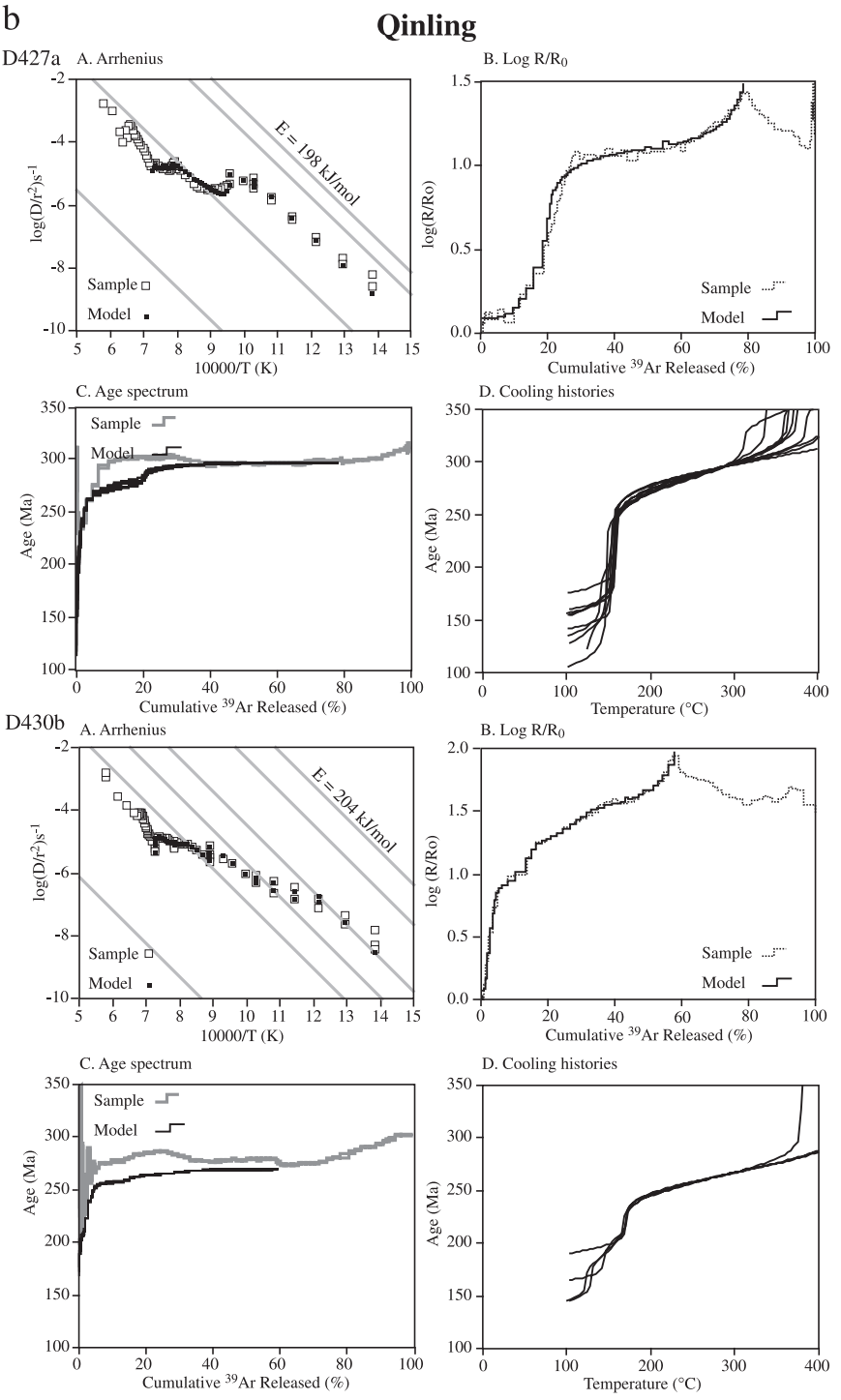

Fig. 4 (*continued*).

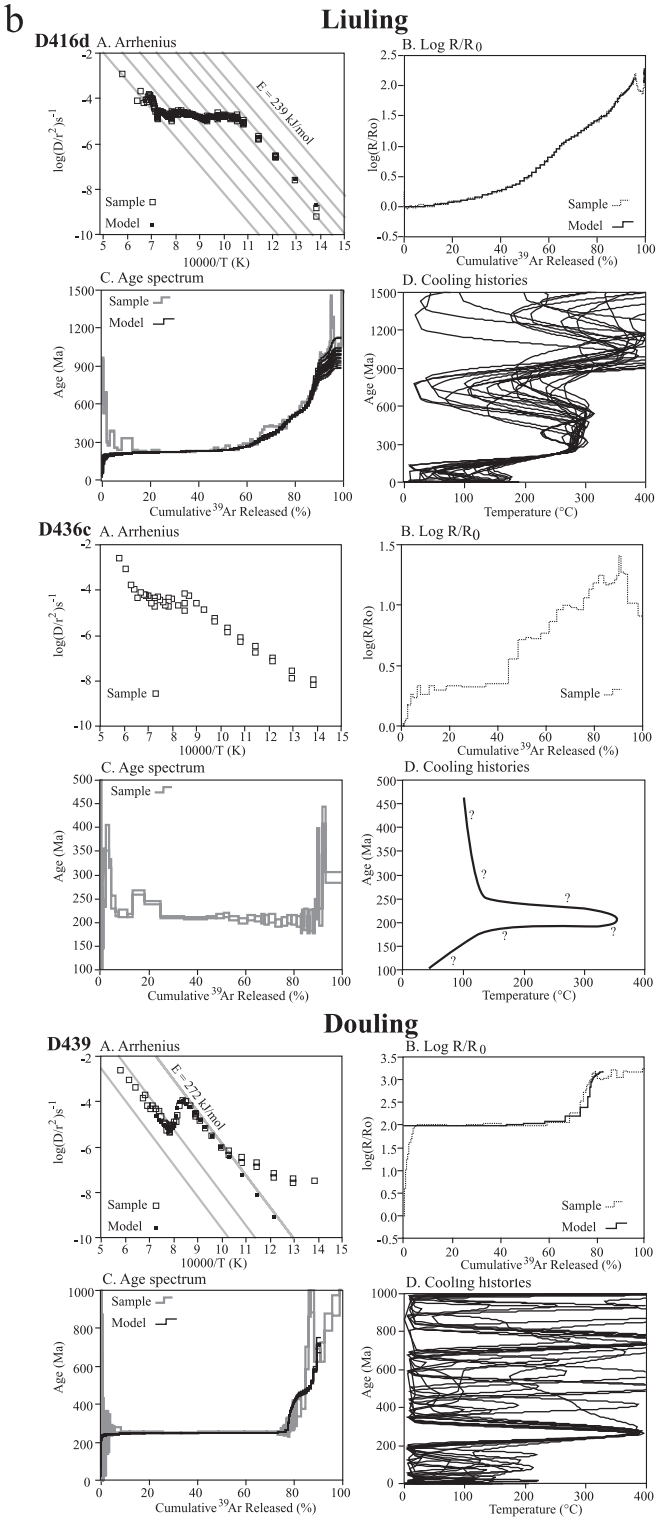

Fig. 4 (*continued*).

Table 1
Geochronology sample descriptions and locations

Sample	Description	N Latitude	E Longitude
Late Jurassic–Early Cretaceous granitoids			
D405	weakly deformed granite	33°43.19′	112°45.87′
D410	moderately deformed tonalitic orthogneiss	33°33.61′	112°28.53′
D419	polymetamorphic pluton in Erlangping	33°29.74′	111°41.60′
D428d	weakly discordant, ductile undeformed dike in Shang–Dan fault zone	33°39.75′	110°20.15′
Erlangping			
D415a	youngest felsic dike cutting D415b	33°17.16′	112°36.85′
D415b	moderately deformed, deep-seated diorite	33°17.16′	112°36.85′
D418c	greenschist-facies andesite	33°26.18′	111°40.78′
D431	granitoid, Qinling/ Danfeng contact	33°41.89′	110°22.38′
D431b	amphibolite, Danfeng complex	33°41.89′	110°22.38′
Qinling			
D427a	late, ductile undeformed granitic dike	33°48.58′	110°15.98′
D427c	early orthogneiss	33°48.58′	110°15.98′
D430b	weakly deformed late granitic dike	33°42.33′	110°22.55′
D435	retrogressed eclogite, Songshugou	33°34.69′	110°58.03′
Liuling			
D222b	amphibolite, Guishan or Nanwan Fm.	31°48.45′	115°15.15′
D416d	mafic mylonite in Shang–Dan fault zone	33°15.31′	111°47.56′
D436b	Shang–Dan fault zone; garnet + muscovite + biotite + kyanite	33°32.74′	110°38.93′
D436c	Shang–Dan fault zone; potassium–feldspar	33°33.00′	110°39.00′
D436f	Shang–Dan fault zone; garnet + muscovite + biotite + kyanite	33°33.90′	110°39.00′
D436k	"molasse" (metamorphic polymict conglomerate)	33°33.90′	110°39.00′
Douling			
D437d	banded retrogressed amphibolite	33°18.94′	110°54.73′
D438c	weakly mylonitic granite in Yaolinghe	33°19.30′	110°56.00′
D439	quartz–potassium–feldspar vein in amphibolite	33°19.37′	110°56.20′
Yangtze			
D449c	Wudang blueschist	32°25.55′	111°01.47′
D459	garnet metagabbro intrusive into Wudang Group	32°38.29′	110°42.74′

late Proterozoic ages to correlate lower Qinling with the crystalline basement of the Yangtze craton, which, unlike the Sino-Korean craton, contains evidence for a widespread ~750 Ma thermal event. The upper Qinling unit might be correlative with the Kuanping unit (Huang and Wu, 1992).

2.5. Liuling: Paleozoic flysch

The Liuling unit (Fig. 3) comprises siliciclastic to volcaniclastic slate, sandstone, conglomerate, amphibolite, and minor carbonate (You et al., 1993). Correlative rocks include the Xinyang Group in Tongbai-Hong'an and the Foziling unit in Dabie. Similar sediments in the Erlangping unit are included in this group by some authors (Liu et al., 1989; Huang and Wu, 1992), who suggest that the Liuling unit was deposited on the Erlangping unit. NW of the town of Danfeng the Liuling unit includes conglomerate with well-rounded, 0.5–1 cm, rarely 3 cm pebbles of gabbro, peridotite, amphibolite, granite, garnet, quartz, and minor hornblende and pyroxene, probably derived from the Qinling unit and interpreted as "molasse" (Mattauer et al., 1985). Yu and Meng (1995) showed that several Devonian conglomerate-bearing deposits occur along the Shang-Dan fault, are associated with turbitites and pyroclastics sediments, are derived from the Qinling unit and an "ophiolitic assemblage", and are locally interbedded with basic volcanic rocks; they suggested an origin along an active continental margin in a fore-arc basin position. In their sections, the fossiliferous Upper Devonian siliciclastics are conformably overlain by a sequence of shallow-marine

carbonates, turbitites, debris flow deposits, and slumps, and a shallowing upward sequence of proven Lower Carboniferous and suspected Carboniferous to Permian age. Yu and Meng (1995), Zhang et al. (1989), and Meng et al. (1995) specifically noted that the Liuling unit is different from the coeval rocks south of the Shan-Feng fault, which are middle Devonian to Carboniferous shallow water to terrestrial clastic rocks that make up part of the Yangtze craton cover. Thus, the Liuling unit is probably composite, encompassing the Qinling unit in the north, flysch units in the center, and locally passive margin sediments in the south; these interpretations remain speculative.

Devonian fossils in the Tongbai area (Du, 1986; Niu et al., 1993) have been used to infer a Devonian depositional age for the entire Liuling unit. From the conglomerate near Danfeng (northernmost Liuling unit), we obtained U/Pb SHRIMP ages (Table 3) on 10 zircons; the results include 403 ± 7 Ma (three overgrowths, probably metamorphic), 782 ± 11 Ma (three detrital grains), and 1.0 Ga (three detrital grains). $^{40}Ar/^{39}Ar$ ages from the Liuling unit are 401 (Niu et al., 1994), 316 (Zhai et al., 1998), <498 Ma (this study, Fig. 4a, Table 2) on hornblende, 301 and 247 Ma on muscovite, and 314, 297 and 264 Ma on biotite (Mattauer et al., 1985). One K-feldspar records reheating and rapid cooling in the Triassic (this study, Fig. 4b, Table 2); there are also two muscovite K–Ar ages of 450 and 433 Ma (Chen et al., 1993). In western Hong'an, the Sujiahe complex separates the dominantly siliciclastic Liuling unit (called the Nanwan formation) in the north from the HP and UHP rocks of central Hong'an in the south and contains arc volcaniclastic rocks, ''mélange'', and eclogite (Fig. 2). Tuff yielded a Rb/Sr whole-rock age of 391 ± 13 Ma (Ye et al., 1993), eclogite yielded U/Pb zircon ages of 377–400 Ma (Jian et al., 1997), 310 Ma (SHRIMP spot ages from zircon rims formed at eclogite-facies conditions; Sun et al., 2002), 350–440 Ma (SHRIMP spot ages from zircon cores; Sun et al., 2002), and eclogite Sm/Nd and Rb/Sr ages of 446 ± 23 and 444 ± 31 Ma (Li et al., 1998). Xu et al. (2000) presented two ~ 400 Ma phengite ages from eclogite-bearing gneisses. In aggregate, these ages indicate deposition during the Silurian–Devonian before metamorphism at ~ 400 Ma, erosion and deposition of 350–440 Ma arc rocks, and local Late Carboniferous eclogite-facies metamorphism in an accretionary wedge setting, followed by a low-temperature Triassic overprint. The metamorphism produced garnet amphibolite in mafic rocks and kyanite + garnet + biotite in pelitic rocks (≥ 700 °C and ≥ 900 MPa) of the northern Liuling unit; during subsequent deformation, the kyanite was replaced by sillimanite.

2.6. Devonian batholith: a ~400-Ma continental margin arc

Intruding the Erlangping, Qinling (Xue et al., 1996a), Kuanping (Zhai et al., 1998) and, possibly, Xiong'er (R.G.S. Henan, 1989) units is a suite of relatively undeformed Late Silurian–Early Devonian plutons (Figs. 2 and 3). This batholith pins the youngest possible age of these four units. It also provides a younger bound to the coalescence of the Kuanping and Erlangping units because at least one of the plutons intrudes their contact. Although no single pluton truncates the contact between the Qinling and Erlangping units, the batholith straddles the contact and thus likely also provides a younger bound to the amalgamation of the Qinling and Erlangping units. Significantly, none of the 400-Ma plutons crop out south of the Shang-Dan fault. Plutons cutting the Qinling unit tend to be granites–granodiorites with initial $^{87}Sr/^{86}Sr$ ratios ≥ 0.707, whereas those cutting the Erlangping unit are gabbro–quartz monzodiorite with initial $^{87}Sr/^{86}Sr$ ratios ≤ 0.706 (Xue et al., 1996a), implying that the magmas were influenced by their crustal substrate. These rocks yielded Pb/Pb zircon ages of 397 (Reischmann et al., 1990), 402 (Xue et al., 1996a), and 437 Ma (Wang and Li, 1996), U/Pb zircon ages of 422 ± 14, 406 ± 4, 410 ± 11, 401 ± 14 and 395 ± 6 Ma (Lerch et al., 1995), Rb/Sr isochrons of 403 ± 17 (Li et al., 1989) and 383 ± 8 Ma (Li et al., 1992), $^{40}Ar/^{39}Ar$ hornblende ages of 402 and ~ 400 Ma (this study, Fig. 4a, Table 2), and K/Ar ages of unknown type of 370, 384, 398, 403 and 407 Ma (R.G.S. Henan, 1989).

Metamorphism of the country rocks of the Devonian batholith can be interpreted as ''regional contact metamorphism'' in the mid-crustal levels of a magmatic arc (Hu et al., 1993; Zhai et al., 1998). Metamorphism in the Kuanping unit is biotite- to kyanite-grade and inverted, such that the lowest temperature

Table 2
Summary of $^{40}Ar/^{39}Ar$ data[a]

Sample	J	Weight (mg)	Grain size (μm)	Interpretation
Potassium–feldspar				
Late Jurassic–Cretaceous granitoids				
D405	0.0040738	1.5	400	cooling from ~ 300 °C at 112 Ma to ~ 100 °C at 103 Ma
D410	0.0040535	1.3	400	slow cooling from ~ 280 to 260 °C between 73 and 63 Ma and fast cooling to 150 °C at 55 Ma
Erlangping				
D415a	0.0041086	2.5	400	>300 Ma rock, reheated to ~ 370 °C at ~ 210 Ma, cooled to ~ 200 °C at ~ 150 Ma
D418c	0.0040163	1.6	400	>400 Ma rock, reheated to ~ 230 °C at ~ 100 Ma, cooling to 100 °C at 75 Ma
D431	0.0040396	2.4	400	>300 Ma rock, slow cooling from 300 to 180 °C between 290 and 240 Ma
Qinling				
D427a	0.0040451	1.6	400	>300 Ma rock, linear cooling from ~ 300 °C at ~ 300 Ma to 160 °C at 250 Ma
D430b	0.0040489	2.2	400	>300 Ma rock, linear cooling from 300 to 180 °C between 270 and 240 Ma
Liuling				
D416d	0.0041966	10.6	200	>1000 Ma, reheating to ~ 300 °C between 600 and 300 Ma, cooling to 200 °C at 200 Ma
D436c	0.0040663	1.7	400	>300 Ma rock experienced 205 ± 5 Ma thermal event
D439	0.0040267	1.6	400	>1000 Ma rock, rapid cooling from ~ 380 °C at 250 Ma

Sample	Mineral	J	Weight (mg)	Grain size (μm)	TFA (Ma)	IA (Ma)	MSWD	$^{40}Ar/^{36}Ar$	WMPA (Ma)	Steps used	% ^{39}Ar used
Hornblende and mica											
Late Jurassic–Cretaceous granitoids											
D419	bio	0.0041216	0.4	250	101.4 ± 0.3	102.5 ± 0.3	0.57	*225.9 ± 5.4*	*101 ± 2*	3–22/24	90
D428d	hbl	0.0042202	6.9	150	157.8 ± 0.3	n/a	n/a	n/a	*152 ± 2*	n/a	n/a
Erlangping											
D415b	hbl	0.0041987	9.4	400	441.8 ± 0.8	*402.4 ± 3.9*	2.1	3055 ± 218	n/a	12–19/20	66
D431b	hbl	0.0041893	7.3	400	376.2 ± 0.9	*385 ± 1.4*	0.12	305.8 ± 5.8	385.8 ± 1.3	25–30/30	29
Qinling											
D427c	hbl	0.0041775	9.0	400	387.1 ± 0.7	n/a	n/a	n/a	n/a	n/a	n/a
D435	hbl	0.0042078	11.1	200	1047 ± 2	~ 420	9.5	~ 1574	n/a	10–23/36	
Liuling											
D222b	hbl	0.0042145	8.7	300	1254 ± 2	n/a	n/a	n/a	n/a	n/a	n/a
D436b	bio[b]	0.0041241	0.5	400	296.0 ± 0.6	297.5 ± 0.7	1.9	332 ± 37	297.7 ± 0.6	14–24/24	44
	mus[b]	0.0041652	0.5	200	355.5 ± 7.3	*281 ± 11*	0.61	563 ± 107	301.3 ± 5.9	2–20/26	83
D436f	bio[b]	0.0041266	0.4	300	263.3 ± 0.7	263.4 ± 0.8	0.67	346 ± 60	263.8 ± 0.6	2–24/24	98
	mus	0.0041611	0.3	300	247.9 ± 0.7	246.0 ± 1.0	0.14	466 ± 101	246.7 ± 0.6	6–27/28	81
Douling											
D437d	hbl	0.0042182	8.7	400	953.2 ± 1.5	220–240	>10	~ 3000	n/a	1–7/50	
D438c	mus	0.0041627	1.4	400	789.6 ± 1.1	807.9 ± 1.4	n/a	n/a	806.2 ± 1.4	107–122/124	37
Yangtze											
D449c	mus	0.0041560	0.4	400	218.0 ± 0.5	*231.3 ± 0.9*	0.38	353 ± 25	231.7 ± 0.8	26–32/32	10
D459	hbl	0.0041751	9.6	200	235.8 ± 0.5	236.6 ± 0.6	0.64	286 ± 14	*236.6 ± 0.6*	29–37/37	37

Table 3
U/Pb data measured by sensitive high-resolution ion microprobe at the Australian National University (sample D436k)

Label	U	Th (ppm)	Th/U (ppm)	$^{204}Pb/^{206}Pb$	$^{207}Pb/^{206}Pb$	$^{238}U/^{206}Pb$	$f206$ (%)	Age (Ma)
1.1	222	216	0.97	0.00005 ± 0.00003	0.0757 ± 0.0010	5.57 ± 0.15	0.09 ± 0.06	1063 ± 27[a]
1.2	731	6	0.01	0.00089 ± 0.00028	0.0763 ± 0.0019	15.22 ± 0.38	1.62 ± 0.51	403 ± 9[b]
2.1	271	71	0.26	0.00007 ± 0.00003	0.1500 ± 0.0013	3.77 ± 0.13	0.10 ± 0.05	1515 ± 48
3.1	222	101	0.46	0.00012 ± 0.00005	0.0720 ± 0.0010	5.86 ± 0.20	0.20 ± 0.08	1013 ± 31[a]
4.1	726	317	0.44	0.00007 ± 0.00004	0.0676 ± 0.0011	8.02 ± 0.28	0.13 ± 0.06	756 ± 25[c]
5.1	642	160	0.25	0.00004 ± 0.00002	0.0707 ± 0.0008	7.67 ± 0.21	0.08 ± 0.03	789 ± 20[c]
5.2	523	55	0.11	0.00009 ± 0.00004	0.0687 ± 0.0017	10.58 ± 0.31	0.16 ± 0.07	581 ± 16
6.1	1226	390	0.32	0.00002 ± 0.00001	0.0693 ± 0.0006	7.67 ± 0.18	0.03 ± 0.01	789 ± 17[c]
7.1	392	178	0.45	0.00019 ± 0.00007	0.0566 ± 0.0009	15.31 ± 0.53	0.35 ± 0.13	406 ± 13[b]
7.2	304	131	0.43	0.00016 ± 0.00007	0.0532 ± 0.0015	15.89 ± 1.30	0.28 ± 0.13	392 ± 31[b]
8.1	1085	106	0.10	0.00005 ± 0.00002	0.0609 ± 0.0005	12.74 ± 0.52	0.09 ± 0.04	486 ± 19
9.1	250	63	0.25	0.00009 ± 0.00009	0.0793 ± 0.0013	10.06 ± 0.24	0.17 ± 0.15	610 ± 13
10.1	1497	10	0.01	0.00007 ± 0.00004	0.0688 ± 0.0014	10.60 ± 0.37	0.12 ± 0.07	580 ± 19
10.2	262	62	0.24	0.00006 ± 0.00006	0.0742 ± 0.0013	5.66 ± 0.18	0.10 ± 0.11	1047 ± 31[a]

Number before decimal identifies a specific grain; number after decimal identifies specific analysis within that grain. 1.2 is definitely a rim, and grain 7 has a core/rim with no age difference; either the core was reset as the rim grew (unlikely), the entire grain was reset at 400 (unlikely), or the whole grain grew at 400 as a metamorphic. Interestingly though, it has a markedly different Th/U than 1.2. $^{204}Pb/^{206}Pb$, $^{207}Pb/^{206}Pb$, $^{238}U/^{206}Pb$ ratios are as measured (i.e., no common Pb correction). $f206$ is the percentage of common Pb as estimated from the difference between the measured $^{207}Pb/^{206}Pb$ ratio and the extrapolated concordant age (^{207}Pb method). 206/238 age corrected for common Pb as given by $f206$. All errors ± 1σ.

[a] Weighted mean age of 1043 ± 17 Ma.

[b] Weighted mean age of 403.3 ± 7.2 Ma.

[c] Weighted mean age of 782.0 ± 11.5 Ma.

rocks are farther south, probably implying S-directed thrusting over the Qinling and Erlangping units (Mattauer et al., 1985). Metamorphic grade decreases monotonically from granulite facies in the Qinling unit to amphibolite to upper greenschist facies in the Erlangping unit (Zhai et al., 1998). The characteristic

Notes to Table 2:
Italics: preferred age interpretation.
Abbreviations: bio, biotite; hbl, hornblende; mus, white mica.
Explanatory notes on ages:
D222b hbl: saddle-shaped spectrum, with minimum age of 497.5 ± 1.8 Ma; suggestion from the isochron of a 200- to 440-Ma thermal event.
D415b hbl: incomplete analysis because of hardware failure; good isochron age of 402.4 ± 3.9 Ma.
D419 bio: weakly disturbed spectrum with WMA 101 ± 2 Ma.
D427c hbl: serially increasing spectrum from ≥ 395 Ma to ≤ 380 Ma; suggests initial closure at ≥ 395 Ma, with subsequent reheating after 380 Ma.
D428d hbl: typical excess Ar spectrum plus isotopic cluster; probably Cretaceous.
D431b hbl: serially increasing spectrum suggesting initial closure at ≥ 385 Ma and reheating at ≤ 330 Ma.
D435 hbl: classic U-shaped excess Ar spectrum; a restricted set of decreasing-age points from 960–1105 °C *suggest* a thermal disturbance at 420 ± 30 Ma.
Original crystallization age unknown, but may be ~ 1.7 Ga.
D436b bio: serially increasing spectrum suggesting closure at 296 ± 4 Ma.
D436b mus: plateau at 301 Ma.
D436f bio: plateau at 263.8 ± 0.6 Ma.
D436f mus: plateau 246.7 ± 0.6 Ma.
D437d hbl: isotopic ratios of early high K/Ca steps imply a ~ 220- to 240-Ma thermal event; the bulk of the steps, which are low K/Ca, imply an early age, strongly masked by excess Ar of ~ 1.0 ± 0.1 Ga.
D438c mus: serially increasing spectrum from ~ 700 to 806 Ma; interpret initial cooling as 806 Ma.
D449c mus: classic loss profile from 232 Ma down toward ~ 150 Ma.
D459 hbl: relatively flat, with minor loss; high T end is 236.6 ± 0.6.
[a] Raw data are available at http://www.geol.ucsb.edu/faculty/hacker/suppleData.
[b] Unreliable, likely homogeneously released excess ^{40}Ar.

aluminum silicate of the Qinling unit is sillimanite, overgrowing kyanite (You et al., 1993). Maximum pressures of 0.9–1.0 GPa at 700–800 °C are suggested by local occurrences of biotite + garnet + kyanite (Hu et al., 1993) and garnet granulites (Kröner et al., 1993). Maximum temperatures, reached in biotite + sillimanite + garnet + orthoclase rocks, were 650–800 °C at 500–900 MPa (Spear, 1993); garnet amphibolites yield similar conditions of 700 °C and 600–800 MPa (Hu et al., 1993), and hornblende granulites formed at 500–700 MPa and ≥600–700 °C (Zhai et al., 1998). Metamorphic mineral ages for this ''regional contact metamorphism'' include $^{40}Ar/^{39}Ar$ hornblende ages of 404 ± 5 (Zhai et al., 1998) and 421 ± 2 Ma (Li and Sun, 1995) on Erlangping amphibolite, 404 ± 2 Ma on Qinling granulite (Zhai et al., 1998), 420 ± 30 Ma on the amphibolite at Songshugou (this study, Fig. 4a, Table 2), 401 (Niu et al., 1994) and 316 Ma (Zhai et al., 1998) from the Liuling unit, eight K/Ar muscovite and biotite ages on Qinling unit metamorphic rocks that range from 480 to 354 Ma (Zhang et al., 1991; R.G.S. Henan, 1989), and one Rb/Sr whole-rock isochron on greenschist-facies pillowed basalts of 402 ± 6 Ma (Sun et al., 1996).

2.7. Douling: Proterozoic Yangtze basement

The Douling unit is composed of micaceous gneiss and schist with subordinate hornblende gneiss, quartz keratophyre, pyroclastics, and massive to pillowed Ti-rich basalt (Fig. 3; R.G.S. Henan, 1989; Hao et al., 1994). It has been correlated with Yangtze basement exposed in the Huangling area based on lithology and age (Hao et al., 1994). Geochronology suggests that the Douling unit rocks formed in the Proterozoic: Sm/Nd whole-rock gneiss age of 1.9 ± 0.3 Ga, Rb/Sr whole-rock gneiss age of 422 ± 16 Ma (Shen et al., 1997), Pb/Pb single zircon gneiss ages of 747 (R.G.S. Henan, 1989) and 1.7 ± 0.2 Ga, amphibolite hornblende $^{40}Ar/^{39}Ar$ age of 833 ± 17 Ma (Shen et al., 1997), Sm/Nd mineral isochron on quartz diorite of 979 ± 12 Ma (Hao et al., 1994), K/Ar ages of unknown type of 718 (Li et al., 1992), 795 and 880 Ma (R.G.S. Henan, 1989), a U/Pb age of unknown type of 725 ± 29 Ma (Zhang et al., 1997), $^{40}Ar/^{39}Ar$ ages on hornblende of ~ 1.0 Ga, and muscovite age of ~ 800 Ma (this study, Fig. 4b, Table 2).

2.8. Yangtze craton

The oldest rocks of the Yangtze craton are Archean and exposed in the Yangtze Gorge in the Shennong and Huangling (Kongling) areas and comprise gneissic trondjhemites with ~ 2.9 Ga zircons (U/Pb SHRIMP ages); paragneisses have detrital zircons of 3.3–2.9 Ga (Qiu et al., 2000; Ames et al., 1996). Granites intruded the Archean basement at ~ 1.9 Ga. Many of the zircons from the Huangling area experienced Pb loss at ~ 1.0–0.9 Ga (Figs. 2 and 3; R.G.S. Hubei, 1990; Qiu et al., 2000). Farther north, the Hong'an, Suixian, Wudang, and Yaolinghe Groups are typified by intercalated mafic and felsic volcanics, siliciclastics, and carbonates (R.G.S. Hubei, 1990). Numerous zircons from these units and from the Douling unit and the Dabie Shan HP–UHP rocks are ~ 750–800 Ma (Fig. 2 and Hacker et al., 1998, 2000); we obtained a $^{40}Ar/^{39}Ar$ muscovite age from the Yaolinghe unit of 806–750 Ma (Fig. 4a, Table 2).

Overlying the Precambrian basement are ~ 12 km of weakly metamorphosed Upper Sinian to Triassic sedimentary rocks. Cambrian through Carboniferous rocks are mostly platform-shelf carbonates and shelf-slope clastic rocks formed on the north-facing passive margin of the Yangtze craton, except for minor Lower Silurian (423–443 Ma) volcanic flow and volcaniclastic rocks. Locally, Lower, Middle, and Upper Devonian fluvial conglomerate, quartz sandstone, and mudstone lie unconformably on Upper Silurian rock. Permian platform-facies carbonates give way upsection to coal-bearing clastics and phosphorites indicative of restricted shelf and lagoonal deposition (R.G.S. Hubei, 1990). Early and Middle Triassic evaporite, carbonate, and argillite indicate shallow marine platform sedimentation with restricted circulation (R.G.S. Hubei, 1990). The shift to continental sedimentation occurred on the Yangtze craton in Late Triassic time.

3. New $^{40}Ar/^{39}Ar$ data

3.1. Hornblende, white mica, and biotite ages

We obtained $^{40}Ar/^{39}Ar$ ages on 23 mineral concentrates (Fig. 4a, Tables 1 and 2). Five of the spectra (D436b and D436f, both with white mica and biotite

from mylonitic gneiss; D459, hornblende from a garnet gabbro) yielded plateau ages. However, the discordance in ages between D436b and D436f, and the younger age for muscovite rather than biotite from D436f are cause for concern as the two samples are less than 2 km apart; these spectra might reflect homogeneously released excess ^{40}Ar. Four spectra (D427c, hornblende from an orthogneiss; D431b, hornblende from an amphibolite; D438c, white mica from a mylonitic granite; D449c, white mica from a blueschist) have serially increasing ages that can be interpreted as the result of an early Ar retention event overprinted by a younger Ar loss event. The spectra for D427c and D431b plausibly record initial argon retention at ~ 400 Ma. Likewise, we propose initial retention ages of ~ 806 and ~ 232 Ma for samples D438c and D449c, respectively; the inferred Ar loss event at ~ 750 Ma for D438c is consonant with abundant other information for an event of this age on the Yangtze craton (Hacker et al., 1998). The remaining four spectra are more problematic. D222b (hornblende from an amphibolite) likely underwent Paleozoic Ar loss, D415b (hornblende from a diorite) probably crystallized at 400–480 Ma, and D419 (biotite from a granite) is certainly a Cretaceous pluton, whereas D428d (hornblende from a dike) probably represents a Cretaceous dike affected by excess ^{40}Ar.

3.2. Potassium–feldspar ages

Ten, mostly metamorphic K-feldspars (Fig. 4b, Tables 1 and 2) were analyzed to constrain low-temperature thermal histories. Qualitative assessment of K-feldspar spectra are consistent with geochronology of other phases, and quantitative modeling of argon release places reasonable and interesting constraints on moderate to low temperatures (350–150 °C) of critical units. All except one K-feldspar sample released ^{39}Ar apparently by volume diffusion and are modeled with multi-domain diffusion analysis (Lovera, 1992; Appendix A). Two K-feldspars from likely Early Cretaceous granitoids in the Sino-Korean craton were analyzed. Under the assumption of monotonic cooling, D405 indicates linear cooling from 300 °C at 112 Ma to ~ 100 °C at 103 Ma; allowing reheating puts the peak of reheating at 120 Ma. D410 shows an age spectrum that climbs from 55 to 85 Ma with a flat segment at 73 Ma. The modeled spectrum indicates slow cooling from ~ 280 to 260 °C between 73 and 63 Ma and faster cooling to 150 °C by 55 Ma. If reheating is allowed, cooling follows a thermal spike at 85 Ma. Three K-feldspar samples come from the Erlangping unit. D415, a felsic dike cutting a diorite with a ~ 400-Ma hornblende age, released significant amounts of excess ^{40}Ar at low temperatures, but yielded model cooling histories of ~ 370 °C at 210 Ma, followed by linear cooling to 200 °C by 150 Ma and to 160 °C by 100 Ma. Because most of the gas released below incremental melting (~ 1150 °C) yielded a descending age spectrum, there is considerable uncertainty in this cooling history. Climbing ages in the final 30% of the ^{39}Ar released suggests 400–350 Ma cooling, consistent with the hornblende age. The spectrum and diffusion modeling of D418c implies a pre-400 Ma history with a 230 °C reheating event at 100 Ma followed by cooling to 100 °C by 75 Ma. Modeling of the spectrum of D431, an unfoliated granitoid intruding the Danfeng amphibolite ($\geq$ 385 Ma hornblende), indicates slow and linear cooling from 300 to 180 °C between 290–240 Ma and a ~ 300 to 320 Ma reheating, consistent with the $\leq$ 330 Ma reheating event inferred from hornblende. Ductile flow in the Danfeng amphibolite must therefore be older than 300–330 Ma. Two K-feldspar samples come from the Qinling unit. D427a is a dike cutting the Qinling orthogneiss (~ 390 Ma hornblende). Modeling yields linear cooling from 300 °C at 300 Ma to 160 °C at 250 Ma followed by very slow cooling to 150 °C by 200 Ma. The 300 to 250 Ma cooling should be considered a minimum rate given complexity in the first 30% of ^{39}Ar released, the sample may have cooled through 250 °C as early as 300 Ma. Ductile deformation in the Qinling unit is thus pre-300 Ma. D430b, a low-*T* ductile to brittlely deformed granitic dike, has a complicated spectrum indicating linear cooling from 300 to 180 °C between 270 and 240 Ma and then nearly isothermal cooling to 200 Ma. Like D427a, the cooling may be somewhat older (270 Ma) if ages ascribed to excess argon are accurate. Two K-feldspar samples are from the Shang-Dan fault zone of the northern Liuling unit. D416d is a well-rounded K-feldspar clast in a thin ultramylonitic acid metavolcanic layer in mylonitic amphibolite; the rocks show evidence of low-*T* ductility (~ 300 °C) overprinting a high-*T* fabric (>500

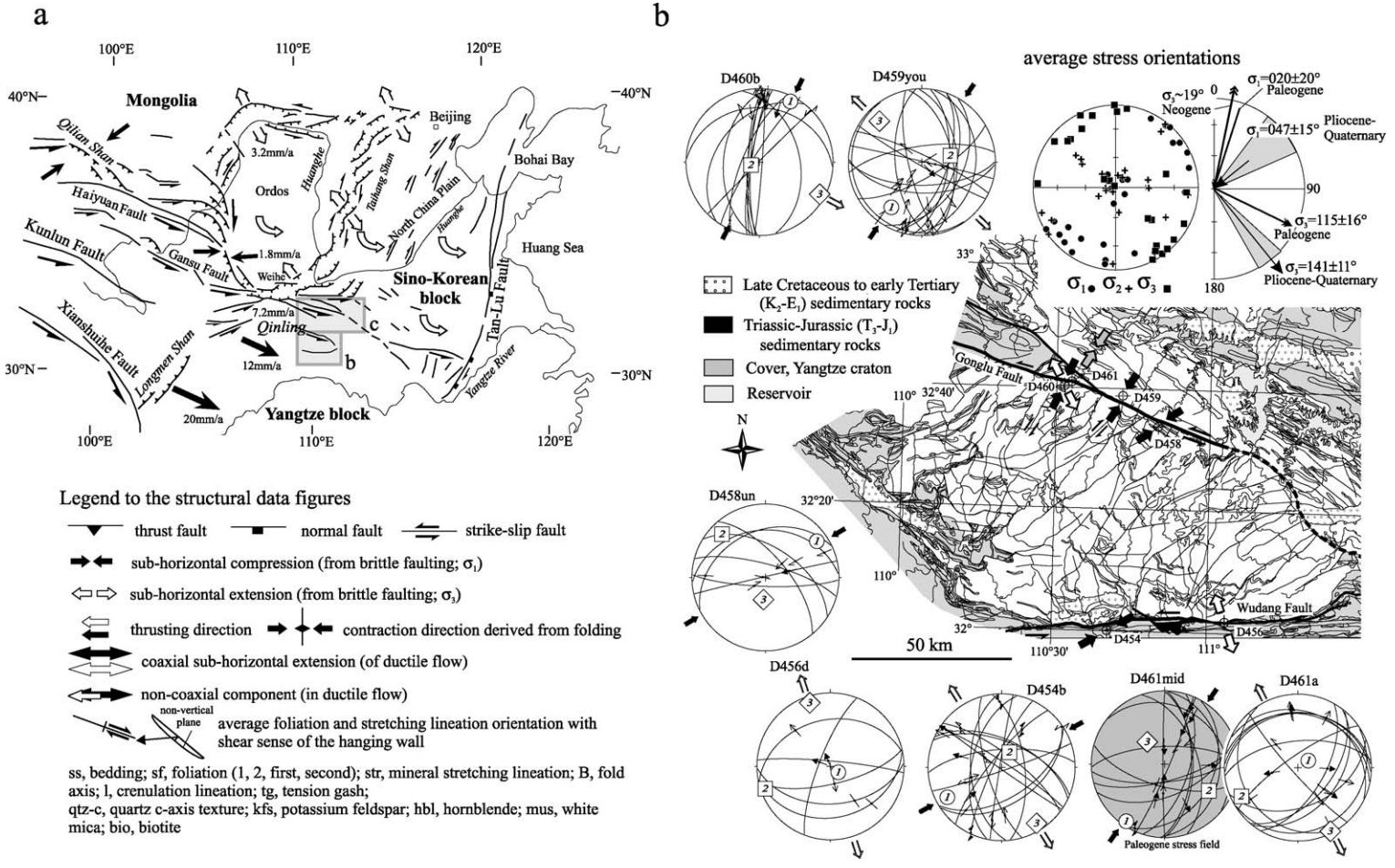

Fig. 5. (a) Simplified map of late Cenozoic extension and strike-slip tectonics in central China, modified from Zhang et al. (1995, and references therein). (b) Lower hemisphere, equal-area stereogram, upper right summarizes principal stress orientations attributed to Cenozoic deformation; orientation rose to the right suggests separation into three distinct stress fields, based on consistent overprinting criteria and neotectonic features associated with the Pliocene–Quaternary fault sets. Remaining stereograms show fault-slip data and principal stress orientations 1–3 and are plotted around simplified geological map of the Wudang Shan showing late Cenozoic faulting. The lower hemisphere, equal-area stereograms are as follows: Faults are drawn as great circles and striae are drawn as arrows pointing in the direction of displacement of the hanging wall. Confidence levels of slip-sense determination are expressed in the arrowhead style: solid, certain; open, reliable; half, unreliable; without head, poor. Arrows around the plots give calculated local orientation of sub-horizontal principal compression and extension. Shading discriminates plots related to different stress fields; the same shading is applied to the arrows indicating principal stress directions in the map. (c) As in b, but showing the Qinling east–southeast of Xian. Our map interpretation is based on 1:500,000 map of R.G.S. Shaanxi (1989), and incorporates evaluation of Peltzer et al. (1985) and Zhang et al. (1995). Double-headed arrows and attached numbers give location and amount of offset across basins and along strike-slip faults; extension across half-graben basins was estimated from a planar fault-triangular half graben model and offset along strike-slip faults used Cretaceous and younger lithological markers. Legend of structural data applies to this figure up to Fig. 8.

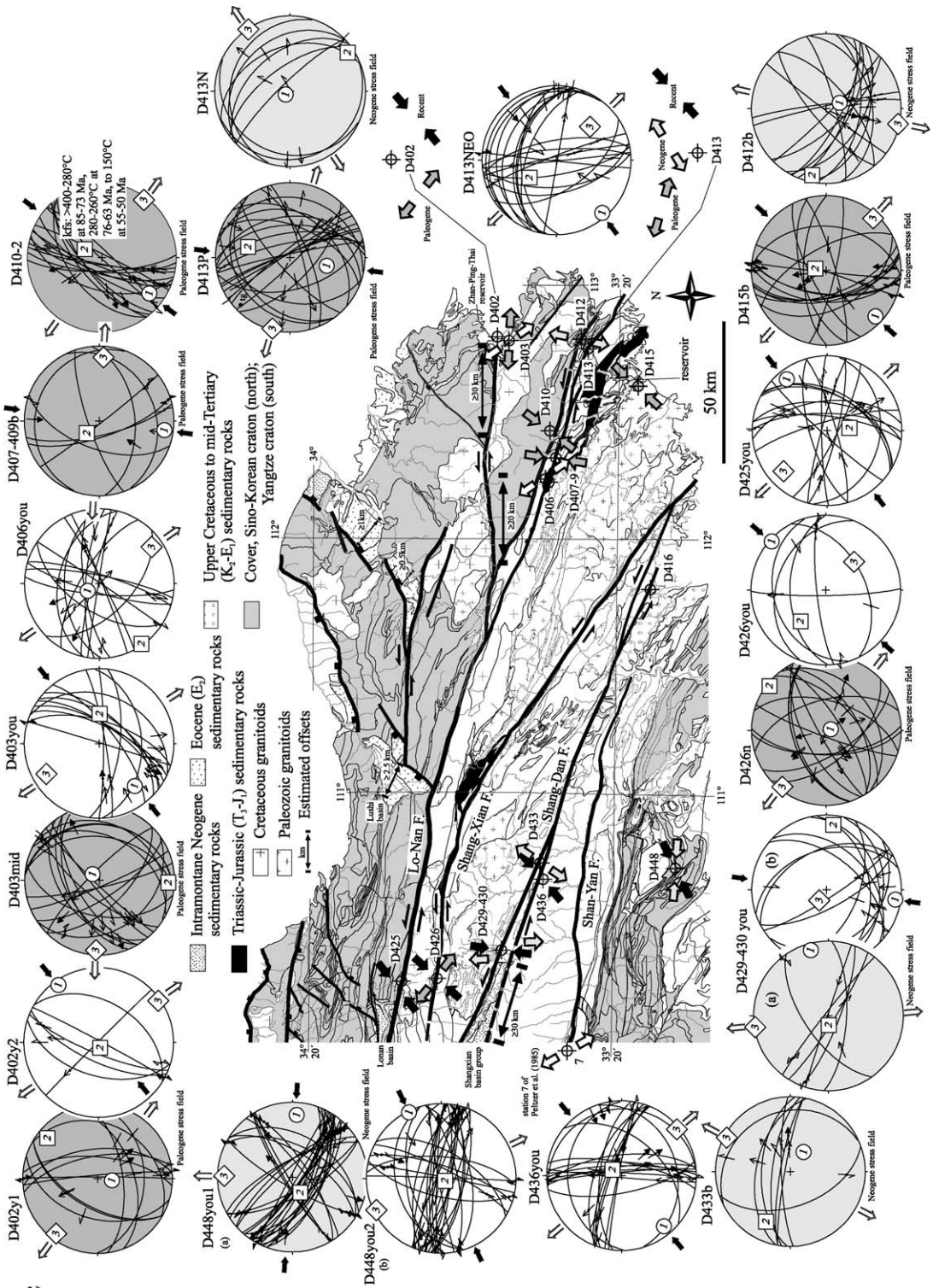

Fig. 5 (*continued*).

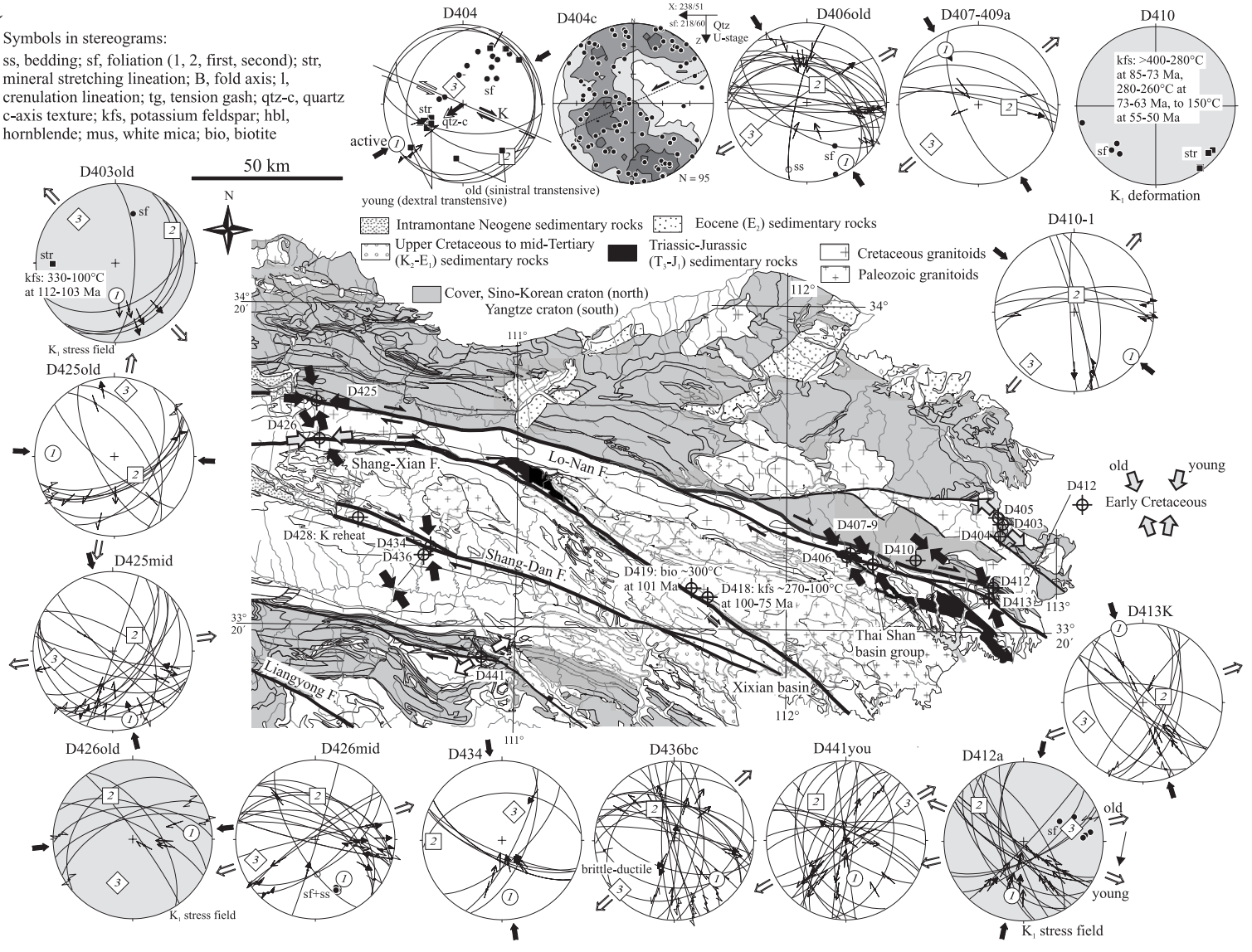

Fig. 6. Cretaceous structural data from the eastern Qinling belt (a) and the Wudang Shan area (b). See Fig. 5 for legend to the structural data. Quartz U-stage data show single *c* axes and distributions contoured with Kamb's method. K, Cretaceous; relevant thermochronologic data plotted close to the structural station plots or, where no structural data available, onto the map.

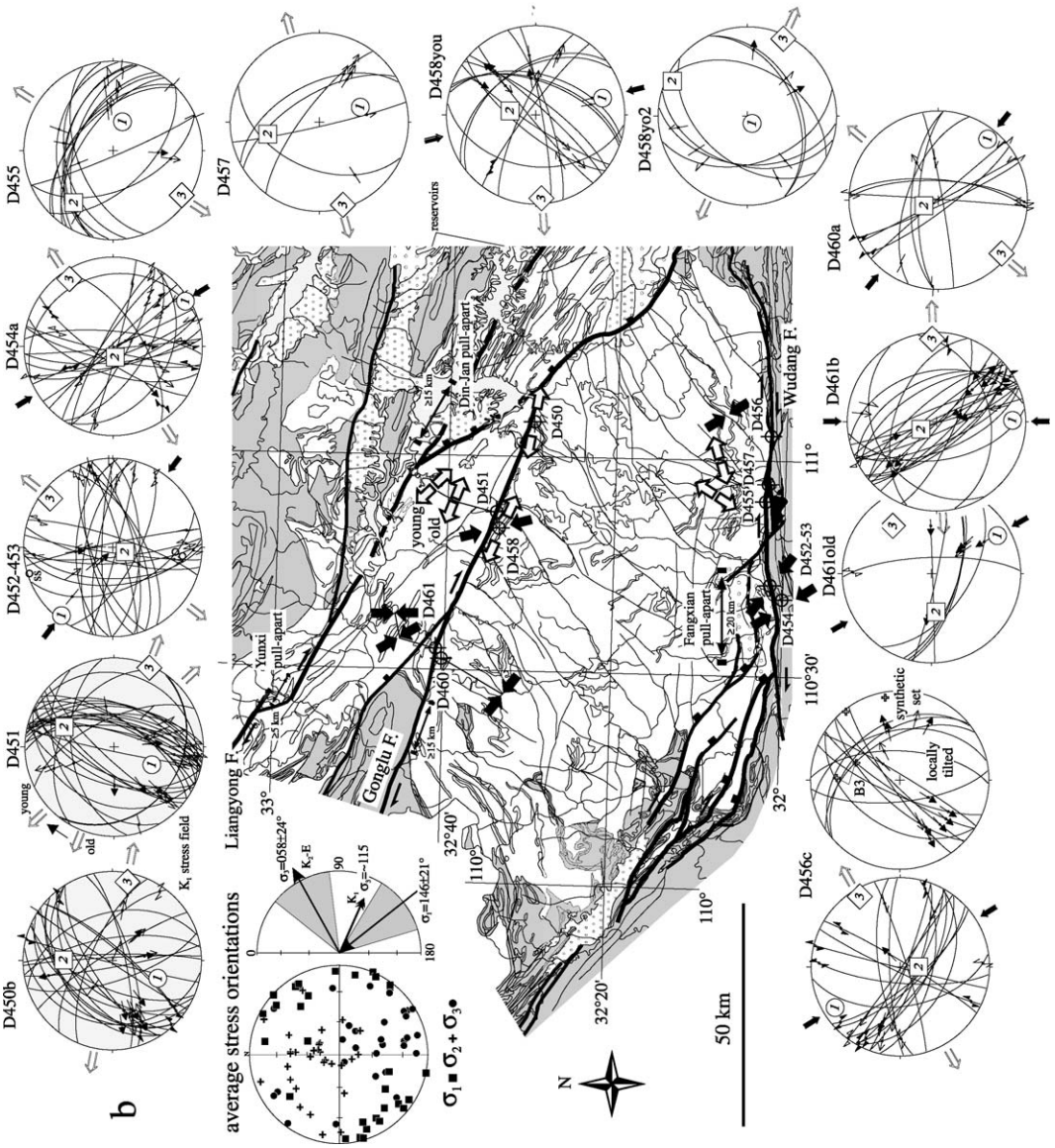

Fig. 6 (*continued*).

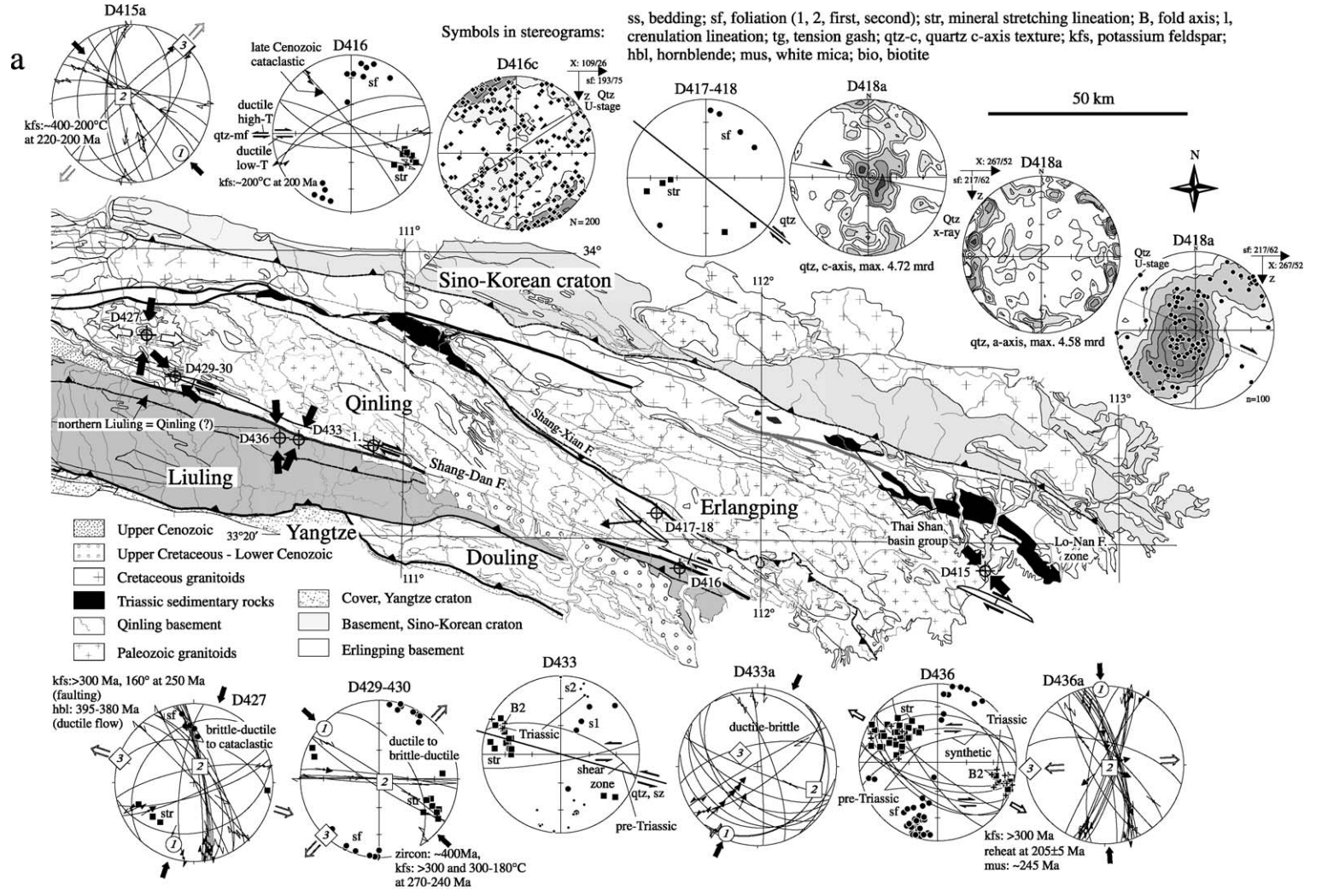

Fig. 7. Triassic structural data from the (a) eastern Qinling belt, (b) the northern, and (c) the central and southern Wudang area. Double arrows in some plots give the sense of shear (hanging wall displacement) interpretation. See Fig. 5 for legend to the structural data and Fig. 6 for further structural and age explanations. X-ray texture goniometer *c* and *a* axes data (*c* axes orientations are derived from orientation distribution function), contoured in multiples of random distribution. (1) in (a) marks the Songshugou ophiolite; the structural interpretation is from Song et al. (1998). Rotated structural data: given is trend of rotation axis, angle of rotation, and sense; ccw, counterclockwise.

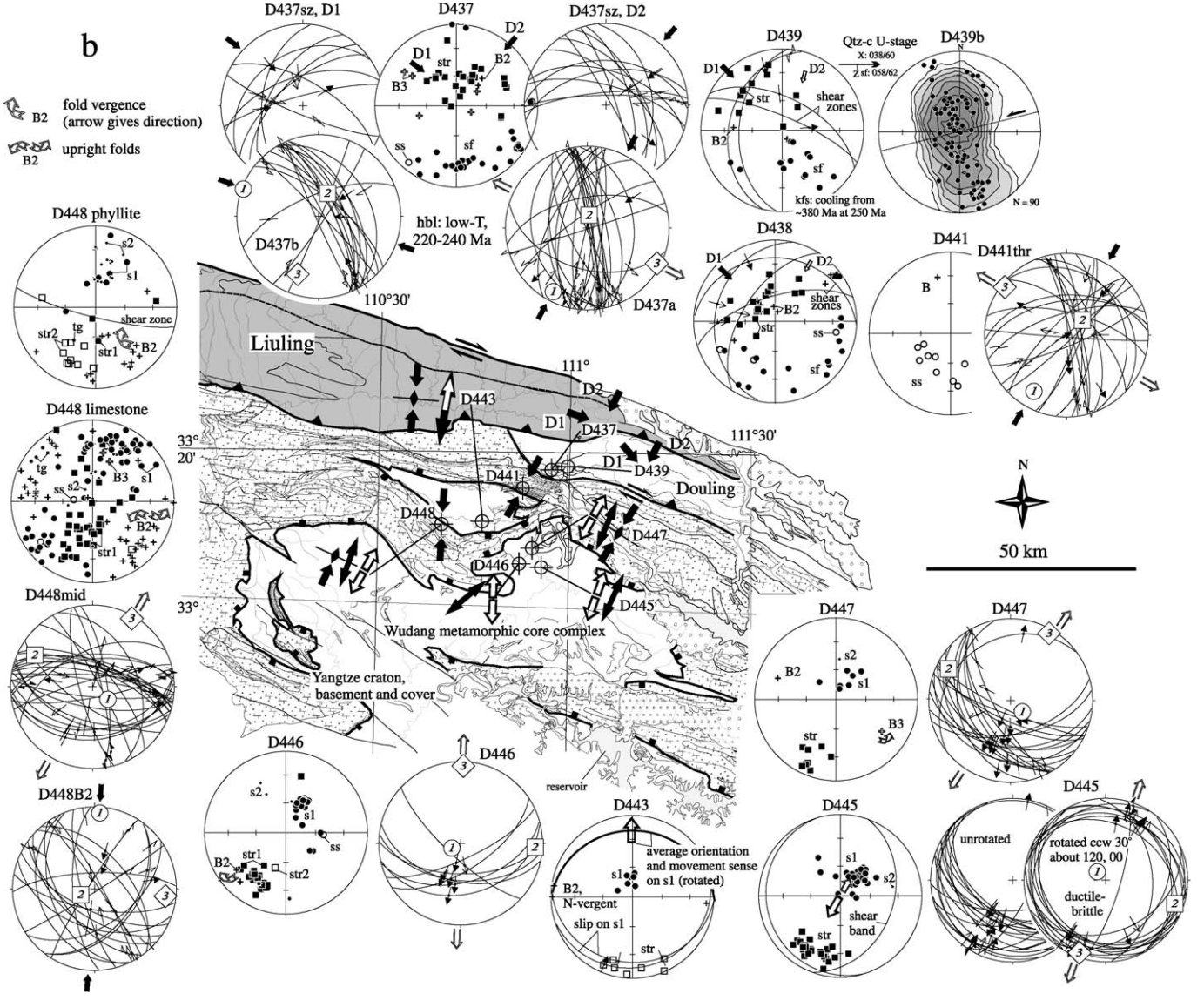

Fig. 7 (*continued*).

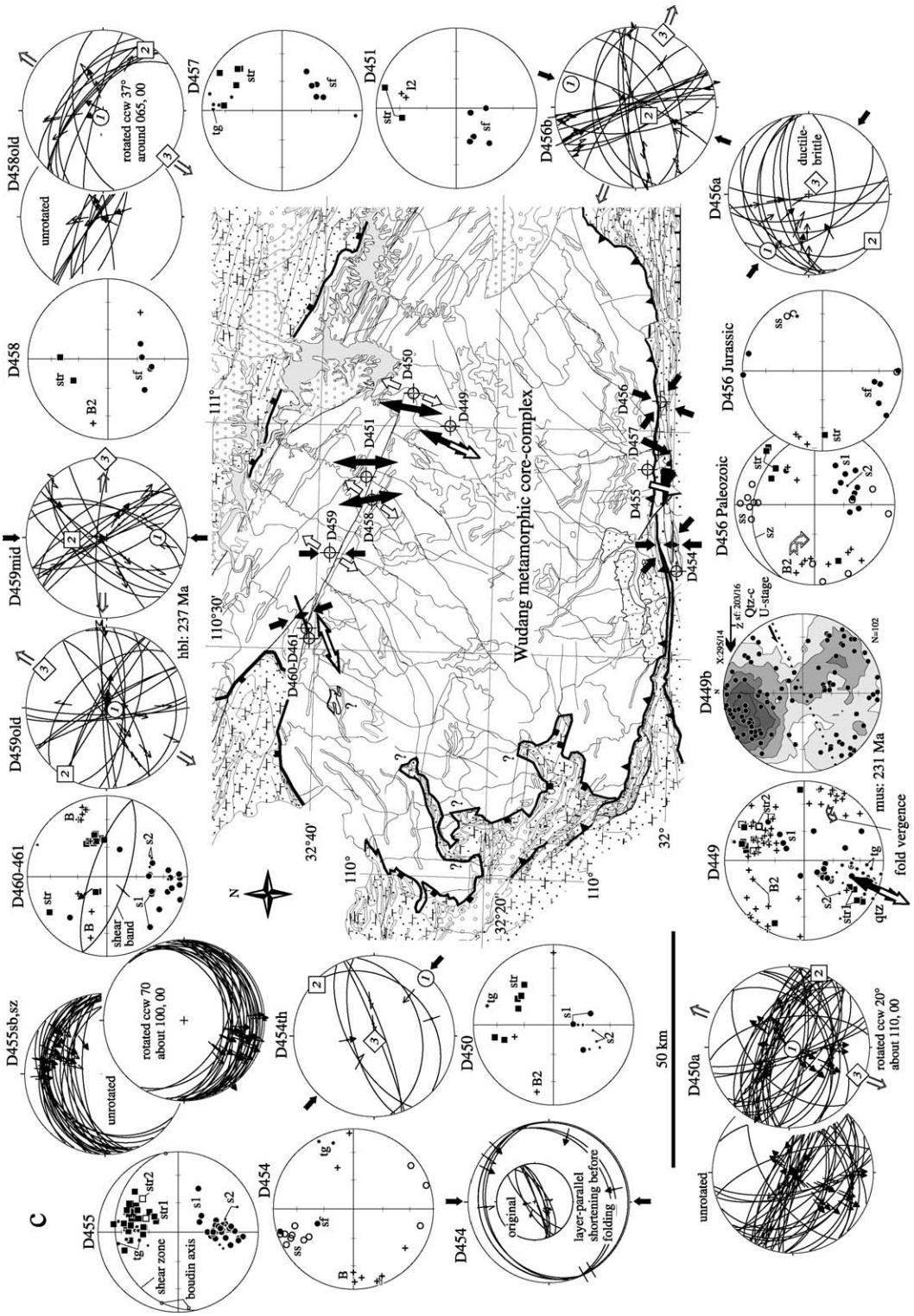

Fig. 7 (*continued*).

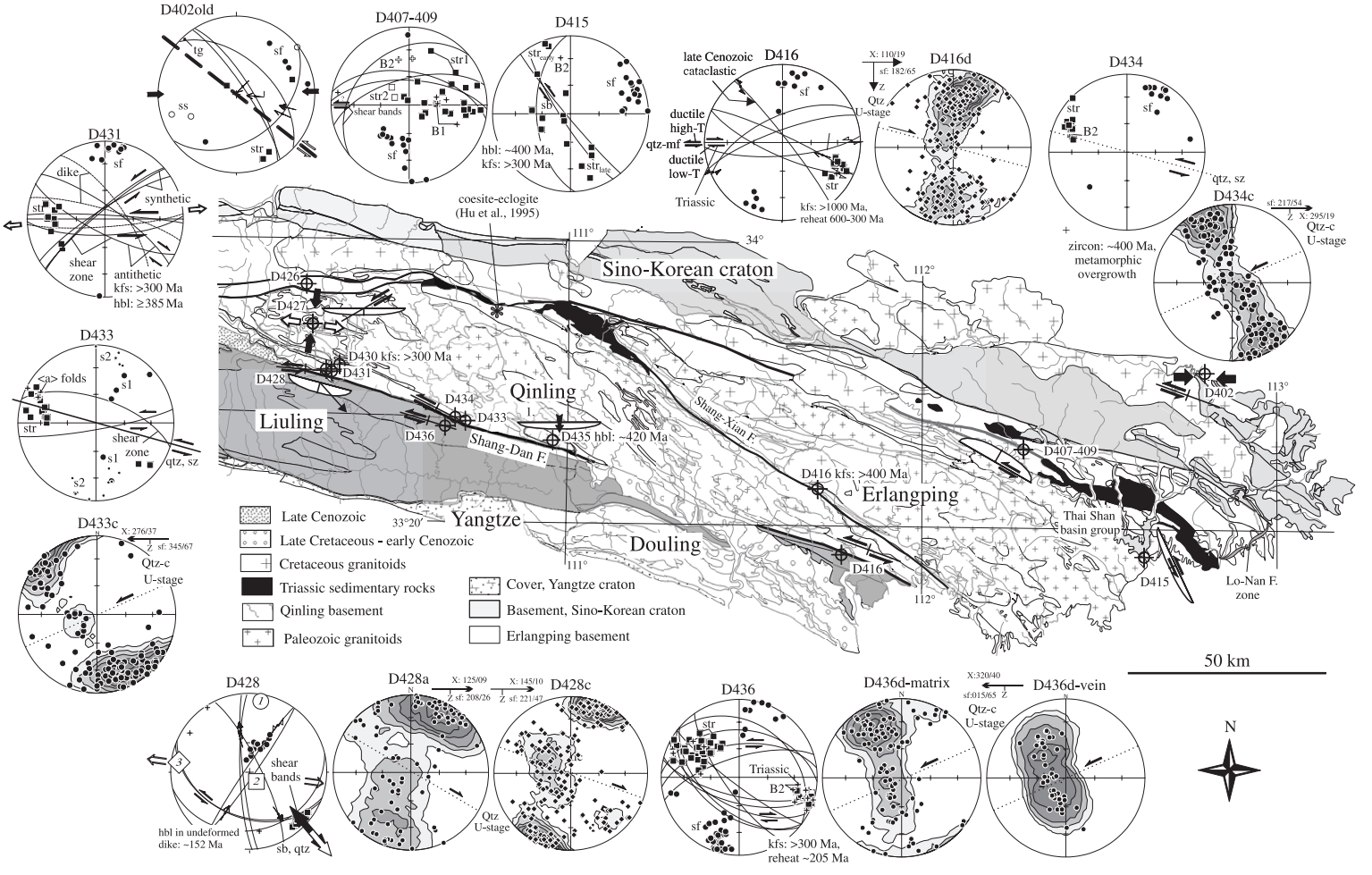

Fig. 8. Silurian–Devonian structural data from the eastern Qinling belt. See Fig. 5 for legend to the structural data and Fig. 6 for further structural and age explanations. (1) marks the Songshugou peridotite ophiolite; the structural interpretation is from Song et al. (1998).

°C). The sample reveals a spectacular age gradient from 1200 to 220 Ma. Models allowing reheating show a thermal spike at 300 °C between 600 and 300 Ma followed by cooling to 200 °C by 200 Ma. High-*T* mylonitisation along the Shang-Dan fault zone is thus older than ~ 300 Ma and the ductile–brittle to brittle faulting is Triassic. D436c, a quartz + potassium feldspar vein in a retrograde phyllitic gneiss (245–300 Ma muscovite and biotite ages, but see Section 3.1), indicates a thermal event at 205 ± 5 Ma. We infer that the sample was affected by reheating because of the older mica ages. D439 is from a quartz + potassium feldspar vein in mid- to low-*T* mylonitic Douling unit amphibolite (~ 800 Ma hornblende, sample D438). Modeling shows rapid cooling from ~ 380 °C at 250 Ma. In summary, the K-

Table 4
Location of stations and parameters of the deviatoric stress tensor: Cenozoic stress field

Site and set name	Lithology	Latitude	Longitude	Method	*n*	σ_1	σ_2	σ_3	*F*	*R*
D402y1[a]	dolomite, shale (?Cambrian)	33°47.351′	112°51.836′	NDA	13 13	187 74	039 14	307 08	19°	0.7
D402y2	dolomite, shale (?Cambrian)	33°47.351′	112°51.836′	NDA	15 15	055 06	255 84	145 02	15°	0.7
D403mid[a]	volcanics (?K)	33°42.673′	112°45.9.39′	NDA(45)	19 19	041 80	182 08	273 06	25°	0.8
D403you	volcanics (?K)	33°42.673′	112°45.9.39′	NDA	13 13	230 26	091 57	330 19	12°	0.5
D404	*granitoid (K) (sampleD405)*	33°39.156′	112°46.477′	PBT	07 07	239 02	149 09	318 81		
D406you	granitoid–marl (J)— red bed (K_2)	33°33.813′	112°15.218′	NDA	16 16	328 75	235 01	145 15	23°	0.9
D407-9b[a]	amphibolite–gneiss (Pt)—red bed (K_2)	33°33.532′	112°14.753′	NDA	08 08	188 12	315 71	094 15	12°	0.1
D410-2[a]	*low-T orthogneiss (?K)*	33°33 61′	112°28.531′	NDA	16 15	217 21	026 69	126 04	13°	0.8
D412b[b]	subvolcanic rocks (K)	33°29 373′	112°45.68′	PBT	16 16	157 74	282 09	192 01		
D413P[a]	limestone (Sinian), J_1 and K_2 sedimentary rocks	33°27.111′	112°44.557′	NDA	23 23	193 48	014 41	284 01	29°	0.7
D413N[b]	as D413K	33°27.111′	112°44.557′	NDA	8 8	324 84	146 08	056 00	16°	0.5
D413neo	as D413K	33°27.111′	112°44.557′	NDA(45)	20 20	229 06	327 54	135 36	25°	0.4
D415b[a]	*granitoid, orthogneiss (pre-300 Ma)*	33°21.02′	112°39.288′	NDA	17 17	223 10	010 78	132 06	25°	0.4
D425you	granitoid (K)	34°01.385′	110°14.316′	NDA	17 16	052 13	173 65	317 21	31°	0.9
D426n[a]	marble	33°54.106′	110°15.432′	NDA	16 16	164 18	038 03	308 04	13°	0.3
D426you	marble	33°54.106′	110°15.432′	NDA	06 06	042 02	309 45	134 45	19°	0.3
D429-30you(a)[b]	*granitoid (pre-300 Ma)*	33°42.5′	110°22.6′	PBT	06 06	075 09	268 80	359 00		
D429-30you(b)	*granitoid (pre-300 Ma)*	33°42.5′	110°22.6′	NDA	11 11	188 07	096 13	305 76	17°	0.2
D433b[b]	gneiss	33°34.597′	110°39.842′	NDA	08 08	124 64	296 26	028 03	16°	0.5
D436you	*phyllite, quartzite, micaschist (pre-300 Ma)*	33°32.743′	110°38.927′	NDA	20 20	230 12	034 78	140 03	23°	0.7
D448you(a)[b]	phyllite, limestone	33°08.323′	110°42.535′	NDA	34 34	094 17	243 71	001 09	21°	0.5
D448you(b)	phyllite, limestone	33°08.323′	110°42.535′	NDA	30 30	064 04	211 85	334 03	20°	0.5
D454b	limestone	32°00.351′	110°40.882′	NDA	06 06	241 16	028 71	148 10	20°	0.4
D456d	dolomite, conglomerate (J)	32°01.923′	111°03.492′	NDA	06 06	127 79	251 06	342 09	18°	0.5
D458un	basement (Wudang)	32°34.465′	110°50.541′	nc		~ 55				
D459you	*hyperbysal (Wudang) (T_2 heating)*	32°38.288′	110°42.743′	PBT	19 14	214 26	077 57	314 20		
D460b	basement (Wudang)	32°40.822′	110°31.284′	NDA	13 12	027 07	252 80	118 07	11°	0.5
D461mid[a]	basement (Wudang)	32°40.857′	110°31.316′	PBT	14 13	214 06	121 30	322 88		
D461a	basement (Wudang)	32°40.857′	110°31.316′	NDA	13 13	056 76	243 14	153 02	15°	0.3

For methods used to calculate stress tensors, see Appendix B; PBT, pressure–tension axes method; NDA, numeric dynamic analysis technique ((45) indicates usage of an angle of 45° instead of 30° for the orientation of σ_1 in respect to the fault plane); nc denotes qualitative interpretation. Italic lettering in the lithology column indicates available radiometric dating (see Tables 1 and 2). In the measurement column (*n*), first number is number of measurements, second is number of measurements used for calculation. For $\sigma_1 - \sigma_3$, azimuth (first number) and plunge (second number) of the principal stress axes are given. The stress ratio *R* is $(\sigma_2 - \sigma_3)(\sigma_1 - \sigma_3)^{-1}$ (where 1 is axial confined extension, 0 is axial confined compression). The fluctuation *F* gives the average angle between the measured slip and the orientation of the calculated theoretical shear stress. K, Cretaceous (K_2, Late Cretaceous); J, Jurassic (J_1, Early Jurassic); T, Triassic (T_2, Middle Triassic); Pt, Proterozoic.

[a] Paleogene stress field.

[b] Neogene stress field, all others Pliocene–Quaternary stress field.

feldspar data record a thermal event in the Late Cretaceous and earliest Tertiary as far south as the Shang-Dan fault zone and a Triassic event as far north as the Erlangping, overprinting rocks older than Carboniferous (probably the Devonian batholith) and late Proterozoic.

4. Deformation history

4.1. Overview

Silurian–Devonian ductile sinistral transpression established the major deformation zones of the Qinling. Triassic Sino-Korean–Yangtze craton collision caused dextral transpressive reactivation of existing shear zones in the consolidated Devonian block north of the Triassic suture in the Liuling complex, subhorizontal crustal extension within core complexes along the northern margin of the Yangtze craton, and N–S shortening by folding and thrusting throughout the belt. The Cretaceous faulting history started with NW–SE (trans)tension, coeval with Early Cretaceous crustal extension and sinistral transtension in Dabie. This was followed by regionally ubiquitous dextral wrenching during or after deposition of widespread Late Cretaceous (K_2) deposits. There were three successive Cenozoic stress fields, the most pervasive a Pliocene–Quaternary field with NW–SE extension and NE–SW compression.

Our structural data supporting this view are detailed in the following and summarized in Figs. 5–8 and

Table 5
Location of stations and parameters of the deviatoric stress tensor, cretaceous stress field

Site and set name	Lithology	Latitude	Longitude	Method	*n*	σ_1	σ_2	σ_3	*F*	*R*
D403old[a]	volcanics (Pt?), granite (K)	33°42.673′	112°45.939′	NDA	05 05	178 56	060 18	320 28	14°	0.5
D406old	subvolcanic (K?), J_1 and K_2 sedimentary rocks	33°33.813′	112°15.218′	NDA	19 18	147 10	030 69	240 19	27°	0.1
D407-409a	gneiss amphibolite	33°32′	112°15′	PBT	06 06	329 20	095 58	230 23		
D410-1	*low-T orthogneiss (?K)*	33°33.61′	112°28.531′	NDA	08 08	128 09	007 72	220 15	07°	0.5
D412a[a]	hyperbysal rocks	33°29.373′	112°45.68′	NDA	20 20	192 30	309 38	075 37	16°	0.3
D413K	limestone (Sinian), J_1 and K_2 sedimentary rocks	33°27.111′	112°44.557′	NDA	13 13	342 01	074 68	252 22	41°	0.4
D425old	*granite (J)*[b]	34°01.385′	110°14.316′	NDA	11 11	273 23	131 61	010 16	21°	0.7
D425mid	*granite (J)*[b]	34°01.385′	110°14.316′	NDA	17 17	166 11	054 62	262 26	16°	0.2
D426old[a]	marble, K_1 sedimentary rocks	33°54.106′	110°15.432′	NDA	08 08	084 26	333 38	199 41	09°	0.5
D426mid	as D426old	33°54.106′	110°15.432′	NDA	19 18	144 38	003 44	251 21	22°	0.6
D434	metaconglomerate, gneiss	33°34.521′	110°40.074′	NDA	09 09	172 28	269 14	023 58	10°	0.3
D436bc	*phyllite, quartzite, micaschist (pre-300 Ma)*	33°32.743′	110°38.927′	NDA	10 10	146 14	013 70	239 14	31°	0.6
D441you	limestone (Cambrian)	33°14.345′	110°51.854′	PBT	22 21	167 49	322 38	059 10		
D450b[a]	basement (Wudang)	32°30.19′	111°04.756′	NDA	26 25	201 44	001 44	101 10	16°	0.6
D451[a]	basement (Wudang)	32°34.761′	110°51.929′	PBT	32 28	211 51	021 39	112 00		
D452-453	quartzite, limestone	32°01′	110°42′	NDA	24 23	307 04	200 78	038 11	27°	0.6
D454a	limestone	32°00.351′	110°40.882′	NDA	22 18	148 04	260 80	057 10	17°	0.5
D455	basement (Wudang)	32°02.272′	110°54.856′	NDA	15 14	108 62	307 27	213 08	30°	0.7
D456c	dolomite, conglomerate (J)	32°01.923′	111°03.492′	NDA	19 19	328 14	180 73	060 09	15°	0.6
D457	basement (Wudang)	32°02.489′	110°57.854′	NDA	06 06	160 49	347 40	254 03	06°	0.5
D458you	basement (Wudang)	32°34.465′	110°50.541′	PBT	15 13	166 23	009 66	266 06		
D458yo2	basement (Wudang)	32°34.465′	110°50.541′	NDA	08 08	237 82	025 07	115 04	29°	0.7
D460a	basement (Wudang)	32°40.822′	110°31.284′	NDA	11 11	129 12	339 76	220 07	20°	0.5
D461old	basement (Wudang)	32°40.857′	110°31.316′	NDA	07 07	150 15	263 54	051 31	28°	0.5
D461b	basement (Wudang)	32°40.857′	110°31.316′	NDA	23 23	170 15	334 74	087 07	23°	0.5

See Table 4 for explanation.

[a] Early Cretaceous fault setting.

[b] Unpublished Chinese U/Pb zircon age of 168 Ma, no analytical data available.

Tables 4–6. In the field, we characterized the contacts of the main rock units along two traverses across the orogen by studying the relative amount of deformation, the sense of displacement or shear, and the pressures and temperatures of deformation. The amount of deformation was judged from the shape of deformed objects such as reduction spots, the thickness and spacing of deformed zones, and the degree of grain-size reduction. Sense of shear was established in the field and in thin section by means of criteria such as offset markers, σ and δ clasts, shear bands, asymmetric boudinage, schistosité–cisaillement (S–C) fabrics, and lattice-preferred orientation (texture) measurements of quartz. Our quartz texture interpretation is based on comparisons with textures from deformation zones where the path and temperature have been established by independent criteria, and from polycrystal-plasticity models and experimental data. To understand the kinematics of fault arrays, we applied "stress" inversion techniques to mesoscopic fault-slip data (Appendix B). We refer the reader to Passchier and Trouw (1996), Angelier (1994), and Twiss and Unruh (1998) for recent, comprehensive summaries and critical discussions of these structural methods.

4.2. Cenozoic

Although to a first approximation the existence, sense, and slip rates of Cenozoic strike–slip faults within the Qinling belt have been established (Peltzer et al., 1985; Bellier et al., 1988, 1991; Zhang et al., 1995, 1998, 1999), little is known about the regional

Table 6
Location of stations and parameters of the deviatoric stress tensor: Triassic stress field

Site and set name	Lithology	Latitude	Longitude	Method	n	σ_1	σ_2	σ_3	F	R
D415a[a]	*gneiss (~ 400 Ma)*	33°17.164′	112°36.846′	PBT	15/13	135 11	311 79	042 00		
D427[b]	*gneiss (~ 400 Ma)*	33°48.579′	110°15.976′	NDA	19/19	198 18	021 72	288 01	15°	0.5
D429-30[a]	volcanics-shale	33°42.5′	110°22.6′	NDA	8/8	313 06	116 83	223 02	26°	0.6
D433a[b]	gneiss	33°34.597′	110°39.842′	NDA	15/14	205 06	112 23	308 67	7°	0.2
D436a[b]	*phyllite, quartzite, micaschist (>300 Ma)*	33°32.743′	110°38.927′	NDA	23/22	357 04	121 84	267 05	15°	0.5
D437a[b]	*marble, amphibolite, schist (~ 935 Ma)*	33°18.937′	110°54.734′	NDA	28/27	208 12	008 77	117 04	22°	0.5
D437b[a]	*marble, amphibolite, schist*	33°18.937′	110°54.734′	NDA	17/16	290 01	021 65	200 25	21°	0.5
D441thr[b]	limestone (Cambrian)	33°14.345′	110°51.854′	NDA	21/20	210 14	038 76	301 02	26°	0.5
D445-rotated[c]	basement (Wudang), dolomite (cover)	33°05.892′	110°56.117′	NDA	20/20	314 78	109 11	200 05	12°	0.4
D446[c]	basement (Wudang), dolomite (cover)	33°06.006′	110°53.494′	NDA	08/08	242 80	093 09	002 05	13°	0.5
D447[c]	phyllite, metavolcanic (Yaolinghe)	33°06.842′	110°54.739′	PBT	23/23	146 73	297 15	030 10		
D448mid[c]	phyllite, limestone	33°08.323′	110°42.535′	NDA	30/29	129 70	299 20	030 03	17°	0.7
D448B2[b]	phyllite, limestone	33°08.323′	110°42.535′	NDA	21/21	004 07	246 75	096 13	25°	0.5
D450a-rotated[c]	basement (Wudang)	32°30.19′	111°04.756′	PBT	38/38	208 86	112 00	202 08		
D454[b]	limestone	32°00.351′	110°40.882′	nc	06/06	000 00				
D454th[b]	limestone	32°00.351′	110°40.882′	NDA	06/06	132 03	042 04	261 85	21°	0.3
D456a[a]	dolomite, conglomerate (J)	32°01.923′	111°03.492′	NDA	13/12	306 14	216 01	122 76	18°	0.5
D456b[b]	dolomite, conglomerate (J)	32°01.923′	111°03.492′	NDA	21/20	020 15	211 74	111 03	20°	0.4
D458old-rotated[c]	basement (Wudang)	32°34.465′	110°50.541′	NDA	10/10	313 82	125 08	215 01	11°	0.5
D459old[a]	*hyperbysal (Wudang) (heating ~ 235 Ma)*	32°38.288′	110°42.743′	NDA	18/18	191 81	302 03	032 09	24°	0.6
D459mid[b]	*hyperbysal (Wudang)*	32°38.288′	110°42.743′	NDA	18/16	180 36	356 54	089 02	27°	0.6

See Table 4 for explanation.
[a] Strike–slip setting (orogenic interior).
[b] Thrust setting (fold-thrust belt).
[c] Normal fault setting (core-complex formation).

distribution of Tertiary and Quaternary faulting and associated regional stress fields. In the course of our fieldwork on the Mesozoic orogeny, we collected microtectonic data to determine the extent to which the Paleozoic–Mesozoic Qinling was reactivated during the Cenozoic.

Geomorphologic features, historic seismicity (e.g., Ma, 1986) in the vicinity of faults traceable in the field, and zones of weakly consolidated cataclastic rocks affecting Late Cretaceous and Cenozoic rocks demonstrate that the entire Qinling was reactivated during the Cenozoic (Fig. 5). On the basis of observations from 16 stations, we obtained regionally consistent σ_1 and σ_3 trends of $047 \pm 15°$ and $141 \pm 11°$ (Table 4), respectively, for the latest Cenozoic deformation; this stress field affected Neogene deposits along the Shang-Dan (e.g., Shangxian basin group, Fig. 5c) and Lo-Nan faults (Lonan basin, Fig. 5c) and is associated with active deformation along the Lo-Nan, Shang-Xian, Shang-Dan, and Shan-Yan faults (Fig. 5b,c). For example, the Cenozoic Lo-Nan fault constitutes a broad zone of cataclasites with scarps and clay gouge at the Zhan-Ping-Tai reservoir (Fig. 5c, stations D402, D403). The Shang-Dan fault shows an up to 100-m-wide exposure of cataclasite including clay gouge in easternmost Shaanxi, where the Shangxian basin sediments, if interpreted as strike–slip related basins, demonstrate Neogene activity and a few tens of kilometers of syn- to post-Neogene offset (Fig. 5c, stations D429-430(b), D436). Arrays of NE-trending, dextral to dextral transtensional faults, conjugate with a few regionally prominent, ESE-trending, sinistral faults (Gonglu and Wudang faults), characterize the Wudang basement dome (Fig. 5b).

Both the Lo-Nan and the Shang-Dan faults record older Cenozoic normal faulting; σ_3 trends $\sim 019°$ (five stations, e.g., D429-430(a), D433b; Fig. 5c, Table 4). These faults are also present in the Neogene Shangxian basin sediments and are thus Neogene or younger. Eight stations along the Lo-Nan, Shang-Xian, and Gonglu faults (Fig. 5, Table 4) record an even older stress field ($\sigma_1 = 020 \pm 20°$, $\sigma_3 = 115 \pm 16°$); related faults, commonly mineralized, overprint fault sets loosely constrained as K_2 (see below). The width of Eocene half-graben basins (lengthening estimated from a planar fault—triangular half-graben model, e.g., Brun and Choukroune, 1983) and the disruption of pre-Cenozoic markers suggest ≥ 25 km offset along the Lo-Nan fault alone (Fig. 5c).

4.3. Cretaceous

Late Cretaceous–Paleogene (K_2–E) sedimentary basins, shear/fault zones, and principal stress orientations calculated from homogeneous, single-outcrop fault-striae sets are shown in Fig. 6 (Table 5). The deformation history started with local ductile flow with NE–SW shortening and NW–SE stretching. Coeval brittle–ductile to brittle faulting depicts similar compression and extension directions; three of the five stations show a clockwise change in time in the orientation of the sub-horizontal principal extension direction (σ_3). Along the Lo-Nan fault (stations D403, D404, D410, D412, D426, Fig. 6a), deformation related to this early event is associated with quartz + biotite + chlorite growth on fault planes, local low-T quartz ductility (250–300 °C) along faults, and cooling of probable Cretaceous granitoids through ~ 300–100 °C at 112–103 Ma (D405, Table 2) and through >400–280 °C at ~ 85–73 Ma (D410, Table 2); ductile deformation in these granitoids, also indicating NE–SW shortening associated with NW–SE stretching (stations D404, D410), may have occurred earlier in the Cretaceous.

Younger faults are regionally ubiquitous, have σ_1 and σ_3 trends of $146 \pm 21°$ and $058 \pm 24°$, respectively (20 stations), and are associated with deformation along the Lo-Nan, Shang-Xian, Shang-Dan, Liangyong, Gonglu, and Wudang faults (Fig. 6a,b); the widespread K_2–E deposits of the Qinling are associated with these fault zones. Along the Lo-Nan fault, we studied profiles incorporating probable Cretaceous granite and Lower Jurassic (J_1) and Upper Cretaceous (K_2) sedimentary rocks (basins north of Thai Shan; stations D406 and D413). At D406, both foliation and bedding are vertical and lower-greenschist facies metamorphism accompanied dextral transpressive faulting in the granite. Dextral strike–slip faulting following the earlier NW–SE extension (see above) affected a probable Cretaceous orthogneiss (D410) north of the Thai Shan basin group and the main strand of the Lo-Nan fault. K-feldspar thermochronology (D410) shows slow cooling at 280–260 °C from 73 to 63 Ma consistent with K_2 sedimentation along the fault. At a similar structural

position, brittlely deformed sub-volcanic rocks at D412 demonstrate clockwise rotation of sub-horizontal σ_1 and σ_3. Stations D413 and D425, ~250 km apart along the Lo-Nan fault, reveal complex post-J_1 (deformed granitoid) and syn-K_2 (basin formation) faulting indicating clockwise rotation of σ_3. The Shang-Xian fault zone, little studied by us, is dextral, and is associated with several K_2–E basins; faulting accompanied cooling from ~300 to 100 °C at 101–75 Ma (biotite in granitoid at D419, K-feldspar in greenschist-facies andesite of D418). The Shang-Dan fault was a dextral strike–slip fault (stations D434, D436) in the Late Cretaceous as indicated by the shape and distribution of sedimentary basins, particularly the Xixian basin (Fig. 6a, see also Mattauer et al., 1985). K_2–E basins (e.g., Yunxi, Din-Jan, Fangxian, Fig. 6b) along the Liangyong, Gonglu, and Wudang fault zones are interpreted as pull-aparts related to dextral slip. From these basins alone, cumulative strike–slip displacement of a few tens of kilometers is evident (Fig. 6b). The Cambrian strata mantling the NW margin of the Wudang basement complex is offset at least 15 km dextrally along the Gonglu fault (Fig. 6b). Several of the stations studied in the Wudang area record the clockwise rotation of σ_3 typical of the Cretaceous deformation. The Jurassic Wudang thrust (see later) was reactivated during the K_2–E and is a sub-vertical dextral strike–slip fault southeast of the Fangxian basin (station D452–D457, Fig. 6b); temperatures during faulting reached ≥150 °C as estimated from ductile flow of calcite (type II twinning, Burkhard, 1993).

4.4. Triassic–Jurassic

Much of the Yangtze and Sino-Korean cratons shown in Fig. 2 have WNW-trending folds and craton-directed thrusts of millimeter to kilometer scale (Mattauer et al., 1985; R.G.S. Henan, 1989; R.G.S. Shaanxi, 1989; R.G.S. Hubei, 1990). For example, the basement and cover of the Yangtze craton were imbricated along south-directed thrust faults in the Wudang Mountain area (Fig. 2) in mid-Triassic or younger time (Huang, 1993). Triassic sandstones and slates show greenschist-facies metamorphism that was likely coeval with formation of the fold-thrust belt (You et al., 1993). On the Sino-Korean craton, the north-directed Lu Shan thrust, placing crystalline basement over Paleozoic cover was active in the Middle Triassic and Late Jurassic (Huang and Wu, 1992). Huang and Wu (1992) also suggested that the Qinling unit was thrust over the Erlangping, Danfeng and Liuling units. They correlate the Kuanping unit with the Qinling unit and identify a series of Mesozoic (first stage: Middle Triassic; second stage Late Triassic–Cretaceous) south-directed thrusts imbricating the Luanchuan (a part of the Sino-Korean basement and cover north of Kuanping), Kuanping, Qinling, Erlangping-Danfeng, Liuling, and Douling units, the Yangtze cover, and the Wudang basement and cover.

Here we present structural and age data for some of the major fault zones in the Qinling area, proceeding from north to south (Fig. 7). Late Triassic to Early Jurassic (T_2–J_1) volcanogenic sandstone, shale, and coal along the Lo-Nan fault zone (e.g., Thai Shan basin group) are openly folded and show low-grade metamorphism. Brittle–ductile faulting at station D415 (gneiss metamorphosed at ~400 Ma; Table 2) occurred with chlorite + epidote + calcite + quartz + hematite + limonite mineralization on the fault planes, probably during reheating to ~400–200 °C at 220–200 Ma (K-feldspar, D415a, Table 2). The Shang-Xian fault zone is dextral transtensive within partly mylonitic, intermediate volcanic rocks at station D418; the quartz texture indicates upper greenschist-facies flow. The Shang-Dan fault zone shows greenschist-grade Triassic dextral transpressive and contractional overprinting of high-grade Devonian sinistral shearing (see below). At station D416, tight to isoclinal, post-mylonitic folding and dextral shearing (e.g., low-*T* quartz texture, D416c) is dated at ~200 Ma (cooling to ~200 °C, K-feldspar, Table 2). Song et al. (1998) reported dextral low-grade shearing along the boundaries of the Songshugou peridotite, just north of the Shang-Dan fault. A gneissic to partly mylonitic ductile fabric with chlorite-coated shear bands is followed in kinematic continuity by a ductile–brittle and cataclastic fault fabric at stations D429-430; both fabrics are low-*T*, indicate dextral slip, and overprint a ~400 Ma (unpublished Chinese U/Pb zircon age) granitoid. A granitic dike affected by the low-*T* fabric experienced cooling from 300 to 180 °C between 270 and 240 Ma, after which the rock stayed at ~180 °C until ~190 Ma (D430b, K-feldspar, Table 2). Eastward along the fault zone (station D433), ductile–brittle faults and

small-scale shear zones and shear bands accompany a vertical, second foliation, all indicating top-NNE thrusting. Similarly, along the northern edge of the Liuling unit at station D436, mostly phyllitic quartzite, micaschists, hornblende + garnet + plagioclase quartzose gneisses and felsic metavolcanic rocks reveal a steep fabric caused by E–W-trending folds. The mica ages from this station are difficult to interpret (see above), but the muscovite plateau age of ~ 247 Ma and the evidence from K-feldspar of a 205 ± 5 Ma thermal event imply that folding and faulting at stations D433 and D436 were Triassic; the ~ N–S shortening is commonly accommodated by vertical and horizontal, E–W, stretching (boudinage).

The Liuling unit is structurally complex and its internal structural geometry has not been resolved; detailed structural analysis is also hampered by the monotonous, generally phyllitic lithology. The northern part of the Liuling unit (e.g., station D433) likely is part of the Qinling unit; it contains mylonitic K-feldspar + plagioclase augen gneiss, garnet + biotite ± hornblende gneiss with intercalations of amphibole- and quartz-rich layers (bimodal volcanic rocks), and metaconglomerate (station D434). The remainder of the Liuling unit we studied (southern stretches of profile represented by station D436) is mostly phyllitic quartzite, micaschists, and hornblende + garnet + plagioclase gneissic quartzites and felsic volcaniclastic rocks, resembling the Fuziling unit of Dabie and the Nanwan unit of Hong'an. Deformation in this phyllitic unit is characterized by ~ N–S shortening, commonly accommodated by vertical and horizontal, E–W stretching.

The Douling unit encompasses granitoid gneiss, bimodal to acid metavolcanic rocks, amphibolite, marble and dolomite, and calcschists at the stations we have studied (D437–D439); overall these rocks are similar to the passive margin of the Yangtze craton and equivalent to the Huwan and Luzhenguang units of Hong'an–Dabie. At stations D437 and D439, low-temperature (greenschist) mylonites in calcite marbles, calcschists, and quartz-rich acid metavolcanic rocks represent a top-SE (dextral transpressive) major shear zone with asymmetric boudinage at the m–dm scale and phyllitic S–C fabrics with ribbon quartz and dynamic recrystallization at ~ 300 °C. Late-stage shear is associated with folding (B2 in the structural plots, Fig. 7b), partly indicating extreme shortening. A second deformation with top-SW (sinistral transpression) brittle–ductile shear-fault zones with late folding (B3) indicates bulk N(E)–S(W) shortening with S(W) vergence, probably related to folding in the Liuling unit and the Yangtze craton. The accompanying low-grade metamorphism indicates that this ductile to ductile–brittle shearing and faulting is Triassic; at D437 (Table 2) the early high K/Ca steps of a hornblende $^{40}Ar/^{39}Ar$ spectrum imply a 220- to 240-Ma thermal event and K-feldspar in hornblende + plagioclase + K-feldspar segregation veins (D439) records rapid cooling from ~ 380 °C at 250 Ma. These stations detail the "Douling thrust" of Huang and Wu (1992). These 250–220 Ma ages represent relatively early stages of the thermal evolution of the Triassic Qinling–Dabie belt (compare the ages compiled in Fig. 2 and Hacker et al., 2000) and date overall top-S imbrication with a change from NW–SE (dextral transpression) to NE–SW shortening.

A foreland fold-thrust belt overprinting an extensional core complex characterizes the Triassic structure of the northern Yangtze craton cover and basement; in the following, we report data from the Wudang area ("Wudang core complex"). Strong regional refolding (Fig. 2), commonly leading to apparent thrusting along original normal faults, has hindered the recognition of the extensional nature of this basement dome (Fig. 7b,c). Stations D443 to D448 record basement deformation and extensional detachment contacts at the northern margin of the Wudang core complex. The footwall comprises blueschist–greenschist-facies acid to basic metavolcanic and metasedimentary rocks of the Yaolinghe complex; Sinian marbles (mostly dolomite) form the hanging wall. At station D443, in the center of the small basement dome at the northern margin of the core complex, a relic, complex and unresolved deformation is overprinted by a penetrative, sub-horizontal first foliation (s_1) related to top-N normal faulting and second deformation folding (D_2). At stations D445–D447, all deformation postdated blueschist-facies metamorphism. The stretching direction of the first deformation (D_1), as portrayed by the mineral lineation and elongated vesicles in metavolcanic rocks, changed in a clockwise sense during progressive deformation. The mostly greenschist-grade footwall is strongly ductilely deformed with intrafolial isoclinal folds. Deformation in the basement is generally

pure shear sub-horizontal stretching from ductile flow to ductile–brittle faulting (e.g., symmetric boudinage and clasts, conjugate shear bands–shear zones and fault sets), but locally has clear non-coaxial fabrics (e.g., asymmetric boudinage) with top-S normal fault geometry. Outcrop-scale faulting at these stations along the northern margin of the Wudang basement dome is mostly top-S, possibly reflecting antithetic slip to a synthetic master detachment with top-N displacement. Folds (B_2) at station D447 are mostly isoclinal and cut by late-stage ductile–brittle normal faults; these folds and the associated sub-horizontal foliation probably originated under sub-vertical shortening. Late, large-scale kink folds (B_3) verge NNE and indicate late shortening. At station D448, the detachment contact (Cambrian limestone against blueschist–greenschist-grade phyllite and acid metavolcanic rocks) is a steeply S-dipping shear/fault zone with a clear metamorphic hiatus between the blueschist–greenschist footwall and the weakly metamorphic hanging wall. An early deformation is complex and multiphase and not resolved in detail. The first resolvable deformation is syn- to post-blueschist-facies metamorphism, shows extreme boudinage, is mylonitic in part, and contains isoclinal folds in phyllite and limestone. As at station D447, there are multiple sub-horizontal stretching events, indicated by multiple, initially probably sub-horizontal foliations (s_2 is always less steeply dipping than s_1) and normal faults interfering with WNW-trending folds. The late faulting (D448B2 in Fig. 7b) is related to the widespread regional folding. Stations D449–D451 and D458–D461 portray structural geometry, kinematics, and deformation–metamorphism relationships in the generally bimodal metavolcanic basement rocks of the north–central part of the Wudang core complex (Fig. 7c). At station D449, there is a clear kinematic continuity of all structures: s_1 carries greenschist-facies minerals and records sub-horizontal stretching; s_2, a crenulation, is associated with B_2 folds that have an extreme orientation range—tight folds are closer to the stretching direction (NE trending) than open folds. This complex fold pattern probably includes early folds related to sub-horizontal stretching and later folds related to sub-vertical stretching. A third deformation, containing tension gashes and a few faults, postdates WNW-trending B_2 folds, indicating renewed sub-horizontal NNW–SSE stretching. Muscovite from a blueschist at station D449 shows a loss profile from 232 Ma down toward ~150 Ma (Fig. 4a, Table 2), indicating crustal extension before or at ~232 Ma. At D450, calcite + quartz + chlorite-coated faults show sub-horizontal extension that is a progressive kinematic extension of the ductile deformation. Stations D458–D461 comprise typical greenschist-facies metasedimentary and metavolcanic basement. D458 is a good example of the rotation (around mean fold axis (B_2) into sub-horizontal s_1 position), we applied to the ductile–brittle fault pattern (Fig. 7c), which results in interpretable structures that indicate sub-horizontal extension. Throughout the studied area, folding followed extension. At station D459, the extensional deformation is well constrained at 236.6 ± 0.6 Ma by a hornblende spectrum with minor low-T loss. Stations D455 and D457 typify the Wudang core complex structures at its southern margin. The basement is phyllitic to massive quartzose metavolcanic rock. At D455, we have rotated the ubiquitous shear zones and associated shear bands such that s_1 is sub-horizontal, resulting in a sub-horizontal extensional deformation geometry with non-coaxial top-SSE flow; this fits the widespread, pervasive boudinage within s_1. The Cretaceous fault set (see above), indicating NE–SW dextral transtension, does not need to be rotated, indicating that the major folding is pre-Cretaceous. All deformation is late in the metamorphic history, and related to greenschist-facies retrogression.

Stations D441, D454, and D456 characterize the Triassic foreland fold-thrust belt deformation. D441 records folding and top-S thrusting in Cambrian limestone just north of the Wudang core complex (Fig. 7b) and D454 records deformation in the same stratigraphic unit south of the core complex (Fig. 7c); at the latter station, ductile–brittle, layer-parallel shortening was followed by fold buckling and thrusting. Station D456 typifies the Triassic–Jurassic Wudang thrust area, which involves Paleozoic to Jurassic strata. The Lower Jurassic (J_1) rocks are coarse, partly angular alluvial fan conglomerate and sedimentary breccia with ≤ 20 cm cobbles consisting of the metavolcanic basement of the Wudang core complex to the north and Paleozoic limestones and sandstones of the fold-thrust belt cover series. Thus, the core complex basement was already exposed in the Early

Jurassic. Lower Jurassic meta-sandstones lie locally on karstified Cambrian dolomite, testifying to a sedimentary hiatus probably related to Triassic–Jurassic orogeny. S-vergent folding and top-S thrusting is a kinematic continuation of top-SE thrusting of Paleozoic rocks over J_1 rocks. The J_1 rocks are low grade and foliated, but show a clear metamorphic break from the greenschist basement; deformation was accompanied by a phyllitic, anastomosing shear fabric and S-vergent tight to isoclinal folds up to 0.5 m in size. The folding clearly predated dextral strike–slip related to K_2–E basin formation; deformation is thus bracketed between J_1 and K_2.

In summary, the deformation sequence in the Wudang Shan basement massif area encompassed initial relic, unresolved deformation, then sub-horizontal crustal extension within the basement and the basement-cover contact zone, continued with folding and thrusting affecting the basement and the Paleozoic cover sequence, and terminated with folding and faulting incorporating Lower Jurassic deposits, which were subjected to low-grade metamorphism during the propagating deformation. Crustal thinning during the early deformation is demonstrated by original sub-vertical shortening and sub-horizontal stretching associated with prevailing coaxial deformation, excision of parts of the stratigraphic sequence, and deformation associated with condensed Triassic isograds (weakly metamorphosed sedimentary rocks on blueschist–greenschist basement). The Lower Jurassic sedimentary rocks are typical syn-tectonic molasse. From the observation that crustal extension started under at least transitional blueschist–greenschist conditions and proceeded to brittle conditions along the same detachment zone, we estimate that up to 20 km of crustal thinning may have occurred during the formation of the metamorphic core complex. Taking ≥ 230 Ma as a likely age of the HP metamorphism and recognizing that basement similar to that exposed today occurs in J_1 ($\sim$ 200 Ma) deposits, yields an exhumation rate of ≥ 0.6 mm/year.

4.5. Silurian–Devonian

Here we report structural and age data on Silurian–Devonian deformation along several of the fault zones in the Qinling to better understand the Triassic and younger overprint (Fig. 8). It was in the Silurian–Devonian when several of the crustal-scale deformation zones were established as sinistral transpressive wrench zones.

We studied post-Cambrian to pre-Cretaceous, probably Silurian–Devonian, ductile deformation in the Sino-Korean craton at station D402. Reduction spots in greenschist-grade Cambrian shale, intercalated with dolomite, yielded a plane strain deformation ($X/Y/Z = 11.5{:}3.1{:}0.84$, Lodes parameter $= -0.004$, strain intensity factor $= 1.85$) within a ductile shear zone striking $\sim 140°$; deformation is characterized by nearly vertical stretching with a sinistral strike–slip component, which is also reflected in the local brittle–ductile fault pattern.

Stations D407–409 and D415 (Fig. 8) characterize the pre-Triassic Lo-Nan fault zone. At stations D407–409, greenschist- to amphibolite-facies micaschist in mylonitic amphibolite show strong deformation during retrogression. T_3–J_1 rocks cover the deformation zone (Fig. 8). Ductile shear bands indicate sinistral transpression along the NNE-dipping foliation. A first folding was isoclinal with axes parallel to the mineral stretching lineation, a second folding accompanied late-stage sinistral shear, and late faults also record top-WSW sinistral transpression. The monzogranitic gneiss at station D415 is cut by an undeformed aplitic dike with >300 Ma K-feldspar and is intercalated with mylonitic diorite with a hornblende age of $\sim$ 402 Ma, and a crystallization depth of ≥ 5 kbar (Al-in-hornblende barometry, plus magmatic epidote). Surrounding homogeneously deformed quartz + biotite mylonitic gneisses show extremely high strain, isoclinal folds, asymmetric boudinage, and high-T deformation with weak post-deformational quartz annealing, all in a sinistral transpressive setting; the mineral stretching lineation is strongly variable in orientation. High-temperature Lo-Nan fault sinistral shear is thus Early Devonian ($\sim$ 400 Ma).

In orthogneiss and marble of the Qinling unit at station D427, ductile, probably also sinistral transpressive flow (see foliation and lineation orientations plotted with the Triassic fault pattern in Fig. 7a) is constrained by a hornblende spectrum which shows a loss profile from 395 to 380 Ma; the outcrop is cut by a late, undeformed granitic dike with a K-feldspar age >300 Ma. The contact of the Erlangping unit with the Qinling unit is locally a carbonate-matrix "mélange";

near this contact, sillimanite–garnet gneisses of the Qinling unit are retrogressed to andalusite (You et al., 1993). At station D426, the only locality where we studied this unit, the marble is coarse grained and foliated, but not mylonitic. Deformation of the Qinling and Erlangping units is thus older than 300 Ma and most likely $\geq$390 Ma.

The present contact between the Qinling and Liuling units is the brittle and brittle–ductile Shang-Dan fault zone (see Triassic, Cretaceous and Cenozoic deformation structures), which overprints a spectacular earlier ductile shear zone. Mineral stretching lineations and associated fabrics indicate an early sinistral displacement and even earlier dip-slip movement (Zhang et al., 1989). Sillimanite + orthoclase gneisses in the Qinling unit are retrogressed to andalusite approaching the shear zone (Hu et al., 1993); this decrease is compatible with south-directed thrusting. We studied this complex fault zone at five localities encompassing $\sim$130 km along strike. At station D416a, strongly deformed amphibolites are intercalated with low-*T* quartz mylonites with rounded feldspar in a fine-grained matrix, and $\leq$30 cm marble layers; ultramylonite is restricted to felsic layers. The first deformation, D_1, shows dynamically recrystallized high-*T* fabrics in amphibolite, with plagioclase partially recrystallized in porphyroclast strain shadows and sinistral shear. Quartz-rich lithologies show syn- to post-tectonic quartz grain growth in ultramylonite with probable sinistral shear. The quartz texture (D416c) indicates high-*T* sinistral shear. At this station, the age of the deformation is poorly constrained; K-feldspar dating suggests a >1000-Ma protolith that experienced reheating between 600 and 300 Ma. Station D428a from the northernmost part of the Liuling unit, which is different from the typical quartzose-phyllitic part (see above), has marble, ortho- (acid metavolcanic) and paragneiss, some mylonitic amphibolite, and mylonitic to ultramylonitic quartzofeldspathic gneiss with K-feldspar clasts. D_1 was followed by grain growth in quartz within fine-grained mylonite layers ($\leq$1.5 cm thick) and is characterized by isoclinal, possibly sheath folds. Plagioclase recrystallized in strain shadows behind porphyroclasts. The shear sense for the high-*T* deformation history is sinistral from shear bands and quartz textures. Quartz mylonites show late dynamic recrystallization at $\sim$300°C at very high strain. All ductile to ductile–brittle deformation predated a Late Jurassic–Early Cretaceous dike (D428d, Table 2). Station D433, again in the northernmost part of the Liuling unit, has biotite $\pm$ garnet gneiss and schists, acid metavolcanic rocks with amphibolite boudins, and locally up to 10-cm-thick ultramylonite. A sub-vertical foliation, sub-horizontal mineral stretching lineation and isoclinal, lineation-parallel <a> folds outline a sinistral transpressive shear zone (e.g., quartz U-stage texture) with strong E–W stretching. The Songshugou peridotite/eclogite, just north of the Shang-Dan fault zone, shows top-S motion (Mattauer et al., 1985; Song et al., 1998); Ar isotopic ratios from a hornblende from an amphibolitized eclogite tentatively suggest 420 $\pm$ 30 Ma reheating (D435, Table 2). Sinistral transpressive shear along the Shang-Dan fault zone is relatively well dated at station D431; hornblende in amphibolite of the Danfeng unit shows a serially increasing spectrum suggesting initial closure at $\geq$385 Ma and reheating at $\sim$330 Ma. A K-feldspar from the amphibolite is >300 Ma (D430). This unit is intruded by K-feldspar-rich granitoids younger than the foliation in the Danfeng amphibolite. Garnet + carbonate layers exhibit superplastic cataclastic flow and late-stage shear zones have biotite + chlorite. The structural geometry is typical of the early history of the Shan-Dan fault zone, with sinistral synthetic shear bands and large-scale boudinage due to E–W stretching. At station D436, within the northern part of the Liuling unit, mostly phyllitic quartzite, micaschist, and hornblende + garnet + plagioclase gneissic quartzites reveal an early fabric with a relic hornblende + plagioclase + kyanite fabric that is higher in grade than the phyllitic, Triassic overprint. Early shear zones indicate strong E–W stretching with boudinage; sinistral shear zones are synthetic (e.g., quartz U-stage texture). All high-grade deformation at this station was pre-300 Ma (K-feldspar and mica ages) and is probably best dated by the metamorphic overgrowths ($\sim$400 Ma) on zircons from the partly mylonitic conglomerate near Danfeng (Table 3); this station (D434a) shows post-deformation annealing that blurs early high-*T* sinistral shear. Taken together, structural and age data indicate that the Shan-Dan fault zone, the most spectacular fault of the Qinling, was a sinistral transpressive mylonite zone active in the early Devonian ($\sim$400 Ma).

5. Discussion

5.1. Cenozoic faulting: interaction between Pacific subduction and India–Asia collision

Peltzer et al. (1985) proposed sinistral, Tertiary slip of >100 km on the Lo-Nan and Shang-Dan faults of the Qinling area (Fig. 5c), whereas Huang and Wu (1992) favored tens of kilometers of displacement on the same faults since the Late Cretaceous; we established ≥25 km of Cenozoic displacement along the Lo-Nan fault alone. The timing of Tertiary displacements on a regional scale is poorly constrained. Studies of Bellier et al. (1988, 1991) and Zhang et al. (1998, 1999) in the Weihe graben along the southeastern margin of the Ordos block (Fig. 5a) established three successive extensional regimes: ~ WNW–ESE during the Paleogene, ~ NE–SW during the Neogene, and ~ NW–SE during the Pliocene–Quaternary. These authors correlated WNW–ESE extension, recorded in Precambrian basement along the Weihe graben, with major stratigraphic disconformities at 52–45 and 25–27 Ma. A structural and apatite fission-track thermochronology study along the Tan-Lu fault zone of easternmost Dabie provides support for Paleogene faulting within the WNW–ESE extensional regime; there, several samples yielded Eocene ages (~ 55–40 Ma), with thermal history modeling indicating enhanced cooling at 45 ± 10 Ma (Grimmer et al., 2002). These ages are interpreted in terms of tectonic reactivation of the Dabie Shan, rather than prolonged cooling from mid-Cretaceous until Eocene, and correspond to sedimentation ages in half-graben basins. Station D410 along the Lo-Nan fault provides direct dating (K-feldspar thermochronology) of early Cenozoic faulting; this Cretaceous(?) tonalite cooled rapidly from >400 °C, likely due to Cretaceous faulting, remained at 280–260 °C from 73–63 Ma, and thereafter cooled rapidly to <150 °C at 55–50 Ma. We attribute the latter cooling to the significant normal faulting at this station (Fig. 5c). The widespread Eocene sedimentation in half-graben basins and related offset of pre-Cenozoic markers (Fig. 5c) indicates that the Paleogene was the major period of sinistral strike–slip and rifting in Qinling. The geodynamic interpretation of the Paleogene deformation is debated. On one the hand, Paleogene syn-rifting sedimentation in northern and eastern China is generally attributed to intra-arc and/or back-arc rifting along the Pacific–Eurasian plate margin (e.g., Allen et al., 1997), for which Northrup et al. (1995) suggested a dynamic link to Pacific–Eurasia convergence; decreased convergence is correlated with reduced plate coupling, which in turn resulted in extension adjacent to the plate margin. On the other hand, Eocene NE–SW shortening across central Asia and strike–slip and extensional faulting across northeastern Asia may be attributed to the India–Asia collision, following suturing and the onset of intra-continental subduction at ~ 55–50 Ma (e.g., Searle et al., 1997; Roger et al., 2000). One argument against the India–Asia collision causing crustal extension in eastern China is the 1500- to 3000-km distance from the collision; however, it is also difficult to understand why the Weihe graben should have formed as a result of back-arc extension, as it is ~ 2000 km away from the East-Asian margin. No clear distinction in the orientation and onset of extension by "Pacific rifting" or "India–Asia collision" has been worked out in the Cenozoic rifts of eastern Asia. Here we suggest that the Paleogene stress field in the Qinling resulted from the combined effects of Pacific subduction and the India–Asia collision.

The second Tertiary extensional regime, NE–SW oriented, recorded by us and the studies in the Weihe graben (see above), was established at 6 ± 3 Ma according to Bellier et al. (1988, 1991). A geodynamic interpretation for this increasingly recognized regime (Weihe: Bellier et al., 1988, 1991; Zhang et al., 1999; Hong'an–Dabie: Ratschbacher et al., 2000; Tan-Lu and Yangtze foreland fold-thrust belt: Zhang et al., 1999; Schmid et al., 2000; Grimmer et al., 2002) has yet to be made.

The latest Cenozoic deformation in the Qinling involves normal slip on ENE-striking, graben-bounding faults, dextral (with variable normal and reverse components) slip along NNE-trending faults, and mostly sinistral (again with variable dip-slip components) slip along E- to ESE-trending faults. This fault pattern is consistent with NW–SE extension and NE–SW compression (Fig. 5b, average stress orientations). Using faults from the Weihe graben in the north to the Shang-Dan fault in the south, Peltzer et al. (1985) and Zhang et al. (1995) documented cumulative active sinistral slip rates of ~ 7 mm/year for the ESE-trending faults of the Qinling. We interpret the active

Qinling fault system as accommodating the eastward escape of the Yangtze craton caused by the India–Asia collision and Pacific back-arc extension (e.g., Tapponnier and Molnar, 1977; Fig. 5a). Our data highlight the widespread reactivation of the Qinling over a N–S distance of at least 200 km, from the easternmost segments of the Weihe graben in the north to the Wudang fault in the south. The eastward motion of the Yangtze block with respect to Mongolia (Fig. 5a) is thus accommodated by a series of strike–slip faults in the Qinling area, whose spacing increases into the Yangtze interior. The prevailing strike–slip deformation contrasts with the dominantly normal faulting around Ordos in the Sino-Korean craton (see Zhang et al., 1998). Our study suggests that the Lo-Nan and the Shang-Dan faults, and their western continuation, the Qinling fault, as the southern boundary of the Weihe graben, are the major strike–slip fault systems. Both fault systems reactivated Paleozoic subduction–accretion complexes. The interior of the northern Yangtze craton in southern Qinling (e.g., Wudang basement dome) is characterized by arrays of NE-trending dextral faults, conjugate to a few prominent ESE-trending, sinistral faults, for example, the Gonglu and Wudang faults (Fig. 5b). This fault array is identical in geometry and kinematics to partly seismically active faults within the crystalline core of Hong'an–Dabie (Ratschbacher et al., 2000) and suggests that sinistral faulting along the northern margin of the Yangtze craton (Qinling fault system) changes southward to distributed, wholesale NW–SE extension within the craton. The average NW–SE (142°) late Cenozoic extension direction obtained for the Qinling area is within error identical to the direction (134°) we obtained for Hong'an–Dabie (Jinzhai and Tan-Lu fault zones; Ratschbacher et al., 2000; Schmid et al., 2000; Grimmer et al., 2002) and similar to active NW–SE extension imposed by the India–Asia collision (e.g., Zhang et al., 1995, 1998). The Cenozoic Nanyang basin (Fig. 2) makes an interpretation of how active displacement is transferred from the Qinling to the Tongbai–Hong'an–Dabie difficult. The Jinzhai fault can be traced continuously from northern Dabie into central Tongbai (Ratschbacher et al., 2000); a second, less active fault zone in southern Tongbai runs sub-parallel to the Jinzhai fault into the Nanyang basin. Because the Lo-Nan fault splays into numerous smaller faults in the easternmost Qinling and the northern Tongbai, the Shang-Dan fault probably transfers the major component of active sinistral slip from the Qinling into the Jinzhai and other fault zones of Hong'an–Dabie.

5.2. Cretaceous: Pacific subduction and far-field collisions

Cretaceous igneous rocks comprise ~ 50% of the surface exposure of the Dabie Mountains and almost the entire northern half of Dabie consists of Cretaceous igneous rocks and orthogneisses (Fig. 2; Ratschbacher et al., 2000). The Cretaceous igneous signature diminishes westward through Hong'an and Tongbai, where plutons are concentrated along their northern margins (~ 20% of surface exposure; Fig. 2), and reach <20% in the Qinling (Fig. 2). The Cretaceous plutons in the Qinling crop out nearly exclusively in the Sino-Korean craton and the adjacent Kuanping unit; this contrasts with farther east, where plutons are widespread in the Yangtze craton. The extensive magmatic and metamorphic overprint implies a considerable role of Cretaceous unroofing in the exhumation of the Qinling–Hong'an–Dabie orogen. Indeed, the structural architecture of Hong'an–Dabie is dominated by Early Cretaceous structures (Ratschbacher et al., 2000), mostly normal and strike–slip shear zones and faults with an initial ductile flow event accommodating the highest strain. The major crust-shaping event in Dabie was the formation of the magmatic–metamorphic–structural dome of the Northern Orthogneiss Unit under NW–SE sub-horizontal stretching and sub-vertical and subordinate NE–SW shortening, and the activation of the Xiaotian–Mozitang detachment fault (Fig. 2). The characteristic regional structural feature is a clockwise change in the orientation of the sub-horizontal strain/stress axes; that is, the trend of the principal stretching/extension direction changed from early NW to intermediate N to late NE. Ductile flow is well dated in Dabie by pre- to syn-tectonic orthogneisses with U/Pb zircon ages of 137–128 Ma and post-tectonic (undeformed) granitoids of 129–125 Ma, and $^{40}Ar/^{39}Ar$ thermochronology indicates that most of Dabie cooled below 250 °C by ~ 115 Ma, coeval with brittle–ductile and brittle faulting (Ratschbacher et al., 2000).

Surprisingly little Early Cretaceous deformation occurred in the part of the Qinling studied by us, given its dominance farther east. In contrast to Dabie, Early Cretaceous deformation is mostly brittle, and our age constraints ($\geq$ 112 to $\sim$ 75 Ma) indicate it is younger too. Reischmann et al. (1990) established that the Shagou shear zone in western Qinling, regarded as a branch of the Shang-Dan fault zone (Fig. 2), deformed plutons in a sinistral sense at amphibolite-facies temperatures. The time of motion is bracketed by a zircon crystallization age of 211 $\pm$ 8 Ma from a granodiorite protolith, and a Sm/Nd garnet–whole-rock age of 126 $\pm$ 9 Ma from a rock that contains post-kinematic garnet (Reischmann et al., 1990). The shear zone also incorporates K_2 basins and deformation during retrograde, very-low to low-grade metamorphism. Here we interpret the Shagou shear zone as a kinematic and time equivalent to the Xiaotian–Mozitang fault zone of northern Dabie and the other Early Cretaceous deformation we documented in Qinling; we correlate its reactivation with the widespread Late Cretaceous faulting and basin formation throughout the Qinling. We argue against a possible Triassic–Jurassic age of the shear zone, noting that Triassic deformation is dextral transpressive within the Qinling (see above), that high-temperature Jurassic deformation has yet to be documented, and that post-deformational annealing of deformation fabrics is also observed in northern Dabie.

Early Cretaceous strike–slip and extensional deformation in eastern Asia, coeval with that in Qinling–Hong'an–Dabie, seems to be widespread, but is often incompletely dated and structurally analyzed (Fig. 9a); it has been proposed to have occurred from Mongolia to southeastern China (see Yin and Nie, 1996; Ratschbacher et al., 2000; Graham et al., 2001 for summaries). Here we follow our earlier model (Ratschbacher et al., 2000) and suggest that Early Cretaceous deformation in eastern Asia was the result of the combined effects of the Siberia–Mongolia—Sino-Korean and Lhasa–West Burma — Qiangtang–Indochina collisions, and Pacific subduction and related magmatism. This overall plate tectonic framework indicates an Early Cretaceous tectonic setting dominated by eastward tectonic escape and Pacific back-arc extension (Fig. 9a).

As in Hong'an–Dabie, there is ubiquitous evidence in the Qinling for the characteristic regional structural feature of Cretaceous deformation—specifically the clockwise change in the orientation of the sub-horizontal stress axes. This likely records a change in the regional stress field in eastern Asia and not the rotation of a large crustal block; Gilder and Courtillot (1997) and Gilder et al. (1999) demonstrated that both the southern Sino-Korean and the northern Yangtze cratons lack paleomagnetically detectable block rotations younger than Late Jurassic. In the Yangtze foreland fold-thrust belt south and east of Dabie, basement domes expose upper- to mid-crustal rocks of the late Proterozoic Yangtze crystalline basement. In the Lu Shan dome (Fig. 1), NW–SE extension has been constrained between Permian and Early Cretaceous, and NE–SW extension is syn- to post-127 Ma (Lin et al., 2000). Taking the data from Dabie (see review above) and Lu Shan together, the characteristic regional clockwise change in the orientation of the sub-horizontal stress fields, from early NW–SE to late NE–SW extension, is dated between $\sim$ 140 and $\sim$ 115 Ma, with the latter beginning after $\sim$ 127 Ma in the Lu Shan area.

In the Qinling, the basins associated with the ESE-trending dextral fault zones and the NE–SW extensional stress regime are poorly dated due to the continental nature of the sediments; our K-feldspar ages loosely bracket faulting between $\sim$ 101 and 63 Ma. The Dabie Shan was reheated between $\sim$ 100 and 90 Ma and the ESE-trending Xiaotian–Mozitang was dextral and probably conjugate to the sinistral transtensive Tan-Lu fault (Ratschbacher et al., 2000), for which fault gouge yielded 110–90 Ma ages along strands far north of Dabie (Chen et al., 1989). A broad dextral shear belt of unknown width and along-strike length occupies the eastern Tongbai Shan (Webb et al., 1999, 2001); to the west and south, these tectonites are associated with sedimentary basins (K_2, according to R.G.S. Hubei, 1990). At least locally, the shear belt was reactivated at $\sim$ 75 Ma ($^{40}Ar/^{39}Ar$ ages on biotite and pseudotachylite, Webb et al., 1999). Structural analysis in the Yangtze foreland fold-thrust belt documents NW–SE shortening and NE–SW stretching also along ESE-trending dextral and NNE-trending sinistral fault zones that interfere with open folds (Schmid et al., 2000; Grimmer et al., 2002). The majority of apatite fission-track ages from Dabie are between $\sim$ 85 and 56 Ma (Grimmer et al., 2002). Combining the

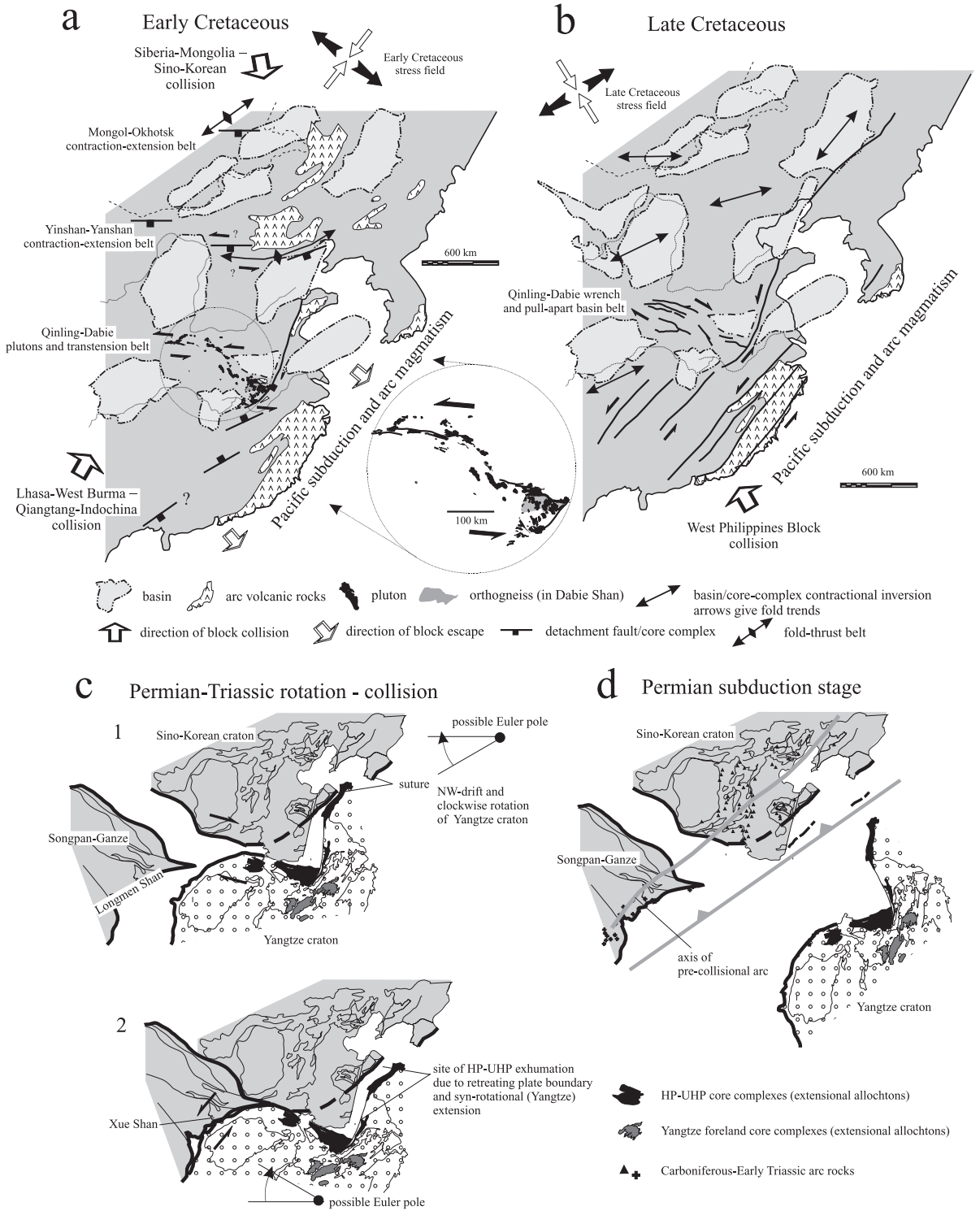
a
Early Cretaceous
Siberia-Mongolia – Sino-Korean collision
Early Cretaceous stress field
Mongol-Okhotsk contraction-extension belt
Yinshan-Yanshan contraction-extension belt
Qinling-Dabie plutons and transtension belt
Lhasa-West Burma – Qiangtang-Indochina collision
Pacific subduction and arc magmatism
600 km
100 km
b
Late Cretaceous
Late Cretaceous stress field
Qinling-Dabie wrench and pull-apart basin belt
Pacific subduction and arc magmatism
600 km
West Philippines Block collision
basin
arc volcanic rocks
pluton
orthogneiss (in Dabie Shan)
basin/core-complex contractional inversion arrows give fold trends
direction of block collision
direction of block escape
detachment fault/core complex
fold-thrust belt
c
Permian-Triassic rotation - collision
1
Sino-Korean craton
possible Euler pole
suture
NW-drift and clockwise rotation of Yangtze craton
Songpan-Ganze
Longmen Shan
Yangtze craton
2
site of HP-UHP exhumation due to retreating plate boundary and syn-rotational (Yangtze) extension
Xue Shan
possible Euler pole
d
Permian subduction stage
Sino-Korean craton
Songpan-Ganze
axis of pre-collisional arc
Yangtze craton
HP-UHP core complexes (extensional allochtons)
Yangtze foreland core complexes (extensional allochtons)
Carboniferous-Early Triassic arc rocks

$^{40}Ar/^{39}Ar$ reheating ages from Dabie and the apatite fission-track ages from Dabie and its foreland, the ~110–90 Ma ages of fault gouge along the Tan-Lu, and the K_2–E stratigraphic ages of sediments east of Dabie, the sinistral normal faulting along the Tan-Lu fault zone of eastern Dabie is constrained to be Late Cretaceous. In conclusion, we suggest that the NW–SE compressional and NE–SW extensional regime affected eastern China from the late Early Cretaceous to the Late Cretaceous; it was associated with important strike–slip faulting, graben formation, and folding (Fig. 9b).

What tectonism produced this Late Cretaceous deformation with the spectacular dextral strike–slip faults in the Qinling, open folding (NE-trending axes) and transtensional rifting in eastern Asia, and what led to a change of ~90° in the orientation of the Cretaceous stress field? Building on the eastern Asian tectonic setting proposed by Charvet et al. (1994) and Lapierre et al. (1997), we suggest that the geodynamic situation changed in southeastern Asia through the Early–Late Cretaceous (Fig. 9): an Early Cretaceous Andean-type continental magmatic arc (producing the plutonic rocks as far north as the Qinling) was followed by a contractional event related to collision of the Yangtze-Indochina Block with the "West Philippines Block" or "South China Sea Landmass" (Faure et al., 1989; Charvet et al., 1994) and coeval and subsequent crustal extension. The collision probably terminated Izanagi Plate subduction (Engebretson et al., 1985), and induced an overall NW–SE compression and NE–SW extension with sinistral slip on (N)NE-trending faults (e.g., the Changle–Nanao tectonic zone in southeast China; Charvet et al., 1990) and dextral slip along ESE-trending fault zones (e.g., the dextral Xiaotian–Mozitang and the faults in Qinling, Fig. 9b).

5.3. Triassic orogenesis: subduction of the Yangtze craton

Formation and exhumation of the HP–UHP rocks of Hong'an–Dabie occurred between 245 and ~225–210 Ma. Hacker et al. (1998, 2000) showed that Triassic zircon, hornblende, mica, and K-feldspar ages are prevalent in Hong'an as far north as the Huwan normal shear zone, south of the Liuling unit, and into the Liuling unit in Dabie (its southern part is called Nanwan in Hong'an and Foziling in Dabie; Fig. 2). Xu et al. (2000) presented a single ~250-Ma white-mica age from the Liuling (called Liangting mélange in their paper) in northernmost Hong'an; however, a 227 ± 3 $^{40}Ar/^{36}Ar$ ratio makes this age questionable. Our thermochronology shows that Triassic orogeny was thermally less significant in the Qinling area than in Dabie. No Triassic zircon ages have been reported from Qinling metamorphic rocks, and there is only one unambiguous Triassic $^{40}Ar/^{39}Ar$ hornblende age, a 237-Ma age from a garnet amphibolite in Wudang. All the K-feldspar spectra we have acquired from pre-Mesozoic rocks in the Qinling area indicate moderate Triassic reheating; this includes rocks in the Erlangping, Qinling and Liuling units. Our best estimate for the time of dextral transpressive slip along the shear/fault zones of the central Qinling (Lo-Nan, Shang-Xiang, and Shang-Dan) is 240–200 Ma; deformation temperatures reached 100–300 °C, locally <400 °C. Well-documented muscovite and hornblende samples from the Wudang basement yielded 237–232 Ma, equivalent to ages from the Huwan detachment and somewhat older than the Hong'an blueschist phengite ages. No mica north of the Wudang blueschists has a clear Triassic age; notably, the Douling unit shows no evidence for resetting of Proterozoic hornblende and mica and,

Fig. 9. Cartoons for the Mesozoic plate tectonic evolution of eastern Asia. (a) Early Cretaceous basin formation, arc magmatism (possibly including plutonism along the Qinling–Dabie belt), wrenching, and extension explained as a result of distant collisions (Siberia–Mongolia—Sino-Korean, Lhasa–West Burma—Qiangtang–Indochina) and Pacific subduction and back-arc extension. (b) 90° change in the orientation of the regional stress field from Early to Late Cretaceous explained by the West Philippines Block–Yangtze collision and concomitant NE–SW extension. (c) Paleomagnetically supported rotation–collision scenario for the Permian–Triassic Sino-Korean–Yangtze approach. Illustrated are the transpressive wrenching along the Qinling–Dabie and Longmen Shan belts and the model of extensional exhumation of the high-pressure and ultrahigh-pressure rocks of Dabie–Sulu caused by an irregular plate margin (retreat of the Sino-Korean plate boundary) and a syn-collisional clockwise rotation of the Yangtze plate, providing space for the exhuming rocks. (d) Formation of a Carboniferous–Permian magmatic arc, oblique to the presently east–west trending Triassic suture along the Qinling–Dabie belt. The pre-Cenozoic shape of the Songpan–Ganze terrain is unknown.

consistent with the K-feldspar thermochronology, implies that the Triassic argon loss event did not reach more than ~300 °C north of the Wudang blueschists. The clear Triassic thermal signature in the Wudang blueschists, and the absence of temperatures >300 °C farther north imply that the Triassic event involved subduction and exhumation of the blueschists.

Both the Sino-Korean and the Yangtze cratons provide sedimentologic clues to Triassic orogenesis (Fig. 3); sediment deposition changed markedly on the Sino-Korean craton in the Early Triassic, when lacustrine-to-alluvial conglomerate, arkosic sandstone, and siltstone were laid down. On the Yangtze craton, Lower and Middle Triassic carbonates indicate shallow marine platform sedimentation (R.G.S. Hubei, 1990). However, Breitkreuz et al. (1994) documented massive breccia deposits within the carbonates, which they took to indicate contractional deformation between the Sino-Korean and Yangtze cratons. The shift to continental sedimentation occurred on the Yangtze craton in Late Triassic time.

As in Hong'an–Dabie, tracing the Triassic suture is difficult at the current stage of mapping and its location can only be inferred from indirect evidence (see, e.g., Hacker et al., 1998 for Hong'an–Dabie). The Yangtze craton stretches as a coherent unit at least to the northern edge of the Douling unit, as indicated by the following (Fig. 2 and inset bottom center; see data review above): (i) Zircon ages of ~700–800 Ma, characteristic of the Yangtze craton, occur south of the Liuling unit. (ii) ~400 Ma metamorphic and magmatic ages occur as far south as the northern Liuling unit. In northwestern Hong'an, Devonian–Carboniferous ages occur as far south as the Sujiahe mélange, which we consider part of the Liuling unit. (iii) The ~240- to 200-Ma thermal event associated with the Triassic collision (and the HP metamorphism) is pervasive as far N as (but not including) the Douling unit in the Qinling. In Hong'an–Dabie, Triassic ages occur as far north as the Qinling–Erlangping units. (iv) Penetrative Triassic deformation characterizes the Yangtze craton up to the southern margin of the Liuling unit. We tentatively place the Triassic suture between the Yangtze and Sino-Korean cratons within the phyllitic–volcaniclastic part of the southernmost Liuling unit (Figs. 2 and 10). We suggest that the plethora of Qinling, and in particular Tongbai–Hong'an area, zircon, hornblende, and mica ages that range from 400 to 250 Ma reflect tectonothermal events in a Devonian to Permian accretionary complex that was built southward of and possibly reworked the Silurian–Devonian accretionary complex (see below). The Devonian batholith and the belt of Carboniferous–Permian andesitic volcanic rocks in the Sino-Korean craton constitute the related arcs (see above and Fig. 1); the northward shift of magmatism from the Silurian–Devonian to the Carboniferous–Permian implies a flattening of the subduction angle (see below). The association of dominantly siliciclastic and acid and basic metavolcanic rocks, and the prevailing greenschist-grade but local HP metamorphism typifies the accretionary setting of the southern Liuling unit. Fig. 10 visualizes the composite, likely continuously active Silurian–Permian Liuling subduction–accretion system as distinct but consecutive subduction zones, emphasizing the probably different subduction geometries and the differently located arc systems.

The Wudang basement massif is a metamorphic core complex that formed in a ~N–S extensional setting and was refolded openly to tightly and involved in a south-directed fold-thrust belt reaching into the Early Jurassic; phases of shortening interfered with stretching. The core complex originated during dominantly pure shear stretching with top-S ductile shearing along its southern and top-N ductile shearing at its northern margins. $^{40}Ar/^{39}Ar$ dating of syn- to post-kinematic hornblende and muscovite puts stretching at or before 230–235 Ma; still unresolved, possibly contractional, deformation predated crustal thinning. Comparing the Wudang and Hong'an–Dabie areas, the northern edge of the extensional dome is located at different positions within the Yangtze craton. The Huwan Formation of northern Hong'an constitutes a lithosphere-scale shear zone (the Huwan detachment) that reactivated the Triassic suture belt (Fig. 2). In Dabie, the Huwan detachment cannot be mapped, as Cretaceous magmatism, metamorphism, and deformation has obliterated earlier fabrics, but it must be south of the Foziling and Luzhenguang units, the latter with clear Yangtze craton affinity and the former with Triassic metamorphic ages, very likely coinciding with the Early Cretaceous Xiaotian–Mozitang crustal-scale shear zone (Hacker et al., 2000; Ratschbacher et

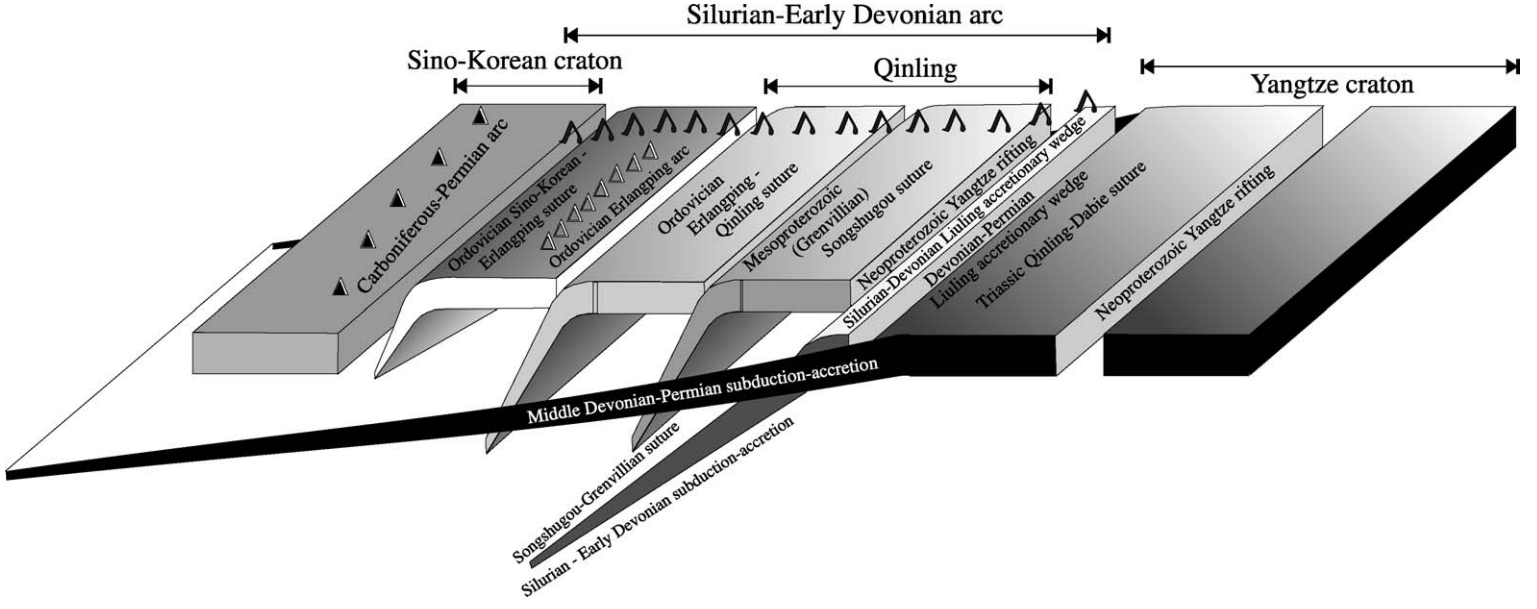

Fig. 10. Cartoon summarizing the late Proterozoic–early Mesozoic assembly of the Qinling area (see Fig. 3 for a summary of the data). The composite, likely continuously active, Silurian–Permian Liuling subduction–accretion system is visualized as two distinct consecutive subduction zones with different subduction geometries and related but differently positioned arcs.

al., 2000). In Qinling, the Douling unit, lithologically equivalent to the Huwan and Luzhenguang units, is non-mylonitic and lacks Triassic HP–UHP metamorphism.

Tentatively, as our age range is still not precise, we correlate dextral transpressive wrenching within the Qinling with crustal thinning and thrusting–folding on the northern Yangtze craton. Although most Yangtze–Sino-Korean collision scenarios contain a component of dextrally oblique convergence (e.g., Yin and Nie, 1996; Zhang, 1997), no model has been based on direct observations. Here we suggest that the dextral strike–slip in Qinling is a result of continental subduction that was oblique to an approximately east–west plate margin in the Qinling, and clockwise rotation of the Yangtze craton (Fig. 9; Zhao and Coe, 1987; Gilder et al., 1999). Note that the range of Triassic ages in Qinling correspond to those in Dabie; the proposed younging and westward migration of collision (e.g., Yin and Nie, 1993; Zhao and Coe, 1987; Zhang, 1997) is not documented geochronologically along Qinling–Hong'an–Dabie. Triassic dextral transpression in the Qinling is compatible with structural data from the Songpan–Ganze allochthon facing the northwestern edge of the Yangtze craton. Burchfiel et al. (1995) showed that the Xue Shan platform of the northern Longmen Shan (Fig. 1) was transported (north)westward during early Mesozoic transpressive tectonism. The entire Triassic Longmen Shan can be considered as a sinistral transpressive belt conjugate to the dextral transpression in Qinling, and both formed under overall N(W)–S(E) shortening (Fig. 9c).

Geological field mapping has outlined several basement domes in the northern Yangtze craton (Figs. 1 and 2). For Wugong Shan, Faure et al. (1996) outlined an extensional origin at 250–230 Ma. Lin et al. (2000, 2001) documented for the Jiuling Shan and the Lu Shan an extensional setting following N–S shortening; they discussed a possible initial stage of formation during the Triassic despite the presence of exclusively Cretaceous U/Pb titanite and $^{40}Ar/^{39}Ar$ mineral ages. We have documented Triassic extension without a Cretaceous overprint in the Wudang Shan. Hacker et al. (2000) showed that the HP–UHP rocks of Hong'an–Dabie were exhumed principally by normal-sense shear from beneath the hanging wall Sino-Korean craton. A detailed discussion of a geodynamic scenario for the extensional setting within the northern Yangtze craton is beyond the scope of this paper; however, we suggest that it was related to widespread subduction of the northern edge of the Yangtze craton to HP and UHP depths (from central Qinling to Sulu, Fig. 1) and subsequent, syn-convergence extensional exhumation due to buoyancy, a retreating plate boundary (Sino-Korean craton), and a clockwise syn-collision–syn-exhumation rotation of the craton (e.g., Zhao and Coe, 1987) which produced local extension during convergence (Fig. 9c).

In spite of this profound subduction and regurgitation of the Yangtze craton, Permian–Triassic magmatism (e.g., an Andean-style arc) is absent from the Dabie, Tongbai, and eastern Qinling areas. Triassic plutons do, however, extend westward ~300 km from Xian (Fig. 2), where they intrude the Kuanping, Erlangping, Qinling, and Liuling units, and, most notably, the Yangtze craton cover. The Triassic granitoids within the Liuling and the Erlangping units in western Qinling are metaluminous, probably I-type with low Sr_i ratios (Reischmann et al., 1990). Zhang (1997), summarizing Chinese geologic, stratigraphic, and geochemical data, outlined a NE-trending belt of Middle Carboniferous to Early Permian andesitic volcanic breccia and tuffs in the eastern half of the Sino-Korean craton, suggesting a pre-Late Permian arc related to subduction; this belt is a direct continuation of the Triassic plutons of the Qinling (Figs. 1 and 9d). Permian and Triassic plutons also occur along the western edge of the Yangtze craton in the Xue Shan, Longmen Shan and in the Songpan–Ganze flysch (Fig. 1). Notable is the NE trend of this Late Carboniferous–Triassic(?) magmatic arc, oblique to the present-day WNW trend of the Triassic suture in Tongbai–Hong'an–Dabie. We suggest that the original trend of the suture in Tongbai–Hong'an–Dabie was modified by crustal extension marked by the metamorphic core complexes in northern Yangtze craton and the Mesozoic–Cenozoic extension in the southern Sino-Korean Hehuai basin, and by the clockwise rotation of the Yangtze craton (Fig. 9c,d).

5.4. Silurian–Devonian orogenesis: oceanic arc accretion and Andean arc

The oldest Paleozoic orogenic event in the Qinling orogen was the formation of the Erlangping intra-

oceanic arc at ~490–470 Ma (Early Ordovician). Subduction was either to the (present) south (Xue et al., 1996b) or to the north; here (Figs. 3 and 10) we adopt northward subduction, thus southward thrusting, as we assign a Kuanping (thus Sino-Korean) affinity to the upper Qinling unit, based on the dominance of marbles in both units. The probable location of coesite-bearing eclogite along the northern margin of the Qinling unit also supports a northward subduction. A back-arc basin may have occupied the intervening region between the intraoceanic arc and the Sino-Korean craton before ~435 Ma when plutons related to the Silurian–Devonian magmatic arc intruded the Kuanping and the craton (see below); the intraoceanic arc thus became amalgamated to the craton between ~470 and 435 Ma.

A magmatic belt straddled the Erlangping, Kuanping, Qinling, and, likely, the Xiong'er (southern Sino-Korean craton) units before 400 Ma (Figs. 3 and 10). The batholiths and related regional contact metamorphism pins the youngest ages of these units. Significantly, none of the 400-Ma plutons crop out south of the Shang-Dan Fault, thus the Liuling unit was not part of this Silurian–Devonian collage. The northern part of the Liuling unit, which we correlate with the Qinling unit, did, however, enjoy the same ~400 Ma regional metamorphism that affected the Kuanping–Erlangping–Qinling units; depth of burial during this kyanite–sillimanite-grade metamorphism was 25–40 km. Silurian to Lower Devonian strata in the northern Liuling conglomerates received metamorphic detritus (Mattauer et al., 1985) from the Qinling and ~780 Ma and ~1.0 Ga detrital zircons (see above). We thus interpret the southern Sino-Korean craton, and units as far as south as the northern Liuling unit, as having been stitched together by the 400-Ma magmatic–metamorphic event and suggest that an Andean-type continental margin arc was built along the amalgamated southern margin of the Sino-Korean craton at this time; we place the subduction zone producing the Silurian–Devonian arc south of the northern Liuling unit.

Late Ordovician (~445 Ma) through Early Carboniferous (~350 Ma) rocks are locally absent from the Sino-Korean craton in the Qinling area, probably reflecting uplift related to the formation of the Andean-style 400 Ma arc. The Douling unit was not influenced by this Devonian event, implying a structural break. During and after the formation of the magmatic arc, the southern margin of the Sino-Korean craton and attached Qinling collage were dissected by sinistral wrenching along the Lo-Nan and Shang-Dan shear systems, with deformation dated at 420–380 Ma. We assume that an oblique subduction imposed these spectacular transpressive wrench zones of Qinling; arc deformation is a common feature along active margins.

Xue et al. (1996b) correlated the Qinling unit with the crystalline basement of the Yangtze craton. We follow them by assigning the lower Qinling unit a Yangtze affinity up until the late Proterozoic, when it was rifted from the Yangtze craton by the late Proterozoic rift system in South China (Figs. 3 and 10). This rifting, dated at ~0.7–0.8 Ga, is probably related to the break-up of Rodinia (Li et al., 1995, 1999); both the lower Qinling unit and the Yangtze craton share the ~0.7- to 0.8-Ga rifting ages. Assembly of the supercontinent Rodinia during the Grenville orogeny (Jinnigian orogeny in China; Li, 1999; Gao et al., 1990) at ~1.0 Ga supports the Qinling–Yangtze connection, as Grenville ages occur in both the lower Qinling unit and the Yangtze craton but are absent from the Sino-Korean craton. It also relates the probable 1.0-Ga eclogite-facies metamorphism within the Songshugou ophiolite to Grenvillian subduction. We object to a Paleozoic Sino-Korean–Yangtze collision and the interpretation of Xue et al. (1996b) that a "highly attenuated marginal basin" formed along the northern Yangtze craton during the collision for three reasons. (1) Paleomagnetic data indicate that the Sino-Korean and Yangtze cratons were separated during the Silurian–Devonian (e.g., Huang et al., 2000). (2) Paleozoic magmatism and metamorphism that might be related to subduction beneath the Yangtze craton or to strong attenuation of the lithosphere, are absent from the Yangtze craton (also from the Douling unit). (3) Silurian–Devonian, ~400 Ma magmatic arc formation on the Sino-Korean craton and the southern abutting Qinling collage and Triassic HP and UHP metamorphism of the northern margin of Yangtze indicate northward subduction.

Figs. 3 and 10 summarize the data and our view of the late Proterozoic–early Mesozoic assembly of the Qinling area. Grenvillian orogeny, involving oceanic subduction with HP metamorphism and ophiolite emplacement (Songshugou ophiolite), assembled the

Yangtze craton, including the lower Qinling microcontinent, into Rodinia. Rifting at ~0.7 Ga separated the lower Qinling unit from the Yangtze craton. Intra-oceanic arc formation (Erlangping–Danfeng–Heihe) between ~490 and 470 Ma was followed by the accretion of the lower Qinling unit to the intra-oceanic arc and the Sino-Korean craton. Oceanward (southward in present coordinates) subduction beneath the northern Liuling unit imprinted the ~400-Ma Andean-type magmatic arc onto the Sino-Korean craton and the previously assembled Qinling collage. Oblique subduction imposed the spectacular early Devonian sinistral transpressive wrench zones. A subduction signature is again evident during the mid-Carboniferous to Late Permian on the Sino-Korean craton, when the Paleo-Tethys was subducted northward, producing the andesitic magmatism on the Sino-Korean craton, and assembling the Devonian–Permian accretionary complex of the southern Liuling unit. In the Late Permian–Early Triassic, the leading edge of the Yangtze craton was subducted to >150 km and subsequently exhumed by crustal extension during clockwise rotation of the craton.

6. Conclusions and outlook

A north–south section from the Sino-Korean to the Yangtze cratons contains the Kuanping accretionary wedge; the Erlangping–Danfeng–Heihe intra-oceanic arc ophiolite; the upper Qinling unit, part of the Sino-Korean cover; the lower Qinling unit, Yangtze craton basement; the northern Liuling unit belonging to the lower Qinling unit; the southern Liuling unit, a Silurian–Permian accretion complex; a continental margin batholith built on the northern Liuling unit to the Sino-Korean craton; the Douling unit, Yangtze basement; and the Yangtze craton. These units were assembled during the late Proterozoic–early Mesozoic. The ~1.0-Ga Grenvillian orogeny, involving oceanic subduction, high-pressure metamorphism, and Songshugou ophiolite emplacement assembled the Yangtze craton, including the lower Qinling unit, into Rodinia. Rifting at ~0.7 Ga separated the lower Qinling unit from the Yangtze craton. Intra-oceanic arc formation at ~470–490 Ma was followed by accretion of the lower Qinling unit to the intra-oceanic arc and the Sino-Korea craton. Oblique subduction beneath the northern Liuling unit imprinted a ~400-Ma Andean-type magmatic arc onto the Sino-Korean craton and the previously assembled Qinling collage, and imposed sinistral transpressive wrench zones within the arc. Devonian–Permian Paleo-Tethys closure built the southern Liuling accretionary wedge (locally incorporating Carboniferous eclogite) and produced andesitic magmatism within the Sino-Korea craton, oblique to and farther into the interior than the Silurian–Devonian arc. In the Late Permian–Early Triassic, the leading edge of the Yangtze craton was subducted to and exhumed from >150 km. The Triassic Yangtze–Sino-Korean suture is within the Liuling complex.

Triassic Yangtze subduction imposed dextral transpressive slip onto pre-existing shear/fault zones (Lo-Nan, Shang-Xiang, Shang-Dan) in the central Qinling at 200–240 Ma, and heated the Erlangping, Qinling, Liuling, and Douling units to 100–300 °C. A >300 and <700 °C thermal signature occurs in the Wudang blueschists of the Yangtze craton, and the absence of temperatures >300 °C farther north implies that the Triassic event involved subduction and exhumation of the blueschists. The Wudang basement massif is a metamorphic core complex formed at ~230–235 Ma with <20 km of crustal thinning at an exhumation rate of ≥0.6 mm/year. The dome was involved in a S-directed fold-thrust belt active into the Early Jurassic. Mapping has outlined several basement domes in the northern Yangtze craton (Wugong, Lu, Jiuling, Wudang, Hong'an–Dabie, Zhangbaling) with proven or suspected crustal extension origin and Triassic age. The extensional setting is related to syn-convergence extensional exhumation of the subducted northern Yangtze craton.

Cretaceous reactivation of the Paleozoic–Triassic Qinling–Dabie orogen started with NW–SE, sinistral (trans)tension, coeval with Early Cretaceous crustal extension and sinistral transtension in the northern Dabie Shan. Only minor Early Cretaceous deformation occurred in the Qinling. However, the Shagou shear zone in the western Qinling Shan is interpreted as a kinematic and time equivalent of the Xiaotian–Mozitang fault zone of northern Dabie, and of other Early Cretaceous deformation in the Qinling. It is suggested that widespread Early Cretaceous strike–slip and extensional deformation in eastern Asia, coeval with that in Qinling–Hong'an–Dabie, was the result of the combined effects of the Siberia–Mongolia—Sino-

Korean and Lhasa–West Burma—Qiangtang–Indochina collisions, and Pacific subduction and related arc magmatism. The characteristic regional structural feature of Cretaceous deformation is a clockwise change in the orientation of the sub-horizontal stress axes; the trend of the principal extension direction changed from NW to NE. It is suggested that the geodynamic situation changed in southeastern Asia through the Cretaceous: an Early Cretaceous Andean-type continental magmatic arc, with widespread Early Cretaceous magmatism and back-arc extension, was followed in the Late Cretaceous by shortening related to the collision of Yangtze–Indochina Block with the West Philippines Block. The collision induced an overall NW–SE compression and NE–SW extension with sinistral slip on (N)NE-trending faults (e.g., the Tan-Lu fault of central–eastern China) and dextral slip along WNW-trending fault zones within the Qinling–Dabie orogen.

The Qinling–Dabie orogen is sliced by ESE-trending Cenozoic faults that have governed the subdivision of the rock units. Commonly mineralized strike–slip and normal faults associated with Eocene half-graben basins record a Paleogene field with NNE–SSW compression and WNW–ESE extension. Direct dating of this faulting comes from K-feldspar thermochronology at 55–50 Ma. Cumulative Cenozoic offsets are tens of kilometers. The Paleogene stress field was a result of the combined effects of Pacific subduction-back-arc extension and the India–Asia collision. A Neogene(?) stress field is characterized by normal faults and a NNE-trend principal sub-horizontal extension. A Pleistocene(?)–Quaternary NW–SE extension and NE–SW compression mostly produced sinistral strike–slip faults. These late Cenozoic faults highlight widespread reactivation of the Qinling belt over a N–S distance of $\geq$200 km, from the Weihe graben in the north to the Wudang fault in the south. The average NW–SE (142°) late Cenozoic extension direction obtained for the Qinling area is within error identical to the direction (134°) obtained for Hong'an–Dabie (Jinzhai and Tan-Lu fault zones) and is similar to active NW–SE extension imposed by the India–Asia collision.

Several first-order problems remain to be addressed within the Qinling–Hong'an–Dabie orogen. (1) The Triassic suture between the Yangtze and Sino-Korean cratons has been placed into the Liuling unit by geochronologic and petrologic constraints; this is an indirectly defined suture and geological mapping must precisely evaluate its surface manifestation. (2) Carboniferous–Permian, Paleo-Tethyan accretionary wedge and oceanic lithosphere remains have only locally been recognized; whether this is due to insufficient documentation and/or specific plate-tectonic processes (e.g., subduction erosion) or is characteristic of UHP orogeny remains to be addressed. The Liuling unit holds the key to defining both the Paleozoic and the Mesozoic sutures and accretionary wedges in Qinling–Dabie. Furthermore, the magmatic arc that resulted from Carboniferous–Permian Paleo-Tethys subduction has to be firmly established (Fig. 9d). (3) A quantitative understanding of the geometry of the Paleozoic and Mesozoic thrust belts in the Qinling is lacking; in particular, the structures related to the Triassic subduction of the leading edge of the Yangtze craton before its exhumation from >150 km are obscure (Fig. 9c). It is to be expected that the cold subduction geotherm (e.g., Liou et al., 2000) prevented extensive ductile flow in the subducting material, favoring discrete brittle faults, which are difficult to document in terrains pervasively deformed by subsequent ductile flow during exhumation. (4) Although buoyant wedge 2D (e.g., Ernst, 2001) and 3D (Hacker et al., 2000) extrusion models have been published for the Hong'an–Dabie section of the orogen, a model providing an unifying exhumation scenario for all Triassic HP and UHP rocks of the Qinling–Dabie–Su Lu area has to be developed. Building on data, partly summarized here, such a model must include plate-tectonic constraints (e.g., an irregular plate margin, clockwise rotation of the Yangtze craton during collision and exhumation), structural constraints (e.g., pervasive extensional deformation and a major component of orogen-parallel rock flow during exhumation), petrologic constraints (e.g., variable subduction depth along strike), and geochronologic constraints (e.g., early Triassic exhumation from mantle to lower crustal depth). (5) The causes of Late Jurassic–Early Cretaceous extension and sinistral transtension and the Late Cretaceous dextral wrenching, folding and transtensional rifting, extension from southern Mongolia (e.g., Graham et al., 2001) to eastern Asia, and of the coincident ~90° change of the stress field remain speculative (Fig. 9a,b). Addressing these problems requires better temporal and regional understanding of Cretaceous deformation of all of Asia and the

dynamics of plate-tectonic processes along the Asian margins. Early Cretaceous magmatism, most probably unrelated to the ~100-Ma older Triassic Qinling–Dabie orogeny, stretches >2000 km into the Asian continental interior; speculative links between low-angle subduction of young Pacific crust and preferred magma ascent along the Qinling–Dabie belt remain to be established. Similarly, little is known about the Yangtze–West Philippines Block collision. (6) Discussion still continues on the role of the India–Asia collision on Cenozoic deformation in eastern Asia; resolution requires a better temporal and regional understanding of geology within Asia and along its margins, in particular the evolution of the Cenozoic basins in eastern Asia, and a knowledge of the time and kinematics of Cenozoic faulting.

Acknowledgements

This research was funded by DFG grants Ra442/14 and 19 and NSF grants EAR-9417958 and EAR-0003568. K-feldspar modeling made use of Frank Spera's IBM 43P computer in the Magma Dynamics Laboratory at UCSB. We thank numerous Chinese colleagues for discussion and field guidance. Gerold Zeilinger and Jürgen Elias contributed U-stage work. Harry Fritz and Wolfgang Unzog are thanked for providing the X-ray texture-goniometer quartz-texture measurement of sample D418. M. Faure and P.H. Leloup provided constructive reviews.

Appendix A. Diffusion-domain K-feldspar thermochronology

We ran modified 1997 versions of Lovera's (1992) modeling routines. A minimum of four steps on the Arrhenius plot were fit with a line to define activation energy E and frequency factor D_0 (Lovera et al., 1989); more steps were added if the fit improved. The number of domains was limited to a minimum of 3 and a maximum of 8. The diffusion-domain theory predicts constant or monotonically increasing age spectra, and spectra that do not fit this ideal must either be rejected or adjusted. In most cases, the samples with abundant excess argon in the first 20–40% of the ^{39}Ar released (D415a, D427a, D430b) yielded similar models for the 50 cooling histories synthesized. Despite their complexity, we present the models because they shed some light on temperature histories for critical portions of the age spectra. Step ages were assigned 2σ analytical uncertainties, except for step ages older than previous steps, for which the uncertainties were expanded until adjacent steps were concordant. In addition, multiple isothermal, low-temperature steps designed to identify Cl-correlated excess ^{40}Ar (Harrison et al., 1994) were all assigned the age of the youngest step in the group. Steps above melting (>1100 °C) that yielded spurious ages were either ignored or made the same as the final 1100 °C step, and steps with low radiogenic yields (<95%) and anomalously old ages were adjusted to provide a smoothly increasing trend. Whereas steps collected at temperatures >1100 °C are not modeled by the program, adjusting anomalously old step ages with low radiogenic yields has no phenomenological justification. Fifty monotonic and non-monotonic cooling histories were generated using age spectrum modeling routines; we only show cooling histories that provide a good fit to the data. Cooling histories and resulting age spectra were modeled with initial ages 50–100 Ma older than the oldest step. By transferring the modeled thermal histories in a cautious way into geological evolution interpretations, we want to make the point that modeling generally involves a simple, numerical fit to complicated, geological data; this is a very subjective process, but it is more valid to present that than a simple closure temperature guess on the cooling history like one is forced to give for hornblendes and micas.

Appendix B. Methods of fault–slip analysis and definition of stress-tensor groups

In the course of our structural studies, fault-slip data were collected from outcrops of known or assumed age. Each station is an outcrop of up to quarry size with uniform lithology. Sense of slip along the faults was deduced from kinematic indicators, for example, offset markers, fibrous minerals grown behind fault steps, Riedel shears, tension gashes. Because errors in slip sense determination may have severe effects on the calculation of principal stress axes, a confidence level was assigned to each slip sense datum. These levels are recorded in the style of the arrowheads expressing the

slip direction of the hanging wall block in the fault slip data diagrams, thus allowing judgment of the quality of the database. Surface morphology of the slickensides (e.g., fiber- or stylolite-coated or polished) and fault size, classified qualitatively based on an estimate of the displacement and the lateral extent of the fault, were recorded. The aim was to discriminate first-order faults and to enable a comparison of faults measured in outcrops with those inferred from mapping. Indications of multiple slip were recorded, and the relative chronology was used for separation of heterogeneous raw data fault sets into subsets. Overprinting relationships such as consistent fault superposition, overgrowths of differently oriented fibers, or fibers with changing growth direction guided the assignment of the subsets to relative age groups. The raw data usually contain several fault slip sets with incompatible slip sense but with consistent overprinting relationships, which were used as the geological constraint for separation. Note, however, that the subsets may contain incompatible data. The latter are included in the stereograms but excluded from the calculations of the stress axes. The derivation of an absolute chronology of faulting events is based on the relationship of faulting to the known age of a rock, the absolute age of its last metamorphism, or a rapid thermal change indicated by thermochronology. Faulting was always evaluated in relation to folding and any sign of post-faulting folding was recorded (e.g., rotated conjugate fault sets with one principal stress direction normal to tilted bedding). Rotations around bedding and foliation have been applied to several faults sets (see, e.g., Fig. 7), but minor rotations ($<20°$) were not performed, as we are more interested in the kinematics/dynamics of regional faulting than in exact stress-field orientations. In all but a few cases, which are stated in the text, data were collected away from major faults. We used the computer program package of Sperner et al. (1993) and Sperner and Ratschbacher (1994) for fault slip analysis to calculate the orientation of principal stress axes and the reduced stress tensors (e.g., Angelier, 1984). Out of this package, we obtained stress axes by the "pressure-tension ($P–B–T$) axes" method and calculated stress tensors by the "numerical dynamic analysis". In addition to stress orientation, the computation of the reduced stress tensor determines the ratio R, which expresses the relationship between the magnitudes of the principal stresses. Extreme values of R correspond to stress ellipsoids with $\sigma_2=\sigma_3$ ($R=0$) or $\sigma_1=\sigma_2$ ($R=1$). The quality and the quantity of field data determined the selection of the method used for calculation. The $P–B–T$ axes method was used with scarce data and where insufficient time was available in the field for careful analysis of fault and striae characteristics.

References

Allen, M.B., Macdonald, D.I.M., Xun, Z., Vincent, S.J., Brouet-Menzies, C., 1997. Early Cenozoic two-phase extension and late Cenozoic thermal subsidence and inversion of the Bohai Basin, northern China. Mar. Pet. Geol. 14, 951–972.

Ames, L., Zhou, G., Xiong, B., 1996. Geochronology and isotopic character of ultrahigh-pressure metamorphism with implications for collision of the Sino-Korean and Yangtze cratons, central China. Tectonics 15, 472–489.

Angelier, J., 1984. Tectonic analysis of fault slip data sets. J. Geophys. Res. 89, 5835–5848.

Angelier, J., 1994. Fault-slip analysis and paleostress reconstruction. In: Hancock, P.L. (Ed.), Continental Deformation. Pergamon, Tarrytown, NY, pp. 53–100.

Bellier, O., Mercier, J.L., Vergely, P., Long, C.X., Ning, C.Z., 1988. Evolution sedimentaire et tectonique du graben cenozoique de la Weihe (Province du Shaanxi, Chine du Nord). Bull. Soc. Geol. Fr., IV 6, 979–994.

Bellier, O., Vergely, P., Mercier, J.L., Ning, C.Z., Deng, N.G., Yi, M.C., Long, C.X., 1991. Analyse tectonique et sedimentaire dans les monts Li Shan (province du Shaanxi—Chine du Nord): datation des regimes tectoniques extensifs dans le graben de la Weihe. Bull. Soc. Geol. Fr. 162, 101–112.

Breitkreuz, H., Mattern, F., Schneider, W., 1994. Mid-Triassic shallow marine evaporites and a genetic model for evaporation during regional compression (lower Yangtze basin, Anhui, China). Carbonates Evaporites 9, 211–222.

Brun, J.P., Choukroune, P., 1983. Normal faulting, block tilting and décollement in a stretched crust. Tectonics 2, 345–356.

Burchfiel, B.C., Chen, Z., Liu, Y., Royden, L.H., 1995. Tectonics of the Longmen Shan and adjacent regions, Central China. Int. Geol. Rev. 37, 661–735.

Burkhard, M., 1993. Calcite twins, their geometry, appearance and significance as stress-strain markers and indicators of tectonic regime: a review. J. Struct. Geol. 15, 351–368.

Charvet, J., Faure, M., Xu, J.W., Zhu, G., Tong, W.X., Lin, S.F., 1990. La zone tectonique de Changle-Nanao, Chine du su-est. C. R. Acad. Sci., Paris 310 (Ser. II), 1271–1278.

Charvet, J., Lapierre, H., Yu, Y., 1994. Geodynamic significance of the Mesozoic volcanism of southeastern China. J. Southeast Asian Earth Sci. 9, 387–396.

Chen, W., Li, Q., Li, D., Wang, X., 1989. Geochronological implications of K/Ar isotope system of fault gouge: a preliminary study. Phys. Chem. Earth 17, 17–23.

Chen, N., Han, Y., You, Z., Sun, M., 1991. Whole rock Sm–Nd,

Rb–Sr and single grain zircon Pb-Pb dating of complex rocks from the interior of the Qinling orogenic belt, western Henan, and its crustal evolution. Geochimica 3, 219–228.

Chen, J., Dong, S., Deng, Y., Chen, Y., 1993. Interpretation of K–Ar ages of the Dabie orogen—a differential uplifted block. Geol. Rev. 39, 15–22.

Chough, S.K., Kwon, S.-T., Ree, J.-H., Choi, D.K., 2000. Tectonic and sedimentary evolution of the Korean peninsula: a review and new view. Earth-Sci. Rev. 52, 175–235.

Cui, Z.-L., Sun, Y., Wang, X.-R., 1995. Discovery of radiolarians from the Danfeng ophiolite zone, North Qinling, and their geological significance. Chin. Sci. Bull. 40, 1686–1688.

Deng, W., 1996. Basic–ultrabasic and volcanic rocks in Chagbu-Shuanghu area of northern Xizang (Tibet), China. Sci. China, Ser. D Earth Sci. 39, 359–368.

Du, D., 1986. Research on the Devonian system of the Qin-Ba region within the territory of Shaanxi Jiaotang University Publishing House, Xi'an.

Eide, L., McWilliams, M.O., Liou, J.G., 1994. $^{40}Ar/^{39}Ar$ geochronologic constraints on the exhumation of HP–UHP metamorphic rocks in east–central China. Geology 22, 601–604.

Enami, M., Zhang, Q., 1990. Quartz pseudomorphs after coesite in eclogites from Shangdong province, east China. Am. Mineral. 75, 381–386.

Engebretson, D.C., Cox, A., Gordon, R.G., 1985. Relative motion between oceanic and continental plates in the Pacific basin. Geol. Soc. Am. Spec. Pap. 206, 1–55.

Ernst, W.G., 2001. Subduction, ultrahigh-pressure metamorphism, and regurgitation of buoyant crustal slices—implications for arcs and continental growth. Phys. Earth Planet. Inter. 127, 253–275.

Faure, M., Marchadier, Y., Rangin, C., 1989. Pre-Eocene synmetamorphic nappe in the Mindoro–Romblon–Palawan area (W. Philippines) and their bearing on the formation of Eurasia. Tectonics 8, 963–979.

Faure, M., Sun, Y., Shu, L., Monié, P., Charvet, J., 1996. Extensional tectonics within a subduction-type orogen: the case study of the Wugongshan dome (Jiangxi Province, SE China). Tectonophysics 263, 77–108.

Gao, S., Zhang, B., Liu, Z., 1990. Geochemical evidence for Proterozoic continental arc and continental-margin rift magmatism along the northern margin of the Yangtze Craton, South China. Precambrian Res. 47, 205–221.

Gilder, S.A., Courtillot, V., 1997. Timing of the North–South China collision from new middle to late Mesozoic paleomagnetic data from the North China Block. J. Geophys. Res. 102, 17713–17727.

Gilder, S.A., Leloup, P.H., Courtillot, V., Chen, Y., Coe, R.S., Zhao, X., Xiao, W., Halim, N., Cogné, J.-P., Zhu, R., 1999. Tectonic evolution of the Tancheng-Lujiang (Tan-Lu) fault via Middle Triassic to Early Cenozoic paleomagnetic data. J. Geophys. Res. 104, 15365–15390.

Graham, S.A., Hendrix, M.S., Johnson, C.L., Badamgarav, D., Badarch, G., Amory, J., Porter, M., Barsbold, R., Webb, L.E., Hacker, B.R., 2001. Sedimentary record and tectonic implications of Mesozoic rifting in southeast Mongolia. Geol. Soc. Am. Bull. 113, 1560–1579.

Grimmer, J.C., Jonckheere, R., Enkelmann, E., Ratschbacher, L., Blythe, A., Wagner, G.A., Liu, S., Dong, S., 2002. Cretaceous–Tertiary history of the southern Tan-Lu fault zone: apatite fission-track and structural constraints from the Dabie Shan. Tectonophysics 359, 225–253.

Hacker, B.R., Ratschbacher, L., Webb, L., Ireland, T., Walker, D., Dong, S., 1998. U/Pb zircon ages constrain the architecture of the ultrahigh-pressure Qinling–Dabie Orogen, China. Earth Planet. Sci. Lett. 161, 215–230.

Hacker, B.R., Ratschbacher, L., Webb, L.E., McWilliams, M., Ireland, T., Calvert, A., Dong, S., Wenk, H.-R., Chateigner, D., 2000. Exhumation of the ultrahigh-pressure continental crust in east–central China: Late Triassic–Early Jurassic extension. J. Geophys. Res. 105, 13339–13364.

Hao, J., Li, Y., Li, X., Zhang, X., 1994. Douling fossil island arc and Wudangshan back-arc basin in East Qinling, central China and their tectonic significance. Sci. Geol. Sin. 3, 265–275.

Harrison, T.M., Heizler, M.T., Lovera, O.M., Wenji, C., Grove, M., 1994. A chlorine disinfectant for excess argon released from K-feldspar during step heating. Earth Planet. Sci. Lett. 123, 95–104.

Hu, N., Yang, J., An, S., Hu, J., 1993. Metamorphism and tectonic evolution of the Shangdan fault zone, Shaanxi, China. J. Metamorph. Geol. 11, 537–548.

Hu, N., Zhao, D., Xu, B., Wang, T., 1995. Petrography and metamorphism study on high-ultrahigh pressure eclogite from Guanpo area, northern Qinling mountain. J. Mineral. Petrol. 15, 1–9 (in Chinese with English abstract).

Hu, N., Yang, J., Zhao, D., 1996. Sm/Nd isochron age of eclogite from northern Qinling mountains. Acta Mineral. Sin. 16, 349–352 (in Chinese with English abstract).

Huang, W., 1993. Multiphase deformation and displacement within a basement complex on a continental margin: the Wudang Complex in the Qinling Orogen, China. Tectonophysics 224, 305–326.

Huang, W., Wu, Z.W., 1992. Evolution of the Qinling orogenic belt. Tectonics 11, 371–380.

Huang, K., Opdyke, N.D., Zhu, R., 2000. Further paleomagnetic results from the Silurian of the Yangtze Block and their implications. Earth Planet. Sci. Lett. 175, 191–202.

Jian, P., Yang, W., Li, Z., 1997. Isotopic geochronological evidence for the Caleodonian Xiongdian eclogite in the western Dabie Mountains, China. Acta Geologica Sinica 10, 455–465.

Kröner, A., Compston, W., Zhang, G.W., Guo, A.L., Todt, W., 1988. Age and tectonic setting of late Archean greenstone-gneiss terrane in Henan province, China, as revealed by single-grain zircon dating. Geology 16, 211–215.

Kröner, A., Zhang, G.W., Sun, Y., 1993. Granulites in the Tongbai area, Qinling belt, China: geochemistry, petrology, single zircon geochronology, and implications for the tectonic evolution of eastern Asia. Tectonics 12, 245–255.

Lapierre, H., Jahn, B., Charvet, J., Yu, Y., 1997. Mesozoic felsic arc magmatism and continental olivine tholeiites in Zhejiang Province and their relationship with the tectonic activity in southeastern China. Tectonophysics 274, 321–338.

Lerch, M.F., 1993. Early Paleozoic tectonic evolution of the Qinling orogenic belt in the Heihe area, central China. PhD Thesis, University of Mainz, Germany.

Lerch, M.F., Xue, F., Kröner, A., Zhang, G.W., Todt, W., 1995. A Middle Silurian–Early Devonian magmatic arc in the Qinling Mountains of central China. J. Geol. 103, 437–449.

Li, X.H., 1999. U–Pb zircon ages of granites from the southern margin of the Yangtze Block: timing of Neoproterozoic Jinning Orogeny in SE China and implications for Rodinia assembly. Precambrian Res. 97, 43–57.

Li, S., Sun, W., 1995. A Middle Silurian–Early Devonian magmatic arc in the Qinling Mountains of central China: a discussion. J. Geol. 104, 501–503.

Li, S.G., Hart, S.R., Zheng, S.G., Liu, D.L., Zhang, G.W., Guo, A.L., 1989. Timing of collision between the north and south China blocks—the Sm–Nd isotopic age evidence. Sci. China 32, 1393–1400.

Li, C., Ma, J., Chen, R., Zhao, J., 1990. New recognition of the stratigraphic sequence and age of the Erlangping Group in Henan province. Regional Geol. China, 181–185.

Li, S., Chen, Y., Zhang, F., Zhang, Z., 1991. A 1 Ga B.P. alpine peridotite body emplaced into the Qinling Group: evidence for the existence of the Late Proterozoic plate tectonics in the north Qinling area. Geol. Rev. 37, 235–242.

Li, X.X., Yan, Z., Lu, X.X., 1992. Granitoids of Qinling–Dabie Mountains Geological Press, Beijing. 218 pp.

Li, Z.-X., Zhang, L., Powell, Ch.McA., 1995. South China in Rodinia: part of the missing link between Australia–East Antarctica and Laurentia? Geology 23, 407–410.

Li, S., Han, W., Huang, F., Zhang, Y., 1998. Sm–Nd and Rb–Sr ages and geochemistry of volcanics from the Dingyuan formation in Dabie Mountains, central China: evidence to the Paleozoic magmatic arc. Sci. Geol. Sin. 7, 461–470.

Li, Z.X., Li, X.H., Kinny, P.D., Wang, J., 1999. The breakup of Rodinia: did it start with a mantle plume beneath South China? Earth Planet. Sci. Lett. 173, 171–181.

Lin, W., Faure, M., Monié, P., Schärer, U., Zhang, L., Sun, Y., 2000. Tectonics of SE China: new insights from the Lushan massif (Jiangxi Province). Tectonics 19, 852–871.

Lin, W., Faure, M., Sun, Y., Shu, L., Wang, Q., 2001. Compression to extension switch during the Middle Triassic orogeny of Eastern China: the case study of the Jiulingshan massif in the southern foreland of the Dabieshan. J. Asian Earth Sci. 20, 31–43.

Liou, J.G., Hacker, B.R., Zhang, R.Y., 2000. Ultrahigh-pressure (UHP) metamorphism in the forbidden zone. Science 287, 1215–1216.

Liu, L., Zhou, D., 1995. Discovery and study of high-pressure basic granulites in Songshugou area of Shangnan, east Qinling. Chin. Sci. Bull. 40, 400–404.

Liu, B.P., Zhou, Z.G., Xiao, J.D., Chen, B.Y., Zhao, X.W., Xin, J.R., Li, X., Du, Y.S., Xin, W.J., Li, G.C., 1989. Characteristics of Devonian sedimentary facies in the Qinling Mountains and their tectono-paleogeographic significance. J. Southeast Asian Earth Sci. 3, 211–217.

Lovera, O.M., 1992. Computer programs to model $^{40}Ar/^{39}Ar$ diffusion data from multi-domain samples. Comput. Geosci. 18, 789–813.

Lovera, O.M., Grove, M., Harrison, T.M., Mahon, K.I., 1989. Systematic analysis of K-feldspar $^{40}Ar/^{39}Ar$ step heating results: I. Significance of activation energy determinations. Geochim. Cosmochim. Acta 61, 3171–3192.

Ma, X.Y. (Ed.), 1986. Lithospheric Dynamic Map of China. Geol. Press, Beijing.

Ma, W., 1989. Tectonics of the Tongbai–Dabie fold belt. J. Southeast Asian Earth Sci. 3, 77–85.

Mattauer, M., Matte, P., Malavieille, J., Tapponnier, P., Maluski, H., Xu, Z.Q., Lu, Y.L., Tang, Y.Q., 1985. Tectonics of the Qinling belt: build-up and evolution of eastern Asia. Nature 317, 496–500.

Meng, Q., Mei, Z., Yu, Z., Cui, Z., 1995. A lost Devonian oldland on the northern margin of the Qinling Plate. Chin. Sci. Bull. 40, 1456–1460.

Niu, B., Liu, Z., Ren, J., 1993. The tectonic relationship between the Qinling Mountains and Tongbai–Dabie Mountains with notes on the tectonic evolution of the Hehuai Basin. Bull. Chin. Acad. Geol. Sci. 26, 1–12.

Niu, B., Fu, Y., Liu, Z., Ren, J., Chen, W., 1994. Main tectonothermal events and $^{40}Ar/^{39}Ar$ dating of the Tongbai–Dabie Mts. Acta Geosci. Sin. 14, 20–34.

Northrup, C.J., Royden, L.H., Burchfiel, B.C., 1995. Motion of the Pacific plate relative to Eurasia and its potential relation to Cenozoic extension along the eastern margin of Eurasia. Geology 23, 719–722.

Okay, A.I., Sengör, A.M.C., Satir, M., 1993. Tectonics of an ultrahigh-pressure metamorphic terrane: the Dabie Shan/Tongbai Shan orogen, China. Tectonics 12, 1320–1334.

Passchier, C.W., Trouw, R.A.J., 1996. Microtectonics. Springer, Berlin, p. 289.

Peltzer, G., Tapponnier, P., Zhang, Z., Xu, Z.Q., 1985. Neogene and Quaternary faulting in and along the Qinling Shan. Nature 317, 500–505.

Qiu, Y., Gao, S., McNaughton, N.J., Groves, D.I., Ling, W., 2000. First evidence of >3.2 Ga continental crust in the Yangtze craton of south China and its implications for Archean crustal evolution and Phanerozoic tectonics. Geology 28, 11–14.

Ratschbacher, L., Hacker, B.R., Webb, L.E., McWilliams, M., Ireland, T., Dong, S., Calvert, A., Chateigner, D., Wenk, H.-R., 2000. Exhumation of the ultrahigh-pressure continental crust in east-central China: Cretaceous and Cenozoic unroofing and the Tan-Lu fault. J. Geophys. Res. 105, 13303–13338.

Reischmann, T., Altenberger, U., Kröner, A., Zhang, G., Sun, Y., Yu, Z., 1990. Mechanism and time of deformation and metamorphism of mylonitic orthogneisses from the Shagou shear zone, Qinling belt, China. Tectonophysics 185, 91–109.

R.G.S. Anhui, 1987. Regional Geology of Anhui Province (in Chinese). Geological Publishing House, Beijing.

R.G.S. Henan, 1989. Regional Geology of Henan Province (in Chinese). Geological Publishing House, Beijing.

R.G.S. Hubei, 1990. Regional Geology of Hubei Province (in Chinese). Geological Publishing House, Beijing.

R.G.S. Shaanxi, 1989. Regional Geology of Shaanxi Province (in Chinese). Geological Publishing House, Beijing.

R.G.S. Sichuan, 1991. Regional Geology of Sichuan Province (in Chinese). Geological Publishing House, Beijing.

Roger, F., Tapponnier, P., Arnaud, N., Schärer, U., Brunel, M., Xu, Z., Yang, J., 2000. An Eocene magmatic belt across central

Tibet: mantle subduction triggered by the Indian collision? Terra Nova 12, 102–108.

Schmid, J.C., Ratschbacher, L., Hacker, B.R., Gaitzsch, I., Dong, S., 2000. How did the foreland react? Yangtze foreland fold-and-thrust belt deformation related to exhumation of the Dabie Shan ultrahigh-pressure continental crust (eastern China). Terra Nova 11, 266–272.

Searle, M., Corfield, R.I., Stephenson, B., McCarron, J., 1997. Structure of the North Indian continental margin in the Ladakh–Zanskar Himalayas: implications for the timing of obduction of the Spontang ophiolite, India–Asia collision and deformation events in the Himalaya. Geol. Mag. 134, 297–316.

Shen, J., Zhang, Z., Liu, D., 1997. Sm–Nd, Rb–Sr, $^{40}Ar/^{39}Ar$, $^{207}Pb/^{206}Pb$ age of the Douling metamorphic complex from eastern Qinling orogenic belt. Acta Geosci. Sin. 18, 248–254.

Song, S., Su, L., Yang, H., Wang, Y., 1998. Petrogenesis and emplacement of the Songshugou Peridotite in Shagnan, Shaanxi. Acta Petrol. Sin. 14, 212–221.

Spear, F.S., 1993. Metamorphic Phase Equilibria and Pressure–Temperature–Time Paths. Mineralogical Society of America, Washington, DC. 799 pp.

Sperner, B., Ratschbacher, L., 1994. A Turbo Pascal program package for graphical presentation and stress analysis of calcite deformation. Z. Dtsch. Geol. Ges. 145, 414–423.

Sperner, B., Ratschbacher, L., Ott, R., 1993. Fault-striae analysis: a TURBO PASCAL program package for graphical presentation and reduced stress tensor calculation. Comput. Geosci. 19, 1361–1388.

Sun, W., Li, S., Sun, Y., Zhang, G., Zhang, Z., 1996. Chronology and geochemistry of a lava pillow in the Erlangping Group at Xixia in the northern Qinling Mountains. Geol. Rev. 42, 144–153.

Sun, W., Williams, I.A., Li, S., 2002. Carboniferous and Triassic eclogites in the western Dabie Mountains, east–central China: evidence for protracted convergence of the North and South China blocks. J. Metamorph. Geol. 20, 873–886.

Tapponnier, P., Molnar, P., 1977. Active faulting and tectonics in China. J. Geophys. Res. 82, 2905–2930.

Twiss, R.J., Unruh, J.R., 1998. Analysis of fault slip inversions: do they constrain stress or strain rate? J. Geophys. Res. 103, 12205–12221.

Wallis, S., Enami, M., Banno, S., 1999. The Sulu UHP terrane: a review of the petrology and structural geology. Int. Geol. Rev. 41, 906–920.

Wang, N., 1989. Micropaleontological study of lower Paleozoic siliceous sequences of the Yangtze platform and eastern Qinling Range. J. Southeast Asian Earth Sci. 3, 141–161.

Wang, T., Li, W.P., 1996. 1:50.000 Regional Geological Surveys of I49E01402 (Shiziping). P.R. China (in Chinese).

Wang, C.Y., Zeng, R.S., Mooney, W.D., Hacker, B.R., 2000. Ultrahigh pressure (27 kb) Dabie Shan orogenic belt: two-dimensional velocity structure from seismic refraction data. J. Geophys. Res. 105, 10857–10869.

Webb, L.E., Hacker, B.R., Ratschbacher, L., Dong, S., 1999. Thermochronologic constraints on deformation and cooling history of high- and ultrahigh-pressure rocks in the Qinling–Dabie orogen, eastern China. Tectonics 18, 621–638.

Webb, L.E., Ratschbacher, L., Hacker, B.R., Dong, S., 2001. Kinematics of exhumation of high- and ultrahigh-pressure rocks in the Hong'an and Tongbai Shan of the Qinling–Dabie collisional orogen, eastern China. In: Hendrix, M.S., Davis, G.A. (Eds.), Paleozoic and Mesozoic Tectonic Evolution of Central and Eastern Asia—From Continental Assembly to Intra-continental Deformation. Geological Society of America, Boulder, CO, Memoir, vol. 194, pp. 231–245.

Xu, B., Grove, M., Wang, Ch., Zhang, L., Liu, S., 2000. $^{40}Ar/^{39}Ar$ thermochronology from the northwestern Dabie Shan: constraints on the evolution of Qinling–Dabie orogenic belt, east–central China. Tectonophysics 322, 279–301.

Xue, F., Kröner, A., Reischmann, T., Lerch, F., 1996a. Palaeozoic pre- and post-collision calc-alkaline magmatism in the Qinling orogenic belt, central China, as documented by zircon ages on granitoid rocks. J. Geol. Soc. (Lond.) 153, 409–417.

Xue, F., Lerch, F., Kröner, A., Reischmann, T., 1996b. Tectonic evolution of the East Qinling Mountains, China, in the Paleozoic: a review and a new tectonic model. Tectonophysics 253, 271–284.

Ye, B., Jiang, P., Xu, J., Cui, F., Li, Z., Zhang, Z., 1993. The Sujiahe terrane collage belt and its constitution and evolution along the north hill slope of the Tongbai–Dabie orogenic belt. Press of Chian University of Geosciences, Wuhan, pp. 66–67. In Chinese.

Yin, A., Nie, S., 1993. An indentation model for the North and South China collision and the development of the Tan Lu and Honam fault systems, eastern Asia. Tectonics 12, 801–813.

Yin, A., Nie, S., 1996. A Phanerozoic palinspastic reconstruction of China and its neighboring regions. In: Yin, A., Harrison, T.M. (Eds.), The Tectonic Evolution of Asia. Cambridge Univ. Press, New York, pp. 442–485.

You, Z., Han, Y., Suo, S., Chen, N., Zhong, Z., 1993. Metamorphic history and tectonic evolution of the Qinling Complex, eastern Qinling Mountains, China. J. Metamorph. Geol. 11, 549–560.

Yu, Z., Meng, Q., 1995. Late Paleozoic sedimentary and tectonic evolution of the Shangdan suture zone, eastern Qinling, China. J. Southeast Asian Earth Sci. 11, 237–242.

Zhai, X., Day, H.W., Hacker, B.R., You, Z., 1998. Paleozoic metamorphism in the Qinling orogen, Tongbai Mountains, central China. Geology 26, 371–374.

Zhang, Z.-J., 1996. Eclogite-facies metamorphism in the amphibolites in the contact with mantle peridotite in the Proterozoic Songshugou ophiolite complex, Qinling mountains, China. Trans. Am. Geophys. Union, EOS 77, 766.

Zhang, K.-J., 1997. North and South China collision along the eastern and southern North China margins. Tectonophysics 270, 145–156.

Zhang, S.C., Tang, S.W., 1983. The discovery of early Paleozoic radiolarian cherts and plate tectonics in northern Qinling. Shaanxi Geol. 2, 1–9.

Zhang, G., Yu, Z., Sun, Y., Cheng, S., Li, T., Xue, F., Zhang, C., 1989. The major suture zone of the Qinling orogenic belt. J. Southeast Asian Earth Sci. 3, 63–76.

Zhang, Z.Q., Liu, D.Y., Fu, G.M., 1991. Ages of the Qinling, Kuanping, and Taowan Groups in the North Qinling orogenic belt, middle China and their implications. In: Ye, L.J., Qian,

X.L., Zhang, G.W. (Eds.), A Selection of Papers Presented at the Conference on the Qinling Orogenic Belt. Northwest Univ. Press, Xi'an, pp. 214–228.

Zhang, B., Luo, T., Gao, S., Ouyang, J., Han, Y., Gao, C., 1994. Geochemical constraints on the evolution of North China and Yangtze blocks. J. Southeast Asian Earth Sci. 9, 405–416.

Zhang, Y.Q., Vergely, P., Mercier, J.L., 1995. Active faulting in and along the Qinling Range (China) inferred from SPOT imagery analysis and extrusion tectonics of southern China. Tectonophysics 243, 69–95.

Zhang, H.-F., Gao, S., Zhang, B.-R., Luo, T.-C., Lin, W.-L., 1997. Pb isotopes of granites suggest Devonian accretion of Yangtze (South China) craton to North China craton. Geology 25, 1015–1018.

Zhang, Y.Q., Mercier, J.L., Vergeley, P., 1998. Extension in the graben system around the Ordos (China), and its contribution to the extrusion tectonics of south China with respect to Gobi-Mongolia. Tectonophysics 285, 41–75.

Zhang, Y.Q., Vergely, P., Mercier, J.L., Wang, Y., Zhang, Y., Huang, D., 1999. Kinematic history and changes in the tectonic stress regime during the Cenozoic along the Qinling and southern Tanlu fault zones. Acta Geol. Sin. 73, 264–274.

Zhang, Z., Zhang, G., Tang, S., Wang, J., 2001. On the age of metamorphic rocks of the Yudongzi group and Archean crystalline basement of the Qinling orogen. Acta Geol. Sin. 75, 198–204.

Zhao, X., Coe, R.S., 1987. Paleomagnetic constraints on the collision and rotation of North and South China. Nature 327, 141–144.